(2)

US Army Corps of Engineers

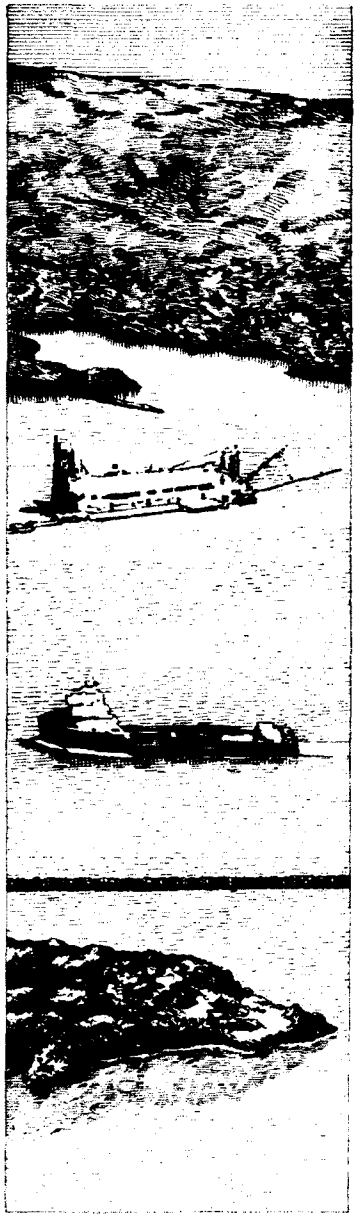

DREDGING RESEARCH PROGRAM

CONTRACT REPORT DRP-92-8

SYSTEM ANALYSIS FOR A KINEMATIC POSITIONING SYSTEM BASED ON THE GLOBAL POSITIONING SYSTEM

by

G. Jeffrey Geier, Peter V. W. Loomis, Alfred Kleusberg

Trimble Navigation Ltd.
645 North Mary Avenue
Sunnyvale, California 94088

December 1992
Final Report

Prepared for DEPARTMENT OF THE ARMY
US Army Corps of Engineers
Washington, DC 20314-1000

Monitored by US Army Topographic Engineering Center
Ft. Belvoir, Virginia 22060-5546

The Dredging Research Program (DRP) is a seven-year program of the US Army Corps of Engineers. DRP research is managed in these five technical areas:

Area 1 - Analysis of Dredged Material Placed in Open Water

Area 2 - Material Properties Related to Navigation and Dredging

Area 3 - Dredge Plant Equipment and Systems Processes

Area 4 - Vessel Positioning, Survey Controls, and Dredge Monitoring Systems

Area 5 - Management of Dredging Projects

REPORT DOCUMENTATION PAGE

Form Approved
OMB No. 0704-0188

1. AGENCY USE ONLY (Leave blank)	2. REPORT DATE	3. REPORT TYPE AND DATES COVERED
	December 1992	Final report

4. TITLE AND SUBTITLE
System Analysis for a Kinematic Positioning System Based on the Global Positioning System

5. FUNDING NUMBERS
DACW72-89-C-0025

6. AUTHOR(S)
G. Jeffrey Geier, Peter V. W. Loomis, Alfred Kleusberg

7. PERFORMING ORGANIZATION NAME(S) AND ADDRESS(ES)
Trimble Navigation Ltd.
645 North Mary Avenue
Sunnyvale, CA 94088

8. PERFORMING ORGANIZATION REPORT NUMBER

9. SPONSORING / MONITORING AGENCY NAME(S) AND ADDRESS(ES)
US Army Topographic Engineering Center
Ft. Belvoir, VA 22060-5516

10. SPONSORING / MONITORING AGENCY REPORT NUMBER
Contract Report DRP-92-8

11. SUPPLEMENTARY NOTES

12a. DISTRIBUTION / AVAILABILITY STATEMENT
Approved for public release; distribution is unlimited.

12b. DISTRIBUTION CODE

13. ABSTRACT *(Maximum 200 words)*

This report documents the findings of a study to design a kinematic positioning system to support U.S. Army Corps of Engineers dredging and hydrographic survey operations. Survey quality GPS receivers are considered, due to the accuracy constraints (10 cm vertical positioning). Use of auxiliary sensors (i.e., INS and high quality clocks) is considered to improve navigation performance when GPS is unavailable. Predicted navigation performance indicates that the accuracy requirements can be met, except at the extremes of the expected separation distances from the reference station. The integer ambiguities associated with the carrier phase measurements can generally be resolved within 7 minutes by processing all available satellites. Measurement gaps of roughly 60 seconds can be tolerated without losing the integers when using a high quality INS.

14. SUBJECT TERMS		15. NUMBER OF PAGES
Dredging	Inertial navigation system	133
Global positioning system	Kinematic survey	16. PRICE CODE
Hydrographic survey		

17. SECURITY CLASSIFICATION OF REPORT	18. SECURITY CLASSIFICATION OF THIS PAGE	19. SECURITY CLASSIFICATION OF ABSTRACT	20. LIMITATION OF ABSTRACT
UNCLASSIFIED	UNCLASSIFIED		

US Army Corps
of Engineers
Waterways Experiment
Station

Dredging Research Program Report Summary

System Analysis for a Kinematic Positioning System Based on the Global Positioning System (GPS) (Contract Report DRP-92-8)

ISSUE: Accurate vessel positioning, survey controls, and dredge-travel monitoring are important to many facets of a dredging program, ranging from the planning phase to contract payment as well as including satisfaction of environmental concerns. Presently, the systems used for horizontal positioning or hydrographic survey vessels and dredges require daily calibration with a known point (shore station). The shore stations are extremely expensive and labor intensive to calibrate and maintain. Further, dredging and survey operations are vertically referenced to the vessel performing the work. This reference is continuously in error by short- and long-term sea surface action. Thus surveyors cannot accurately define the datum at a job site.

RESEARCH: A kinematic positioning system was designed that would support the Corps dredging and hydrographic survey operations. Because of accuracy contraints (10 cm vertical positioning), only survey-quality GPS receivers were considered; use of auxiliary sensors was studied to improve navigation performance when GPS was not available. The analysis included simulation of three important areas of system performance:

- Ability to resolve GPS carrier-lane ambiguities.
- Ability to recover from loss of GPS signal.
- Navigation system accuracy operating with one (or more) differential stations.

Based on the analysis and examination of relevant costs and risk factors, a decision matrix was prepared.

SUMMARY: From the decision matrix, systems emerged as strong candidates as a GPS receiver and for an Inertial Guidance system for maintenance of navigational accuracy during complete GPS outages. The system analysis and decision matrix will be used to develop a prototype GPS that will be field tested.

AVAILABILITY OF THE REPORT: The report is available through the Interlibrary Loan Service from the U.S. Army Engineer Waterways Experiment Station (WES) Library, telephone number (601) 634-2355. National Technical Information service (NTIS) report numbers may be requested from WES Librarians.

To purchase a copy of the report, call NTIS at (703) 487-4780.

About the Authors: The principal authors, all associated with Trimble Navigation Ltd. of Sunnyvale, CA, were Messers. G. Jeffrey Geier, Peter V. W. Loomis, and Alfred Kleusberg. For further information on this work, contact Ms. Sally Froge at (703) 355-2819. For general information on the Dredging Research Program (DRP), contact Mr. E. Clark McNair, Manager, DRP, at (601) 634-2070.

December 1992

PREFACE

The work described in this report was authorized by Headquarters, U.S. Army Corps of Engineers (HQUSACE), as part of the Dredging Research Program (DRP). The work was performed under Work Unit 32479, "Horizontal/Vertical Positioning System Based on the Global Positioning System Satellite Constellation". Mr. Carl A. Lanigan was Principal Investigator. Mr. M.K. Miles (CE-EP-S) was the DRP Technical Monitor for this work.

Mr. Jesse A. Pfeiffer, Jr. (CERD-C) was the DRP Coordinator for the Directorate of Research and Development, HQUSACE. Mr. E. Clark McNair (CEWES-CD-P) was the DRP Program Manager. Mr. George P. Bonner (CEWES-JV-Z) was the Technical Area Manager. The DRP was assigned to the Coastal Engineering Research Center, Dr. James R. Houston, Director, and Mr. Charles C. Calhoun, Jr., Assistant Director.

The work was performed under contract with Trimble Navigation Ltd. The principal authors were Messrs. G. Jeffrey Geier, Peter V.W. Loomis and Alfred Kleusberg.

Mr. Frederick Gloeckler was the Contracting Officer's Technical Representative for the U.S. Topographic Engineering Center. Mr. Regis Orsinger was Director, Topographic Developments Laboratory; Mr. Peter J. Cervarich was Chief, Surveying Division and Mr. Stephen R. DeLoach was Chief, Precise Survey Branch.

Colonel David F. Maune was Commander and Director and Mr. Walter E. Boge was Technical Director of the U.S. Topographic Engineering Center when this study was accomplished.

At the time of publication of this report, Director of WES was Dr. Robert W. Whalin. Commander was COL Leonard G. Hassell, EN.

For further information on this work, contact Ms. Sally Froge at (703) 355-2819 or Mr. E. Clark McNair, Jr., at (601) 634-2070.

TABLE OF CONTENTS

SECTION PAGE

1.0 Summary

This report documents the results of a systems analysis of a Global Positioning System (GPS) based navigation system to support U.S. Army Corps of Engineers (USACE) dredging and hydrographic surveying. A horizontal positioning accuracy of 2 meters is required; however, decimeter level accuracy is highly desired. In the vertical, decimeter level accuracy is required. Due to these stringent accuracy constraints, a significant portion of this effort was dedicated to an accuracy prediction based upon extensive error modeling and simulation. These efforts are summarized in the next section. Based upon the results of the analysis, and examination of relevant cost and risk factors, a decision matrix was prepared (see Table 9.0-1).

The analysis included simulation of three important areas of system performance:

- the ability to resolve GPS carrier lane ambiguities
- the ability to recover from loss of GPS signals
- navigation system accuracy operating with one (or more) differential reference stations.

Decimeter level positioning, using GPS, requires use of carrier phase measurements which have the integer cycles, or lanes, properly resolved.

The first simulation investigated the ability and time required to resolve the lanes, considering the possible receiver types (i.e., P-code, sirgle frequency C/A-code, and dual frequency C/A-code types). The results show that the so-called widelanes can be resolved within 7 minutes using P-code receivers at distances up to 100 km. Widelanes could be resolved only for limited separation distances using dual frequency "codeless" type receivers (which derive second frequency information through "squaring" or "cross-correlating", as explained later in the report). Section 4 describes the simulation and results in detail.

In the second simulation, the use of an Inertial Navigation System (INS), high quality clocks, and a barometric altimeter were examined for their use in maintaining integers during gaps in GPS coverage. Different quality INSs were considered with both partial and complete obscuration of GPS. Maximum tolerable gap lengths (without loss of the integer ambiguities) were determined as a function of the separation distance from the differential reference station. The maximum tolerable gap for total loss of GPS and a high quality INS was found to be about a minute. A detailed reporting of these efforts appears in Section 5.

The third simulation predicted the resultant navigation performance when operating with both single and multiple reference stations operating as a network. Separation distances of up to 120 km are considered. Multiple reference stations were necessary to maintain decimeter vertical accuracy at longer separation distances. The results are reported in detail in Section 6. The conclusions of the study are as follows:

- A decimeter level kinematic positioning system employing differential GPS is feasible.

- The maximum operating range requires use of P-code receivers. Lesser receivers provide only limited range. A suitable receiver is presently on the market, though it is expensive.

- A single reference station can supply decimeter-level accuracy out to about 20 km once single frequency (L1) lanes have been determined.

- Multiple reference stations are needed to maintain decimeter vertical accuracy at distances greater than 20 km. The user must be surrounded by the network stations (interpolation).

- Wide-lanes can be resolved and the system initialized within ≈7 minutes using six available satellites from the full GPS constellation. Use of GLONASS and/or geostationary satellites can speed up the process.

- Integration of a high quality INS allows complete loss of GPS signals for periods up to a minute without having to reacquire the lanes.

2.0 Introduction

2.1 Review of Current Dredging Operations

A major function of USACE is to maintain the Nation's ports, harbors and waterways. Extensive hydrographic surveys are required to support the planning, engineering, design, and construction phases of this effort. Hydrographic surveying and vessel positioning is an essential engineering function to prepare for and administer dredging projects. Presently, horizontal positions of dredges and hydrographic survey vessels are determined using systems that electronically measure multiple ranges or ranges and angles from previously established control points on shore. Most of these systems require the vessel to occupy a calibration point installed near the job site each work day to "initialize" the system. Furtnermore, they all require establishing a series of receiver/transmitters on control stations on shore. Maintaining these control stations, moving receiver/transmitters about, and performing the calibration process is extremely expensive and labor intensive. In addition, all dredging and survey operations are vertically referenced to the vessel performing the work. This reference is generally related to a tide or river gage to reduce the depth readings to some datum, for instance mean lower low water (MLLW). This method assumes that water surface elevations at the gage site accurately represent the surface elevations at the survey site. However, this is not the case and the surface elevations vary significantly between the gage and the survey site. Offshore tide gages have been introduced as a means to produce mathematical models of the surface characteristics of a body of water. However, these are expensive to install, operate and maintain. Furthermore, the models produced are limited in accuracy by various tidal characteristics, and metrological, oceanographic, and hydrological effects. Current technology does not allow surveyors to accurately and efficiently define the vertical datum at a job site. With GPS, vessel altitude is determined relative to the WGS-84 ellipsoid. Once an onshore tide gauge reading has been referenced to WGS-84 ellipsoidal elevation (by collocating a GPS receiver with the tide gauge), vessel depth gage readings can be determined relative to MLLW without the use of water surface modelling.

A system requiring no onsite calibration and only one reference station would significantly increase the efficiency and productivity of the USACE hydrographic surveyor. If this system could simultaneously provide sufficient vertical accuracy it could also serve as a means to rectify the tidal datum. For such a system to be accepted by the community it would have to provide a horizontal positioning accuracy of ± 2 meters, and a vertical accuracy of ± 0.1 meters. Even though a GPS kinematic positioning system may not require calibration to its reference station, it may have to be calibrated or aligned to the local project datum.

With the deployment of GPS, a possibility for a kinematic positioning system meeting these requirements has materialized. Relative positions of a moving antenna meeting the above criteria are possible using GPS. Differential positioning using carrier smoothed pseudo-ranges has demonstrated accuracies of a few meters. Differential kinematic surveys using carrier phase measurements have demonstrated accuracies of a few centimeters.

However, experiments using the later approach employed methods to initialize carrier lane ambiguity which are operationally inappropriate in the marine environment (occupation of known baseline, antenna swaps, static surveys, etc.). Additional operations may be needed to recover full performance after loss of signal and cycle slips. Data transmission, handling, and reduction have not been fully developed for operational use.

2.2 Review of USACE Study Objectives

Currently, there is no kinematic GPS positioning system which meets the operational needs previously outlined. The purpose of this study is to define and analyze possible candidate system approaches, determine their performance, and estimate costs to implement and operate.

2.2.1 Kinematic Positioning System Requirements

For the systems under study to be successful, they must meet the following requirements:

They should provide horizontal positional accuracies equivalent to that obtained with existing systems, approximately ± 2 meters. Decimeter horizontal accuracy is highly desired.

Existing water surface modeling techniques using onsite gages can provide vertical accuracies of about 0.1 meter, however these are not repeatable at this level due to metrological and hydrological conditions, etc. Therefore, the proposed systems should be capable of redefining the vertical datum at the 0.1 meter level or better.

USACE uses automated hydrographic survey systems to produce engineering drawings for the planning, design and construction of major engineering works. These principally include navigation channels and dredged material disposal areas. Most importantly, the results of these surveys are used for budget estimates and contractor payments. As a result, the scale of these surveys requires the positions be computed at least once per second.

It is desired that positions be computed in "real time" so that they may be provided to other on-board systems when the event actually occurred. Alternately, a time tag, accurate to 1 millisecond, must be provided for post-mission matching of soundings and positions.

Survey vessels and dredges must be accurately piloted along a pre-determined course or to a specified position. Horizontal positions must be provided in "real time" to an accuracy of ± 2 meters, for mission navigation. Height in real time is required. Other requirements and desirable system features relative to vessel positioning are summarized below:

- The system must operate in the dynamic conditions experienced in small craft (20 to 65 feet) under all weather conditions in which hydrographic survey operations are performed.

- The system must determine positions of other on-board systems, such as depth sounder transducers, which are not coincident with the GPS antenna(s).

- The system must minimize the need for shore based control and/or reference stations. A single reference station should have a broad coverage area and be capable of servicing multiple users simultaneously.

- It is desired that no special calibration or operational procedures be required to initialize the system to conduct a mission. Any needed pre-mission operations must be within the capability of the vessel crew to perform.

- The system must be robust in operation. It should be designed to minimize loss of GPS data. It is desired that performance degrade gracefully after signal loss. Recovery of full performance should be rapid when sufficient signals are reacquired. It is desired that no special operational procedures be required to restore full performance.

- The system must be reliable with little downtime. When troubles do arise, general repairs will normally be made by survey technicians.

- The system must be relatively small and light weight. Many USACE survey vessels are in the 20 to 25 foot class with limited space and weight capacity. A reasonable weight limit would be 120 pounds or less.

- USACE is anticipating the development of a helicopter mounted LIDAR Bathymeter. A kinematic positioning system developed under this work unit should maintain a goal of interfacing to this helicopter system. This system will have very rigid mission requirements in regards to dynamics, size, and weight; although they are yet to be defined.

- The system should be capable of installation on a buoy to be used as a reference point for establishing off shore tidal datums. Again, the specific requirements for this application have not been defined, but they would certainly be the most rigorous for size and weight limits. However, the data processing application may be the simplest because of the limited motions.

- The system must operate with Block II and Block IIR satellites as well as with the present constellation. It is fully expected that Selective Availability (S/A) and Anti-Spoofing (AS) will be implemented in the Block II constellation. It is desired that the system not require classified access for full performance.

- The system should have lower cost and/or better performance than the present methods for hydrographic surveying.

2.2.2 Summary of Study Activities

The study activities are summarized in the following paragraphs:

- Develop alternate system implementations for analysis.
- Prepare detailed descriptions of selected systems, including hardware, software, and interface requirements, error budgets, reference station location(s), data storage, communications, processing requirements, calibration/initialization, operational procedures and constraints.
- Analyze and simulate system performance for representative operational scenarios. The analysis shall include: accuracy; sensitivity to calibration/ initialization procedures; sensitivity to signal loss; and accuracy degradation and recovery from signal loss and carrier cycle slips.
- For operationally viable system implementations, estimate the system costs including: development; procurement; operation; and data reduction. Identify sources for all components available off-the-shelf. Scope the development effort and assess the risk for items needing further development.
- Identify areas of potential growth and barriers to growth (e.g., helicopter operation).
- Evaluate the tradeoffs between system performance, risk, cost and growth potential.
- Prepare a decision matrix comparing the performance, risk, cost, and growth potential of the alternative system implementations.

2.3 Discussion of Technical Approach

2.3.1 Identification of Critical Issues

Based upon the stated navigation system requirements, four critical technical issues affecting performance were identified:

1. Rapid and reliable acquisition of the lane ambiguities associated with the carrier-phase-derived pseudorange measurements in the expected dynamic environment.
2. Maintenance of positioning capability during partial or complete GPS obscuration and reconvergence to the correct set of carrier-phase integer ambiguities upon reacquisition of GPS signals.
3. Estimation and removal of the correlated errors (i.e., S/A and tropospheric and ionospheric delay) in the GPS measurements over the expected range of separation distances from the reference stations.

4. Maintenance of carrier lock and/or detection and correction of cycle slips for the expected signal dynamics and noise environment.

The ability of the system to satisfy the stringent accuracy requirements is critically dependent on establishing the correct set of lane ambiguities, since each lane error contributes a minimum of roughly 20 cm of ranging error (for the nominal L1 wavelength). These ambiguities must be determined in a dynamic, rather than a static (i.e., survey) environment. The time to acquire the correct set of ambiguities can adversely affect system operations if it is too long. For example, requiring more than 20 minutes for initial convergence (and perhaps reconvergence if the correct set is lost) can make the system unusable for some applications.

The ability to maintain integer count during GPS obscurations requires the use of external sensors, including (generally) a high quality (e.g., rubidium standard) clock and an INS. The required sensor quality will depend upon the length of the measurement gap and the extent of GPS coverage loss (i.e., how many of the minimum required satellites are obscured).

Residual correlated errors in the carrier pseudorange measurements made available for navigation limit the achievable positioning accuracy, since they cannot be filtered (at least in the short term), and are difficult to estimate reliably. These correlated errors can also adversely affect both the speed and reliability of the ambiguity resolution process. It is therefore critical that the ability of single or multiple reference stations to remove these error contributions be quantified.

Loss of carrier lock is readily detected by most GPS receivers within 20 msecs. This detection can be performed reliably by each receiver channel, independent of the other channels, without use of any externally-supplied information. Once a (momentary) loss of track is detected on one channel, a multichannel, state-of-the-art GPS receiver [2,4,36] should be able to determine the number of carrier cycles which were lost when track has again been established. The redundancy available in the additional satellites should permit reconstruction of the (missing) carrier cycles. In addition, if separate tracking of both L1 and L2 carriers is performed within the receiver, this information can be used to determine the number of slipped cycles on one carrier, as long as both carriers do not lose lock over the same time period. Thus, an examination of recovery from carrier loop loss of lock will not be performed as part of this study, since it can and will be done reliably within the recommended GPS receiver architectures [1,8,38]. Current experience with testing Trimble Navigation, Ltd. (TNL) survey receivers indicates that cycle slips are generally induced by interfering sources or poor signal strength; i.e., caused by external radio frequency sources or partial obscuration of the GPS signals. Independent of the cause, methods are used which can detect cycle slips very reliably. Although no comprehensive statistical analysis has been performed for TNL receivers, probabilities of undetected cycle slips of less than one tenth of a percent have been observed in tests of simulated cycle slips over extended time periods (i.e., many hours).

In addition to the critical issues identified and discussed above, certain other technical issues listed below, are addressed in the report:

- Signal reception in the expected multipath and dynamic environment.
- Antenna design, location and mounting.
- System initialization/calibration requirements.
- Referring positions to and time synchronization with other on-board systems.
- Impact of S/A and AS.

2.3.2 Simulation Requirements

The preceding discussion of critical technical issues motivates three separate but related simulation activities:

1. A simulation of the integer ambiguity acquisition (and reacquisition) process.
2. A simulation of the use of external sensors in filling in GPS obscuration periods.
3. A simulation of the use of single and multiple reference stations in removing correlated error components in the GPS measurements.

These three simulations have been used to address the critical issues mentioned above, and are reported on in the following sections of the report.

3.0 System Description and Design Alternatives

3.1 System Overview

The major components of the recommended navigation system are illustrated in Figure 3.1-1. Note that it is comprised of two major subsystems: a ship-based unit, with an associated communications link to a master reference station; and up to three reference stations, including the master and (up to) two monitors. The number of monitor stations required is a function of the desired accuracy and geographic coverage; over reasonably short distances (e.g., 10 km), a single reference station should meet USACE constraints on accuracy.

3.1.1 Ship-Based System

As illustrated in the figure, the ship-based system consists of a GPS receiver with a rubidium frequency standard input, an INS, a barometric altimeter, a communications subsystem and a display. Each of these subsystems interfaces with the central processor, at the heart of the system. The GPS receiver is the primary source of navigation information for the ship: the ultimate accuracy achievable is largely dependent upon the receiver quality. The other navigation sensors (including the rubidium clock) serve primarily to aid GPS, when fewer than the required number of satellites are received. INS provides a full three-dimensional backup navigation capability, and is in fact calibrated during periods of full GPS coverage, while the barometric altimeter and rubidium clock add stability to the vertical and time channels, respectively, when full coverage is unavailable. Note that, even when operating with both monitor stations, the ship-based system need only communicate with the master reference station. The major functions to be performed by the central processor include:

- Providing the interface, in real time, with the navigation sensors, the display and the communications subsystem.
- Implementing the Kalman filter software for integrating the INS, measurements from the GPS receiver, clock and barometrically derived altitude.
- Implementing the differential correction software, based upon data received from the master reference station.
- Implementing the ambiguity resolution algorithms, for initial convergence and needed reconvergence to the correct set of integer ambiguities.
- Providing the interface, in real time, to other on board systems, as required.

The major modules of the real-time kinematic positioning software are illustrated in Figure 3.1.2. As indicated, the operator interface software allows for system control (i.e., starting and stopping) and display, and changing the values of algorithm parameters. The Moding and Sequencing Logic controls the execution of the Ambiguity Resolution Software and the GPS/INS

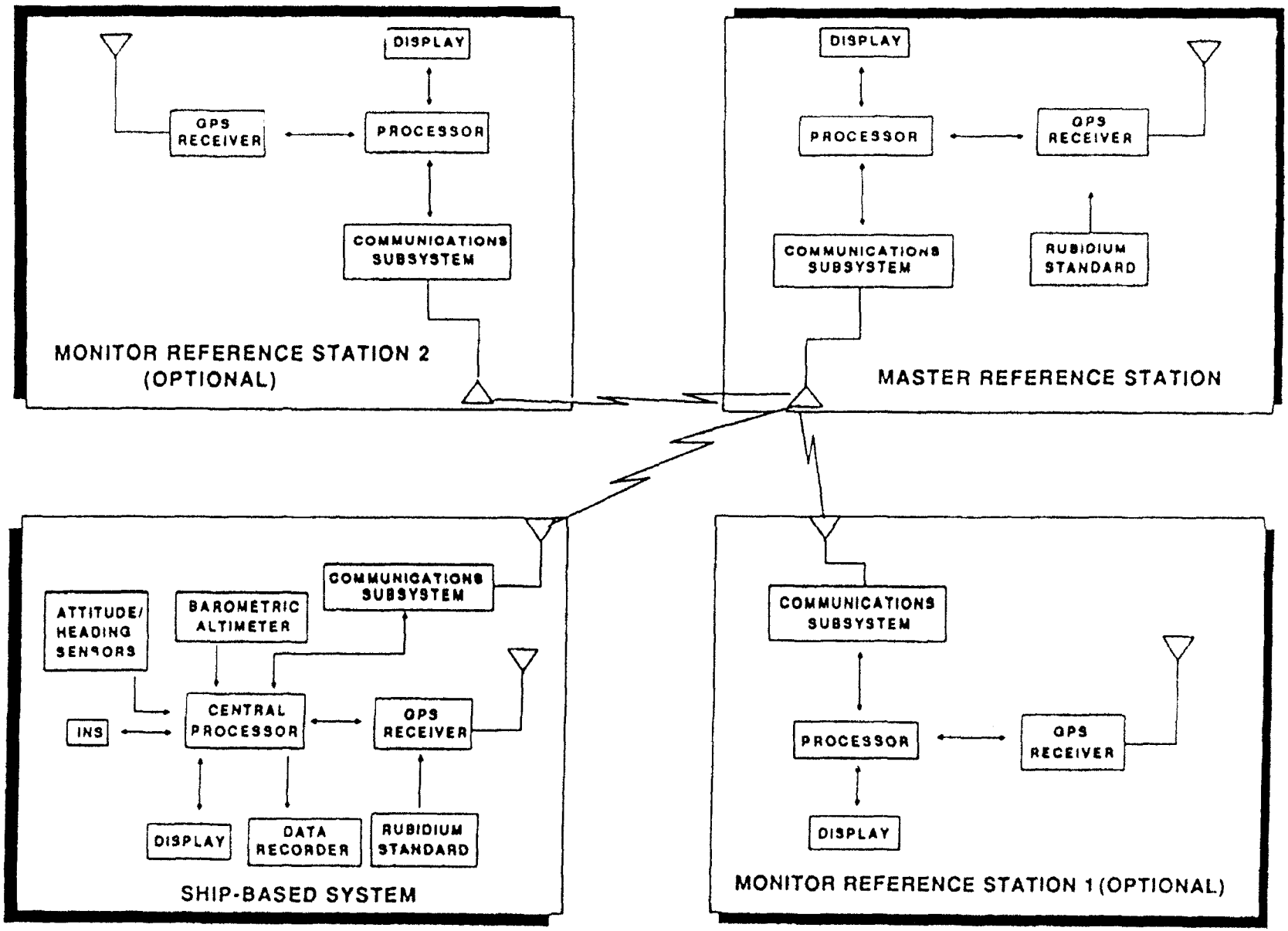

Figure 3.1-1 Navigation System Major Components

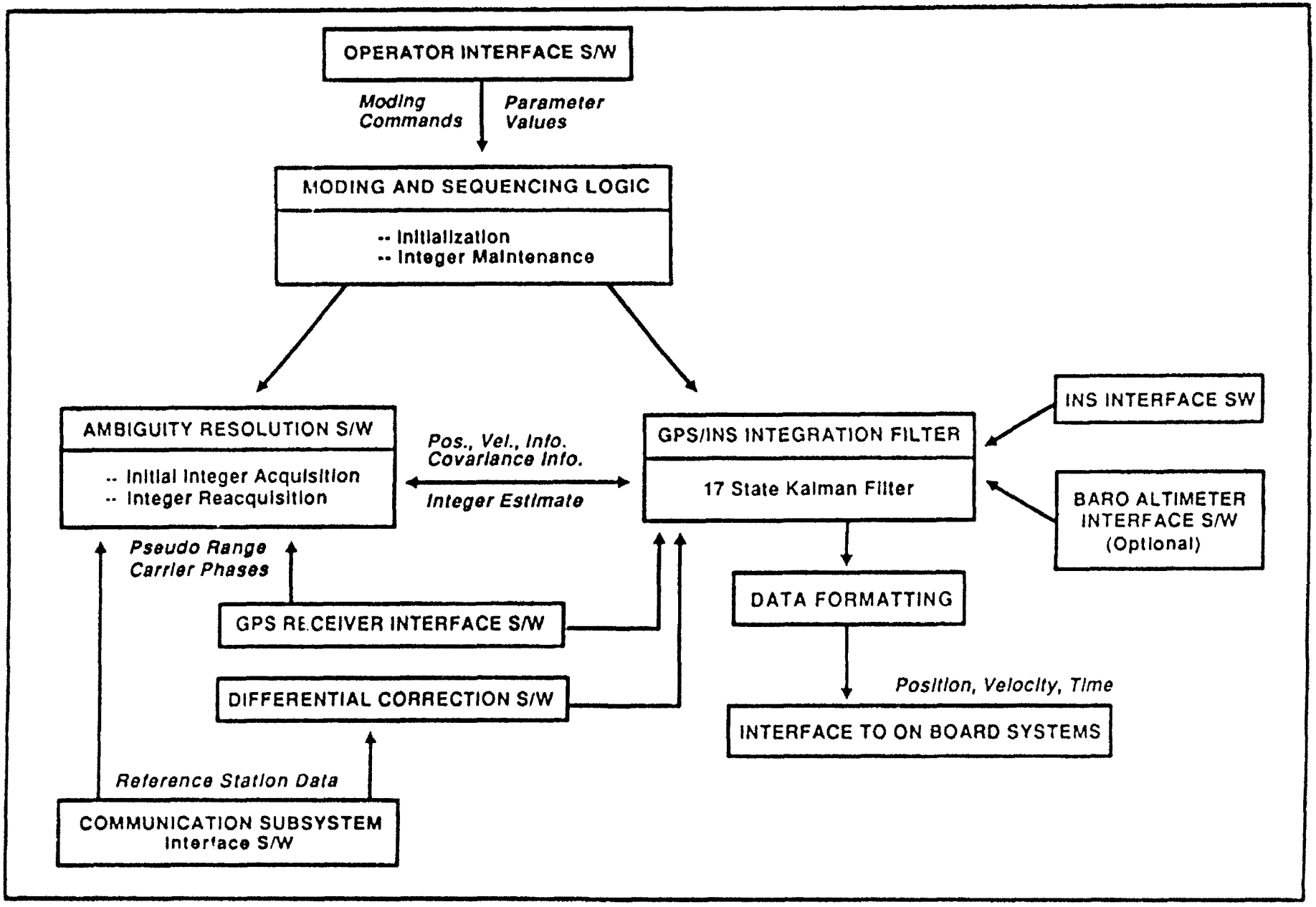

Figure 3.1-2 Major Modules Of The Real-Time Kinematic Positioning Software

Integration Filter to ensure that a correct set of integer ambiguities is maintained: initially, and each time a new GPS satellite is acquired, the Ambiguity Resolution Software must be executed to determine new integers; given a set of integers, the carrier pseudorange measurements can be processed by the GPS/INS Kalman filter. This filter comprises 17 states, which represent a compromise between fidelity (the truth model, as discussed in Section 5, includes 56 states) and imposed computational burden. The modelled states include 3 INS position, 3 INS velocity and 3 INS attitude errors, 3 gyro drifts, 3 accelerometer biases and 2 GPS receiver clock error states. Thus, the Kalman filter and the Ambiguity Resolution Software are running concurrently, with the filter processing carrier pseudorange measurements derived from all satellites for which lane ambiguities have been resolved. The resolved carrier pseudoranges are continuously monitored by the Kalman filter. The cycle slip information output by the GPS receiver can be utilized to resolve any momentary losses of track, and filter residual testing can be used to augment this process. Should a cycle slip be detected by the GPS receiver, the Kalman filter state vector could be augmented in an attempt to solve for the slipped cycles. Thus, "false alarms" will not degrade performance, since the filter's estimate for the unresolved lane ambiguity should not be close to an integer value. For cycle slips which have not been detected by the GPS receiver (a very rare occurrence for most designs), Kalman filter residual (parity) testing can be used to isolate one or more slipped channels if sufficient redundancy exists (six satellite tracking permits isolation of a single cycle slip). When integers have been lost on a satellite which is still in view, (e.g., as induced by obscuration) covariance and position and velocity information is passed to the Ambiguity Resolution Software, to enable an accelerated search process.

Depending upon the outputs of INS (i.e., position and velocity vs. delta velocity and delta angle increments), INS interface software changes significantly. For the Modular Azimuth Positioning System (MAPS) Dynamic Reference Unit (DRU) INS, position and velocity outputs are available at a 5 Hz rate, which is adequate for this application. However, there is a timing uncertainty of 80 msecs associated with the position output; since this cannot be compensated, it can only be modelled as an additional "noise" source by the Kalman filter, with magnitude computed as a function of the expected velocity and acceleration. Interpolation of INS outputs may be needed because the depth sounder can output 6-10 readings/sec. The barometric altimeter interface software is optional, depending on the availability of the barometric altimeter, and supplies altitude information to the filter at a 1 Hz rate. The outputs of the GPS/INS Kalman filter which represent the best estimates of position, velocity, attitude, attitude rate and time, are output for transmission to other shipboard systems; the velocity and attitude rate information can be used to synchronize the supplied position and attitude information.

A secondary usage for INS is as an attitude reference, required for lever arm compensation from the GPS antenna to other points on the ship. Assuming a 20 meter lever arm magnitude, an attitude measurement accuracy of a few milliradians (mrads) is necessary to reduce errors induced by the lever arm

correction to the centimeter level. Such an accuracy is readily achievable using a high quality INS which is periodically calibrated by GPS. If INS is not present, an alternate attitude system is required, as illustrated in Figure 3.1-1. Such a system could be based upon the use of GPS in a multiple (i.e., at least 3) antenna system for three-axis attitude information. Accuracies approaching 0.5 mrad are possible with sufficient antenna separation and an environment relatively free from multipath. Given that the relevant integer ambiguities associated with the carrier difference measurements can be reliably resolved, a differential phase measurement accuracy of 0.5 cm (which includes the effects of both multipath and noise) implies an antenna baseline requirement of 5 meters to achieve 1.5 mrads of accuracy. A relatively low cost rate gyro (which can be calibrated by the GPS-derived attitude) may be used to augment the GPS determined attitude to provide backup attitude information during obscuration periods. Such a backup system is required only for maintenance of continuous attitude, since the integers can be reacquired fairly rapidly for reasonable baseline lengths (e.g., acquisition over a 1 meter baseline can generally be performed in seconds).

The GPS Receiver Interface Software supplies the raw pseudorange and carrier phase measurements to the Ambiguity Resolution and Kalman filter software, along with the required ephemeris data. The Communications Subsystem Interface Software provides the required data received from the master reference station to the Ambiguity Resolution Software and the Differential Correction Software, which computes the differential corrections to be applied to the measurements processed by the Kalman filter.

3.1.2 Reference Stations

The master reference station maintains the required high rate communication with the ship, making possible use of data from two (monitor) reference stations. Data transferred by the master includes the pseudorange and carrier phase measurements on both L1 and L2 for all satellites in view, and spatial derivatives of the differential corrections derived from the monitor station data. This spatial derivative information enables the user to adjust the differential corrections computed by the master station to account for the spatial decorrelation of the ionosphere and SA. Thus, the master station software includes an algorithm for computing these derivatives from the raw measured data. Of course, when operating without the monitor stations, the partial derivative information is absent, and so this software is unnecessary.

Transmissions from the monitor stations to the master occur relatively infrequently (i.e., once per minute) and include the pseudorange and carrier phase measurements on both L1 and L2 for all satellites in view. No special computations are performed by the monitor stations.

3.2 GPS Receiver Designs

Each GPS receiver considered for use in the recommended navigation system must support the following minimum set of requirements:

- Track the worst case expected signal dynamics on the L1 C/A code and carrier with minimum probability of loss of track for the expected minimum signal to noise ratio.

- For dual frequency designs, track the L2 signal with minimum probability of loss of track under the maximum expected dynamics and worst case signal to noise ratio.

- Provide for output of measured pseudorange and carrier phase on L1 (and L2, for dual frequency designs) at 1 Hz for all satellites in view; the pseudorange and carrier phase measurement noise variances should not exceed 1 m^2 and 1 cm^2, respectively, over the full range of signal dynamics and signal to noise ratios.

- Allow for use of an external high quality (i.e., rubidium frequency standard) clock.

Given these minimum set of requirements, four generic receiver designs were considered in this study:

- A P-code dual frequency receiver.

- A C/A-code single frequency receiver.

- A C/A-code dual frequency receiver with codeless extraction of L2 by squaring.

- A C/A-code dual frequency receiver with codeless extraction of L2 by cross correlation with L1.

These two types of codeless L2 tracking receivers deserve further discussion. Since neither design derives L2 information through use of the P-code, they both incur a loss in noise performance relative to a P-code receiver. In addition, both designs require L2 tracking loop aiding by the L1 tracking loop to enable discrimination of the separate satellite signals around the L2 frequency. The squaring process removes the code modulation on each satellite carrier; in so doing, it also removes the ability to isolate specific satellites through code correlation. Similarly, the receiver which cross correlates band-pass-filtered versions of the received signal about L1 and L2 cannot uniquely identify each satellite's signal on L2. The major performance differentiating feature of the two designs relates to the ability to perform wide laning. The receiver which relies upon signal squaring effectively doubles the incoming signal frequency, so can, at best, achieve one-half of the wide lane by combining L1 and L2 carrier phase information.

In addition, optional operation with GLONASS and a geosynchronous satellite was considered to increase the available number of signals for reducing the convergence time of the ambiguity resolution algorithms under study.

3.3 Use of Auxiliary Sensors

As illustrated in Figure 3.1-1, three auxiliary sensors are considered for dynamic aiding during GPS outages; an INS, a barometric altimeter, and a rubidium frequency standard. Three generic INSs were considered in this study, representing high, medium, and low quality designs. The basic concept in using INS aiding is that, once the INS has been calibrated during full GPS coverage, it should enable "coasting" during outages, i.e., maintenance of the correct integer counts for a period of time so that an integer reacquisition may not be necessary when the signals return. Use of either the barometric altimeter or the rubidium frequency standard bounds the error growth during GPS outages in a single direction; for the barometric altimeter, INS altitude error is limited to the residual bias error in the instrument (which has been calibrated by GPS prior to the outage), while the rubidium clock limits the temporal error growth. The rubidium frequency is inherently very stable and its frequency drift has been estimated by the Kalman filter during periods of full GPS coverage.

As an alternative to the use of the barometric altimeter, zero mean vertical velocity damping was considered. This approach relies on the fact that, over many cycles of ocean wave induced oscillation, the average vertical velocity of the ship should be close to zero; thus, the average of INS vertical velocity over an equally long period should be an accurate measure of INS vertical velocity error and can be used to bound the INS error growth in the vertical channel.

3.4 Communications Subsystems

As previously noted, there are (at most) three separate communication links which need to be implemented: as a minimum, data must be transferred from the master reference station to the ship at a fairly high rate (i.e., 1 Hz); optionally, the two monitor stations communicate with the master at a relatively low frequency (e.g., once per minute). The data requirements for the master reference communications are presented in Table 3.4-1. As indicated, approximately 1.0 kbaud is needed to transmit the data from up to 10 satellites at a 1 Hz rate. Note that several special measures have been taken to reduce the required baud rate:

- The ranges for the L1 code and carrier phase and time have been reduced below their maximum possible values; it is therefore necessary to detect "rollovers" of these quantities in the ship computer and make necessary adjustments before these quantities can be used.

- Only the differences between the L1 and L2 code and carrier phases, rather than the whole valued L2 phases are transmitted; the difference variable must therefore only accommodate twice the worst case ionospheric delay, multipath and noise.

Data requirements for the monitor station communications are indicated by Table 3.4-2. Similar measures have been taken to reduce the baud rate of the link, resulting in a requirement of 0.02 kbaud.

Table 3.4-1

MASTER REFERENCE STATION COMMUNICATION REQUIREMENTS

VARIABLE	RESOLUTION	RANGE	REQUIRED NO. OF BITS
L_1 Code Phase	0.1 m	±300 m	16
L_2-L_1 Code Phase	0.1 m	0-200 m	11
L_1 Carrier Phase	$\lambda_1/256$	$\pm N_1\lambda_1$ m	22
L_2-L_1 Carrier Phase	$\lambda_2/256$	$\pm N_2\lambda_2$ m	20
Satellite ID	----	32	5
Satellite Health	----	0-1	1
Time	1 μsec	10 secs	25
Parity	----	----	6 bits/24 bits

Total Bits / Satellite = 125

Assume (worst case) 10 satellites ⇒ 1250 bits/sec ≈ 1.25 kbaud

Table 3.4-2

MONITOR STATION COMMUNICATION REQUIREMENTS

VARIABLE	RESOLUTION	RANGE	REQUIRED NO. OF BITS
L_1 Code Phase	0.1 m	$\pm$48000 m	27
L_2-L_1 Code Phase	0.1 m	0-200 m	11
L_1 Carrier Phase	$\lambda_1/256$	$\pm N_1\lambda_1$ m	30
L_2-L_1 Carrier Phase	$\lambda_2/256$	$\pm N_2\lambda_2$ m	17
Satellite ID	----	32	5
Satellite Health	----	0-1	1
Time	1 μsec	600 secs	31
Parity	----	----	6 bits/24 bits

Total Bits / Satellite = 153

Assume (worst case) 10 satellites $\Rightarrow$ 1530 bits/60 secs = 0.025 kbaud

Mechanization of the communications links can be accomplished using modems and standard telephone lines for data transfer between the monitor stations and the master reference station, and a Very High Frequency (VHF)/ Ultra High Frequency (UHF) line of sight radio link between the master station and the ship. Use of telephone lines for the monitor stations is motivated by the relatively low baud rate; of course, a rental fee would be associated with the use of the telephone lines. The line of sight radio link between the master reference station and the ship can only accommodate the largest expected separation distance (100 km) if a sufficiently large radio tower is utilized and power is sufficiently large. Unless such a tower is already available, its construction could substantially increase the cost of the communication subsystem required.

4.0 Ambiguity Resolution Simulation

This section describes the simulation of the resolution of widelane carrier phase ambiguities in differential kinematic positioning. The ability to resolve the L1 lane ambiguity is not addressed. This limitation of the analysis will be further discussed in Section 6, when resultant navigation performance predictions are presented based upon both widelaning and knowledge of the L1 lane. Generally speaking, acquisition of the L1 lane, given that the widelane has been acquired, is not straightforward. Determination and fixing of the correct integer values of the carrier phase ambiguities is a requirement for sub-decimeter kinematic positioning with GPS. Some useful methods for ambiguity resolution in land kinematic positioning have been developed over the past few years. These methods require a static initialization and are therefore not applicable in an operational marine environment.

Three methods can be used for ambiguity resolution "on-the-fly" (OTF), i.e., while the remote receiver is in motion. The first method resolves ambiguities by combining pseudorange and carrier phase measurements; this has been proved successfully in the field with dual frequency P-code receivers [34], and is chosen for further simulation in this study.

A second method is based solely on redundancy in integrated Doppler measurements to multiple satellites [24,29]. It is analogous to current Doppler survey techniques, but uses three extra satellite signals to track the motion of the vehicle. This method has never been tested in the field; simulation has demonstrated very long convergence times requiring uninterrupted carrier tracking, especially under the effect of differential atmospheric delay and multipath. Consequently, this technique is deemed impractical for real-time kinematic positioning in the context of dredging.

The third method of ambiguity resolution was also considered but rejected because of the perceived risk associated with its use. This method, the ambiguity function method, searches for the most likely set(s) of double-difference integers within the meter-level "coarse" bounds established by double-difference code. With reasonably good code measurements these bounds can be as small as twenty wavelengths (integers) in diameter. To illustrate this method, examine the situation where only four satellites are available. Then three double-difference integers (an integer triplet) are necessary to resolve the ambiguity; there are roughly 6000 triplets within the sphere described by the coarse bounds and any one of them is equally acceptable. If a fifth satellite is added, a fourth double-difference integer that is linearly related to the other three is now required for a full solution. Theory indicates that very few integer triplets will allow a fourth integer that satisfies the linear relationship within the noise bounds of the measurement. This linear relationship can be thought of as a family of planes, a wavelength apart and twice thickness of the carrier phase error, that cuts through the lattice of possible points indicated by the triplets. With a typical carrier noise of 0.05-0.1 wavelength, the percentage of volume in the planes (i.e., satisfying the relationship) is only 1% of the total volume of the space. Thus, the extra restriction eliminates 99% of the

possible triplets of the first three satellite pairs. Once the full GPS constellation is up, one can deperd on six satellites with short outages; this produces two extra restrictions, eliminating 99.99% of the possible triplets. With only 6000 possible triplets, six satellites will usually discriminate the true solution immediately. Similar methods have been used in static survey applications for many years (ambiguity function technique, [5,30]). Recent advances in algorithms and faster microprocessors are combining to make this technique much more practical than previously thought possible (ambiguity search technique,[15,9]).

The difficulty with these ambiguity function and ambiguity search techniques is that in field conditions there is a possibility of large carrier measurement bias, on the order of a centimeter. These biases can last a minute (multipath at the reference station) or many minutes (atmospheric delays over twenty kilometers) or virtually permanent (epsilon orbit error over twenty kilometers). A static receiver can average through these effects, but a kinematic receiver cannot The response of the ambiguity search methods to such biases is nonlinear; although perturbing the measurements very slightly does not change the integer solution at all, a substantial perturbation of a centimeter may cause convergence on a set of integers far from the true solution. The effect that incorporation of additional satellites (e.g., through the inclusion of GLONASS) has on rectifying this problem is a subject of current research activities. This differs from the code/carrier convergence technique chosen for study, which always converges on the correct wave integer. Estimating the biases is possible; if no a priori information on the size of these biases is available, the estimation problem degrades to the multiple satellite integrated Doppler approach mentioned above which converges very slowly unless many satellites are available. The ambiguity techniques do work well in short-baseline static surveys because multipath errors are averaged over a substantial period. The ambiguity function and ambiguity search techniques were not considered as viable real-time kinematic techniques for the following two reasons: OTF performance in field conditions with reference station multipath and atmospheric biases has not been demonstrated; and quality assurance methods have not yet matured to the point that they can be considered reliable for OTF ambiguity resolution. The ambiguity techniques work well in static survey because the data is averaged over a substantial period.

The simulation is performed in two steps for various scenarios. The first step consists of generating GPS measurements based on a particular satellite constellation, a model for the measurement errors and a model for the motion of the remote receiver. In the second step a position and ambiguity determination algorithm tries to recover the carrier phase ambiguities together with the differential position. For the present study, the differential position is a by-product of the algorithm and will not be further analyzed or discussed. Section 4.1 describes the models used in

generating the simulated measurements. Section 4.2 describes the solution algorithm employed to recover the carrier phase ambiguities. Finally, Section 4.3 summarizes the numerical results of the study.

4.1 Measurement Simulation Program

The measurement simulation program generates a file containing satellite coordinates, carrier phase measurements and pseudorange measurements for all visible satellites above 15 degrees of elevation at a one second data rate. The simulated measurements are based on a set of satellite ephemerides, a model for the receiver motion and models for measurement errors. Ephemerides reference epoch is $00^h\ 00^m\ 00^s$ of day 364, 1990.

4.1.1 Satellite Ephemerides

The ephemeris files have identical format for all satellites used in this study. The standard University of New Brunswick GPS ephemeris file format has been used, containing seven records per satellite with the GPS broadcast ephemerides parameters organized according to Table 4.1.1.

For the purpose of this study only nominal orbital parameters are required. These nominal orbital parameters describe circular orbits with constant rate of right ascension, and the resulting ephemeris files contain many zeros. However, the general file format has been retained to enable the processing of real GPS broadcast ephemeris data, if required. The ephemeris files used in this study typically will have the structure as indicated in Table 4.1-2 (xx.xx means non-zero value).

4.1.1.1 GPS Ephemerides

The full GPS constellation used in this study is described in [4-3]. The 24 GPS satellites are irregularly spaced in six orbital planes with 55° inclination, separated by 60° in longitude of the ascending node. The orbits are nominally circular, with a radius of 26,609 km, which leads to an orbital period of 1/2 of a sidereal day. The **eccentricity** and the **argument of the perigee** are set to zero. Thus the ephemerides are given in terms of Keplerian elements **semi-major axis a, inclination i, right ascension of the ascending node Ω** and **mean anomaly M** for the epoch 00:00:00 of November 26, 1989, which is day number 330 of 1989.

For use in this study, the ephemerides must be extrapolated to the simulation epoch on day number 364 of the year 1990. For this ephemerides prediction, the semi-major axis and the inclination are assumed to be constant. The mean anomaly of the nominal orbits repeats every 12 (solar) hours. Therefore, at the epoch 00:00:00 of day 364 of 1990, the mean anomalies of the nominal GPS constellation are identical to the ones listed in [4-5]. Right ascension of the ascending node is subject to a linear drift in first order approximation. Since it is proportional to the cosine of the satellite orbit inclination:

$$d\Omega/dt = \text{constant} \cdot \cos i, \qquad (4.1)$$

Table 4.1-1: Ephemeris File Format

record #1:	I4 - S.V. number	N/A
	I4 - GPS week Weeks from 6 Jan 1990	
	I4 - User range accuracy	Meters
	I4 - S.V. health	N/A
	I4 - Ephemeris fit interval	0 = 4 hrs, 1 = 6hrs
	F10.2 - Age of data ephemeris	Seconds
	F10.2 - Ephemeris reference time	Seconds
	F22.15 - a0 coefficient for S.V. clock	Seconds
record #2:	F22.15 - a1 coefficient for S.V. clock	Sec./Sec.
	F22.15 - a2 coefficient for S.V. clock	Sec./Sec.**2
	F22.15 - MO (mean anolaly at reference time)	Rad.
record #3:	F22.15 - Del N (correction to mean motion)	Rad./Sec.
	F22.15 - Eccentricity	N/A
	F22.15 - A**.5(sq.root of semimajor axis)	Meters **.5
record #4:	F22.15 - w (argument of prerigee)	Rad.
	F22.15 - 10 (inclination angle at ref. time)	Rad.
	F22.15 - I dot (rate of inclination angle)	Rad./Sec.
record #5:	F22.15 - Omega (right ascension of ref. time)	Rad.
	F22.15 - Omega dot (rate aof Omega)	Rad./Sec.
	F22.15 - Cuc (cos harm. term to arg of lat)	Rad.
record #6:	F22.15 - Cus (sin harm. term to arg of lat)	Rad
	F22.15 - Crc (cos harm. term to orbit rad)	Meters
	F22.15 - Crs (sin harm. term to orbit rad)	Meters
record #7:	F22.15 - Cic (cos harm. term to ang of incl)	Rad.
	F22.15 - Cis (sin harm. term to ang of incl)	Rad.
	F22.15 - Group delay differential	Sec.

Table 4.1-2: Ephemerides File Structure for Nominal Orbits

```
 xxxxx 0 0 0    0.00 xxxxxx.xx 0.000000000000000D-00
0.000000000000000D-00 0.000000000000000D-00 x.xxxxxxxxxxxxxxxD-xx
0.000000000000000D-00 0.000000000000000D-00 x.xxxxxxxxxxxxxxxD-xx
0.000000000000000D-00 x.xxxxxxxxxxxxxxxD-xx 0.000000000000000D-00
x.xxxxxxxxxxxxxxxD-xx x.xxxxxxxxxxxxxxxD-xx 0.000000000000000D-00
0.000000000000000D-00 0.000000000000000D-00 0.000000000000000D-00
0.000000000000000D-00 0.000000000000000D-00 0.000000000000000D-00
```

the rate of right ascension for the GPS satellites in the nominal orbits with 55° inclination can be computed from the broadcast rate of right ascension of an existing GPS satellite by using the equation:

$$d\Omega/dt_{55°} = \phi(\cos 55° \cos i) \cdot d\Omega/dt_{i} \qquad (4.2)$$

The resulting rate of right ascension for the nominal constellation amounts to $-7.914 \cdot 10^{-9}$ rad/sec, yielding a change in right ascension of -15.5926° for day 364 of 1990 according to:

$$\Omega \text{ (day 364, 1990)} = \Omega \text{ (day 330, 1989)} - 15.5926°. \qquad (4.3)$$

The value Ω_o transmitted in the GPS broadcast message is not the right ascension in the sense of a Keplerian element. As pointed out in [4-5], Ω_o is referenced to the zero meridian at the beginning of the GPS week. The relation between Ω and Ω_o is given by:

$$\Omega_o = \Omega - GAST_{week} \qquad (4.4)$$

where $GAST_{week}$ is the Greenwich Apparent Sidereal Time at the beginning of the GPS week. For the purpose of this simulation, GAST can be replaced by GMST (Greenwich Mean Sidereal Time) which is given by the Astronomical Almanac (1990) in units of hours:

$$GMST = 6.6265313 + 0.065709824\ d + 1.00273791\ t \qquad (4.5)$$

where d is the day of the year 1990, and t is the time of the day in hours. For the epoch 00:00:00 of day 364 of 1990, this equation yields in units of degrees:

$$GMST = 98.1736°. \qquad (4.6)$$

With equations (4.3), (4.4), and (4.6) we obtain finally the broadcast Ω_o for the simulation epoch:

$$\Omega_o = \Omega - 15.5926° - 98.1736° \qquad (4.7)$$

The resulting broadcast ephemerides for the 24 GPS satellites are listed in Appendix 1. The pseudo random noise (PRN) numbers assigned to the GPS satellites are 1 through 24.

4.1.1.2 GLONASS Ephemerides

The full GLONASS constellation used in this study is described by P.Daly [6]. The 24 GPS satellites are regularly spaced in three orbital planes with 64.8° inclination, separated by 120° in longitude of the ascending node. The orbits are nominally circular at an altitude of 25,507. km which leads to an orbital period of 675.73 minutes. The ephemerides are given in terms of Keplerian elements **semi-major axis a, inclination i, right ascension of the ascending node Ω** and **mean anomaly M** for the epoch 00:00:00 of September 7, 1987, which is day number 250 of 1987.

As for the GPS constellation, the ephemerides must be extrapolated to the simulation epoch on day number 364 of the year 1990. The semi-major axis and the inclination are assumed to be constant. The mean anomaly of the nominal orbits is extrapolated using the mean motion defined by:

$$dM/dt = 2\pi \ / \ 675.73 \text{ minutes} = 0.1549728 \cdot 10^{-2} \text{ rad/sec.} \qquad (4.8)$$

This mean motion yields a phase shift of 196.06° for the mean anomaly between the ephemerides epoch in [6] and the ephemerides epoch for this simulation study.

$$M\ (00{:}00{:}00,\ \text{day } 364,\ 1990) = M\ (00{:}00{:}00,\ \text{day } 250,\ 1987) + 196.06° \qquad (4.9)$$

The change in right ascension of the ascending node is computed from equation (4.2) for the nominal GLONASS constellation and amounts to $-6.102 \cdot 10^{-9}$ rad/sec, yielding a change in right ascension of -35.1906° for day 364 of 1990 according to:

$$\Omega\ (\text{day } 364,\ 1990) = \Omega\ (\text{day } 250,\ 1987) - 35.1906°. \qquad (4.10)$$

As discussed in the previous section, GAST must be subtracted from the right ascension to obtain the value Ω_0 transmitted in the GPS broadcast message. With equations (4.3), (4.4) and (4.10) we obtain the broadcast Ω_0 for the simulation epoch:

$$\Omega_0 = \Omega - 35.1906° - 98.1736° \qquad (4.11)$$

The resulting broadcast ephemerides file for the 24 GLONASS satellites is listed in Appendix 2. The PRN numbers assigned to the GLONASS satellites are 25 through 48.

4.1.1.3 Geostationary Satellite Ephemeris

By definition, a geostationary satellite is in an equatorial orbit (i.e. inclination = 0) with a radius of about 42,000 km. It's elevation and azimuth does not change in time for a fixed receiver location. Since the geostationary satellite to be used in this study is of fictional nature only, we are free to select its position to ensure for the areas of interest a high satellite elevation angle.

The satellite elevation depends primarily on the spherical distance between the receiver position and the satellite footpoint at the equator as shown in Figure 4.1. In general, if the spherical distance, S, increases, the elevation angle, E, will decrease. In order to maximize the elevation angle of the geostationary satellite as seen from different areas of interest, the corresponding spherical distances must be minimized.

The relation between spherical distances and spherical coordinates ϕ, λ is shown in Figure 4.2. To yield maximum satellite elevation at the U.S. East Coast (Washington, D.C., ϕ39°, λ-77°) and in Alaska (Anchorage, ϕ61°, λ-150°), the fictional geostationary satellite is placed at a longitude λ=-130°. This satellite position results in spherical distances of 62° for both locations, yielding a maximum satellite elevation angle of 19°.

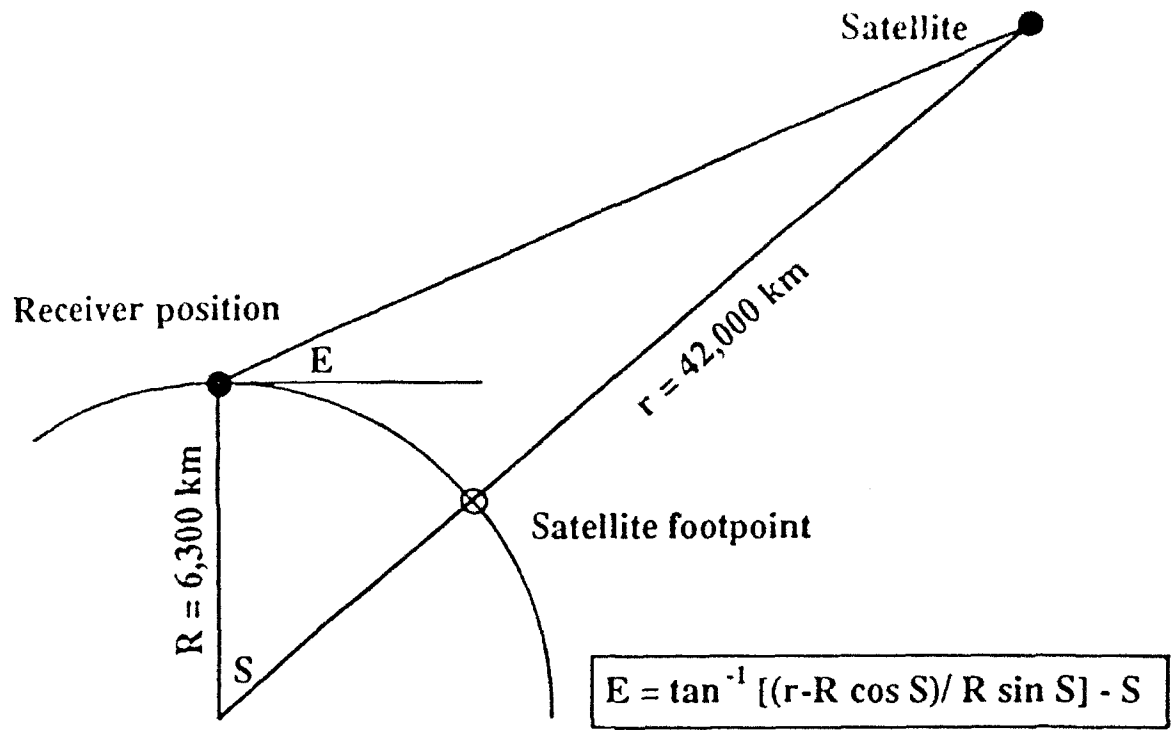

Figure 4.1: Satellite elevation as function of spherical distance between receiver and satellite

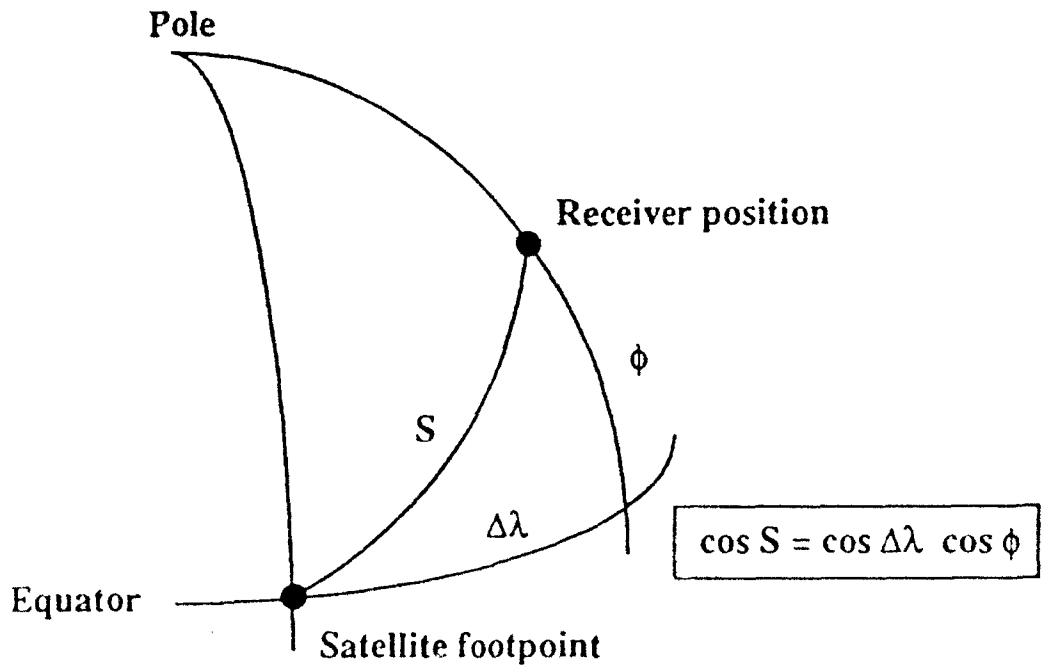

Figure 4.2: Spherical distance between receiver and Geostationary satellite

The ephemerides file (broadcast GPS ephemerides format) for the nominal orbit of a geostationary satellite is of particular simple structure. The inclination is zero by definition, and the mean anomaly cannot be seperated from the right ascension. The only remaining non-zero elements are the right ascension of the ascending node and the semi-major axis of the orbit. Since the broadcast Ω_0 is the right ascension referred to the zero meridian at the beginning of the GPS week, it is identical to the longitude of the ascending node at the beginning of the GPS week. This longitude has been selected above to maximize the satellite elevation angle. Thus we have:

$$\Omega_0 = -130.00°. \tag{4.12}$$

The semi-major axis, a, of a Keplerian satellite orbit can be computed from the orbital period, T, and the gravitational constant, μ, using Kepler's third law:

$$a^3 = T^2 \cdot \mu / (4 \pi^2). \tag{4.13}$$

With $\mu = 3.986008 \cdot 10^{14}$ m^3/sec^2 and $T = 86400$ sec, we obtain from equation (4.13) for the semi-major axis of a geostationary satellite:

$$a = 42,241 \text{ km}. \tag{4.14}$$

The resulting broadcast ephemerides file for the geostationary satellite is listed in Appendix 3. The PRN number assigned to the geostationary satellite is 25.

4.1.2 Receiver Position Consideration

The coordinates of the monitor station and the moving vessel need to be known for the generation of the simulated GPS measurements. Whereas the monitor station coordinates are time invariant, a new position has to be supplied for the moving receiver for every measurement epoch.

4.1.2.1 Monitor Station

The ellipsoidal (geodetic) coordinates longitude, latitude and height of the monitor station are considered to be known with sufficient accuracy. No attempt is made to include models for differential positioning errors resulting from inaccurate monitor station coordinates.

4.1.2.2 Remote Station

For the generation of simulated measurements, a time series of positions of the moving receiver has to be supplied. For the present simulation, this position time series should adequately represent the motion of a dredging vessel. The following equations have been used to generate horizontal coordinates latitude ϕ and longitude λ for the moving receiver:

$$\phi(t_i) = \phi_0 + \Delta\phi(t_i) / R \tag{4.15}$$

$$\lambda(t_i) = \lambda_0 + \Delta\lambda(t_i) / (R \cos\hat{}V\phi(t_i)). \tag{4.16}$$

The initial position (ϕ_0, λ_0) in relation to the coordinates of the monitor station determines the separation between monitor station and user receiver for a particular simulation run. The changes in horizontal coordinates (units of meters) are computed from:

$$\Delta\phi(t_i) = \Delta\phi(t_{i-1}) + v(t_i) \cdot \cos A(t_i) \tag{4.17}$$

$$\Delta\lambda(t_i) = \Delta\lambda(t_{i-1}) + v(t_i) \cdot \sin A(t_i) \tag{4.18}$$

in terms of a continuously changing vessel speed, $v(t_i)$, and a continuously changing vessel heading, $A(t_i)$. Both, speed and azimuth are based on an average value and a series of harmonic variations according to:

$$v(t_i) = v_0 + \sum_{j=1}^{6} v_j \cdot \cos\,(v_j \Delta t_i + \mu_j) \tag{4.19}$$

$$A(t_i) = A_0 + \sum_{j=1}^{3} A_j \cdot \cos(\gamma_j \Delta t_i + \delta_j) \tag{4.20}$$

with: $\Delta t_i = t_i - t_0$. The mean values chosen are:

$$v_0 = 1 \text{ m/sec} \tag{4.21}$$

$$A_0 = 45^\circ \tag{4.22}$$

and the amplitudes, frequencies, and initial phases of the harmonic variations are given by:

$$v_j = (0.055,\ 0.050,\ 0.045,\ 0.040,\ 0.035,\ 0.030) \text{ m/sec} \tag{4.23}$$
$$v_j = (2\pi/10,\ 2\pi/13,\ 2\pi/17,\ 2\pi/23,\ 2\pi/31,\ 2\pi/36) \tag{4.24}$$
$$\mu_j = (20.0\pi,\ 16.9\pi,\ 14.1\pi,\ 11.3\pi,\ 9.0\pi,\ 8.3\pi) \tag{4.25}$$
$$A_j = (8^\circ,\ 7^\circ,\ 20^\circ) \tag{4.26}$$
$$\gamma_j = (2\pi/19,\ 2\pi/37,\ 2\pi/330) \tag{4.27}$$
$$\delta_j = (0.0,\ 16.2\pi,\ 1.2\pi). \tag{4.28}$$

The horizontal components of the vessel trajectory contain constituents of frequencies between 0.1 Hz and 0.0003 Hz. The deviations of the resulting latitude and longitude coordinates from a mean straight line motion (45 degrees of azimuth) is shown in Figure 4.3. The detailed horizontal position variations in the first two minutes of the simulation interval ($0 \le t_i \le 120$ sec) are shown in Figure 4.4.

The vertical motion of the vessel is considered to consist of an initial height, h_0, and a time varying part, $Dh(t_i)$, according to:

$$h(t_i) = h_0 + \Delta h(t_i). \tag{4.29}$$

The time varying part consists of a linear trend and a series of harmonic constituents to simulate tidal variations (linear over half an hour) and more or less periodic height variations due to swell and waves. It is computed

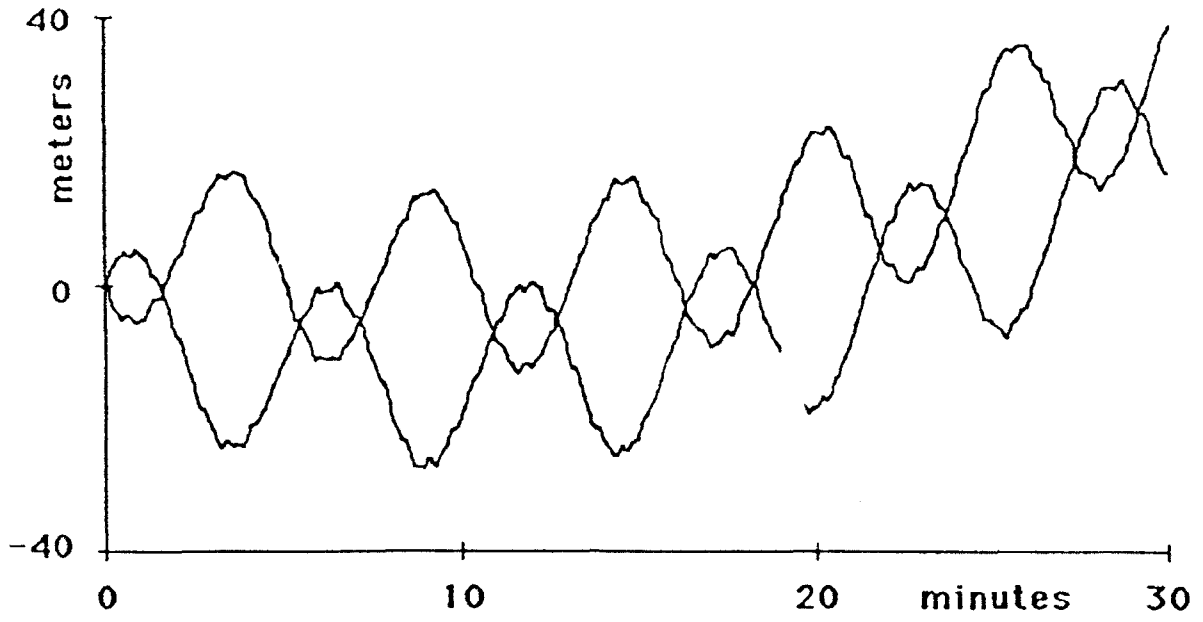

Figure 4.3: Horizontal coordinate deviation of simulated vessel motion from straight line motion for total simulation interval

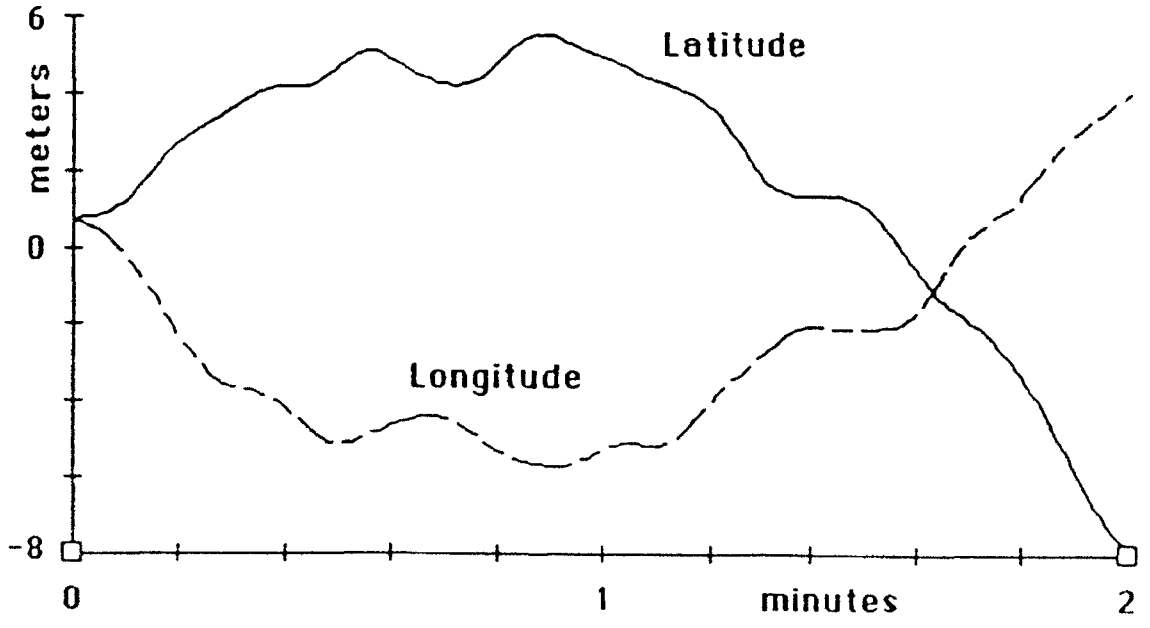

Figure 4.4: Horizontal coordinate deviation of simulated vessel motion from straight line motion for first two minutes

from:

$$\Delta h\ (t_i) = \alpha \cdot \Delta t_i + \sum_{j=1}^{6} h_j \cdot \cos(\psi_j\ \Delta t_i + \xi_j) \qquad (4.30)$$

with

$$\alpha = 0.5\ \text{m} / 3600\ \text{sec} \qquad (4.31)$$

$$h_j = (0.11,\ 0.10,\ 0.09,\ 0.08,\ 0.07,\ 0.06)\ \text{m} \qquad (4.32)$$

$$\psi_j = (2\pi/10,\ 2\pi/13,\ 2\pi/17,\ 2\pi/23,\ 2\pi/31,\ 2\pi/36) \qquad (4.33)$$

$$\xi_j = (20.0\pi,\ 16.9\pi,\ 14.1\pi,\ 11.3\pi,\ 9.0\pi,\ 8.3\pi) \qquad (4.34)$$

The linear term accounts for a height change of 0.5 meters over a time of 1 hour, and the harmonic constituents generate maximum vertical motion amplitudes of 0.5 meters. The periods of the vertical motion range from 10 second to 36 seconds. The total vertical motion profile is shown in Figure 4.5. The detailed vertical position variation in the first two minutes of the simulation time interval is depicted in Figure 4.6.

A data file containing three dimensional position coordinate changes $\Delta h(t_i)$, $\Delta\phi(t_i)$, $\Delta\lambda(t_i)$ at one second intervals for a total time span of one half hour is input to the GPS measurement simulation software.

4.1.3 Measurement Errors

GPS measurements pseudorange, P, and carrier phase, F, can be represented by:

$$P = \rho + dp \qquad (4.35)$$

$$\Phi = \rho + d_\phi \qquad (4.36)$$

where:

$$\rho = \| r - R \| \qquad (4.37)$$

is the geometric distance between the satellite antenna position vector, r, at signal transmission time (as represented by the satellite ephemerides) and the (unknown) receiver antenna position vector, R, at signal reception time. The terms d_p and d_ϕ represent errors and biases in the measurements and consist of

$$dp = d\rho + d_{ion} + d_{trop} + c\cdot(dt - dT) + A_c + \eta_c + \varepsilon_p \qquad (4.38)$$

$$d_\phi = d\rho - d_{ion} + d_{trop} + c\cdot(dt - dT) + A + \eta + \varepsilon_\phi \qquad (4.39)$$

where:

- $d\rho$ is the range error resulting from satellite ephemerides errors,
- d_{ion} is the range error caused by (dispersive) ionospheric signal delay,
- d_{trop} is the range error caused by tropospheric signal delay,
- c is the speed of light in vacuum,
- $c\cdot dt$ is the range error caused by the satellite clock error,
- $c\cdot dT$ is the range error caused by the receiver clock error,
- A_c is the code ambiguity,
- A is the carrier phase ambiguity,
- η_c is the range error caused by code signal multipath,
- η is the range error caused by carrier signal multipath,

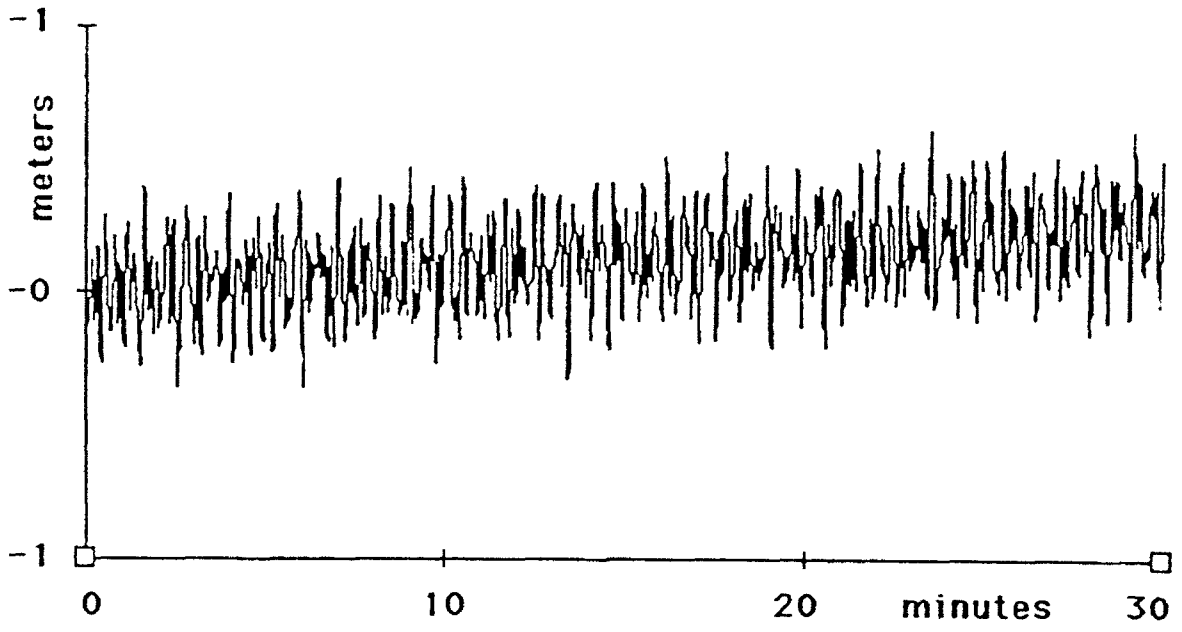

Figure 4.5: Simulated vertical vessel motion for total simulation interval

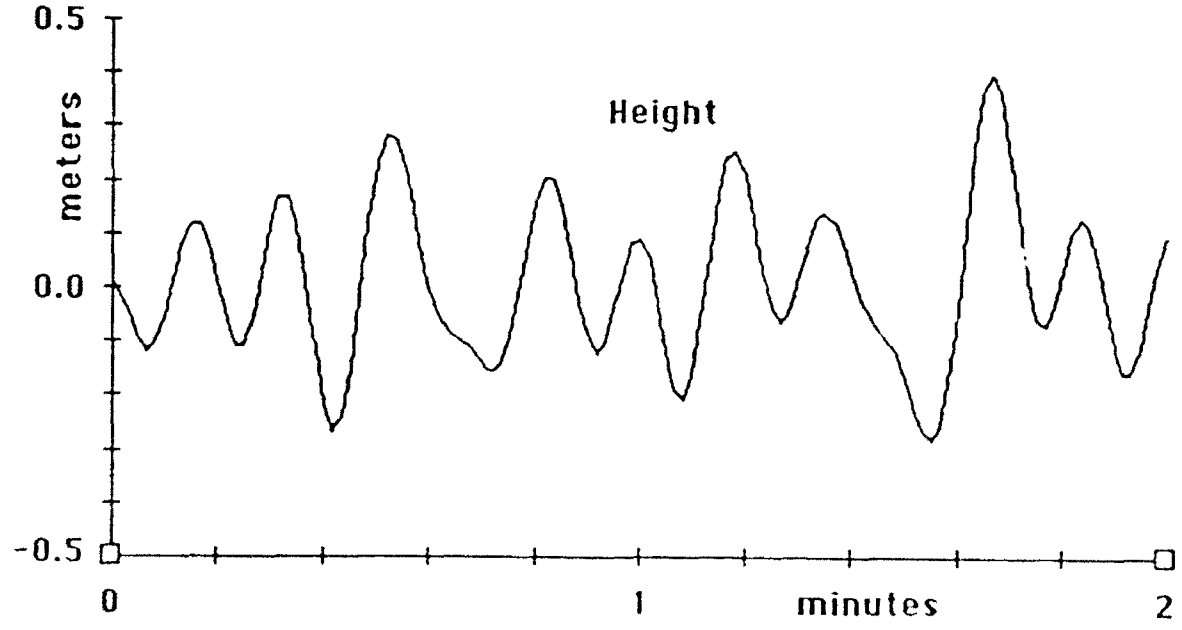

Figure 4.6: Simulated vertical vessel motion for first two minutes

and $\varepsilon_p, \varepsilon_\phi$ are the range errors in pseudoranges and carrier phases caused by measurement noise. For a realistic simulation study, the simulated GPS measurements must be contaminated by artificially generated errors. The following sections discuss the significance of the individual errors and their generation term by term.

4.1.3.1 Satellite Ephemeris Errors

Broadcast satellite ephemerides errors result from imperfections in the prediction process of the satellite orbits. The size of these errors has been assessed recently in [4-12] by comparing Broadcast Ephemerides with the more accurate Precise Ephemerides. This comparison does not yield the actual broadcast ephemerides errors, but it tells us about the order of magnitude of these errors. The authors of the aforementioned study concluded, that the maximum broadcast ephemerides errors for GPS satellites with Cesium clocks (which will be assumed for this study) were of the order of five meters in the along-track component, three meters in cross-track direction and two meters in radial direction. These results were obtained when ephemerides were uploaded three times per day. For the present study, we take the pessimistic view to use these numbers as standard deviations for the broadcast ephemerides errors. The errors are taken to be constant during the simulation time interval.

The geometric pseudorange and carrier phase measurements are based on the true satellite position $\mathbf{r}_{true}$, which is computed according to:

$$\mathbf{r}_{true} = \mathbf{r} + d\mathbf{r} \tag{4.40}$$

with $\mathbf{r}$ being the satellite position from the ephemeris file. The ephemeris error is calculated according to:

$$d\mathbf{r} = R(0,\ 5\ m)\cdot\mathbf{e}_{along} + R(0,\ 3\ m)\cdot\mathbf{e}_{cross} + R(0,\ 2\ m)\cdot\mathbf{e}_{radial} \tag{4.41}$$

where: $R(\alpha, \beta)$ is a normal distribution random number with mean α and standard deviation β. $\mathbf{e}_{along}$, $\mathbf{e}_{cross}$ and $\mathbf{e}_{radial}$ are unit vectors pointing in along-track, cross-track and radial direction respectively. The resulting ephemerides errors are constant for a particular satellite during the simulation interval, but are different from satellite to satellite. These ephemerides errors do not include the orbital error caused by S/A, see section 4.1.3.11.

4.1.3.2 Satellite Clock Errors

The position determination program described in section 3 of this report is based on the analysis of double differences of both pseudorange and carrier phase measurements. In this type of processing, the satellite clock error is effectively eliminated if the measurements at the monitor station and the remote receiver are collected simultaneously. Therefore, the inclusion of simulated satellite clock errors in the present study is not necessary.

4.1.3.3 Ionospheric Dispersive Refraction

The range error caused by the interaction of the GPS signal with the ionosphere depends on the total electron content, TEC, along the path of the GPS signal and the frequency of the carrier signal, f, according to:

$$d_{ion} \approx 40.3 \frac{m^3}{sec^2} \cdot \frac{TEC}{f^2} \qquad (4.43)$$

TEC depends on the electron distribution in the atmosphere, which not only changes with diurnal, annual and solar (11 year) cycles, but is also subject to short periodic variations. The high frequency variations are of concern for signal tracking, and the correction of carrier phase discontinuities [4-4]. Their effect on positions tends to average out in time. Short periodic variations in the ionosphere will not be further discussed in this study. The slowly varying part of the TEC has been shown to lead to biases in the estimated positions [4-6] and is more relevant as far as differential position accuracy is concerned.

To generate range errors due to a slowly varying ionosphere, we consider the following simplified model for the ionosphere [4-4]. The ionosphere is represented by a thin spherical layer at a fixed altitude with a surface density equal to the total vertical electron content, VEC. This surface density is spatially constant, and does not change for the measurement simulation time span. From Figure 4.7 we see, that in this model for a particular GPS signal, the relation between TEC and VEC is

$$TEC = \frac{VEC}{\cos z'} \qquad (4.43)$$

where z' is the zenith angle of the GPS signal at the ionospheric layer. z' can be related to the zenith angle at the surface of the earth, z, through:

$$\sin z' = \frac{R}{R+H} \sin z. \qquad (4.44)$$

Equations (4.42) through (4.44) allow the simulation of ionospheric delay errors, if the height of the ionospheric layer, H, and VEC are specified. Typically, altitudes between 300 and 400 km are chosen for an ionospheric surface layer model. For this study, we shall use H = 350 km. The vertical electron density varies between $1 \cdot 10^{16}$ m^{-2} and $2 \cdot 10^{18}$ m^{-2} depending on solar activity and season of the year [11]. We shall use VEC = $0.5 \cdot 10^{18}$ m^{-2} for our study, which yields an ionospheric range error of about 9 meters for a vertical incident GPS signal and 22 meters range error for a signal at 15° elevation.

Some GPS receivers allow for the measurement of the ionospheric delay difference between the two GPS signals by cross correlating the P-code bit structures on L1 and L2. The measurement can be used to correct single frequency C/A-code pseudoranges for ionospheric delay.

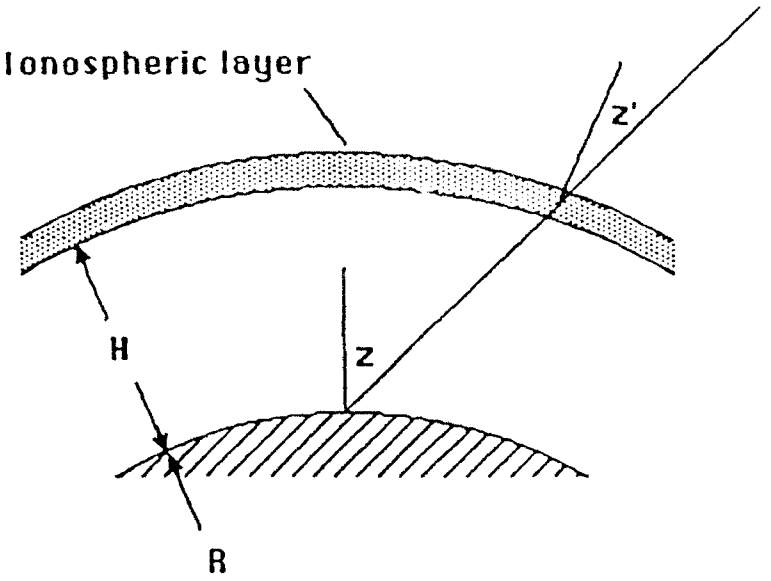

Figure 4.7: Geometry of ionospheric layer and signal propagation path

4.1.3.4 Tropospheric Effects

Tropospheric delay is caused by the lower non-dispersive part of the atmosphere. It can be modelled exactly, if the atmospheric pressure, the atmospheric temperature and the humidity are known along the signal path. Since these quantities can not be measured directly along the signal path, they are approximated be an external model for the vertical profile of the atmosphere, driven by surface meteorological data.

The total tropospheric delay is usually separated in the "dry" delay part and the "wet" delay part. The dry delay depends on pressure and temperature only and amounts to about 2 meters in the zenith direction. It can be very accurately determined from surface meteorological data. The wet delay depends also on the atmospheric humidity and amounts to about 0.3 meters in the zenith direction. Its relative accuracy as determined from surface met, data is not as high as for the dry component, primarily because of irregularities in the vertical humidity profile.

The accuracy of the vertical tropospheric delay as calculated from surface pressure, temperature and humidity is of the order of up to a few centimeters. Its variations over time depend on local weather conditions and cannot be easily and realistically modelled in a simulation. Tropospheric delay is not included in this simulation study.

4.1.3.5 Receiver Clock Error

The double difference processing of pseudoranges and carrier phases in the position determination program eliminates receiver clock error completely if the measurements to different satellites are referenced to the same receiver time tag. This is the case in all relevant types of presently available GPS receivers. Therefore, the inclusion of simulated receiver clock errors in the present study is not necessary.

4.1.3.6 Code Ambiguity

GPS pseudoranges are measured by aligning codes transmitted on the carrier signal with similar codes generated in the GPS receiver. For P-code pseudoranges, this alignment can be done unambiguously. For C/A-code pseudoranges, the code ambiguity in the measured pseudoranges equals an integer multiple of the C/A-code length of 1.10^{-3} sec, which is equivalent to about 300 km. This ambiguity can easily be resolved and needs no further investigation or simulation in the present study.

Codeless pseudoranging utilizes the structure of the code only and not the code itself. If pseudoranges are measured codelessly, their ambiguity is equal to an integer multiple of the code chip length. Since codeless pseudoranging makes sense only with the P-code (C/A-code is freely available), the ambiguity in codeless pseudoranging is a multiple of the P-code chip length of about 30 meters. This ambiguity can be easily resolved using conventional C/A-code pseudoranges, and will not be further investigated or simulated in this study.

4.1.3.7 Carrier Cycle Ambiguity

The carrier phase ambiguity, A, is a constant integer multiple N of the carrier wave length λ for code tracking receiver channels, and an integer multiple of half the carrier wave length for codeless tracking receiver channels.

$$A = N \cdot \lambda, \quad A = N \cdot \lambda/2 \tag{4.45}$$

The correct resolution of the carrier phase ambiguity is of utmost importance in the present study. To enable an easy assessment of the correct carrier phase ambiguity resolution in the position determination software, all simulated carrier phase measurements are generated with a unique ambiguity

$$A = PRN \cdot 1000 \cdot \lambda, \quad A = PRN \cdot 1000 \cdot \lambda/2 \tag{4.46}$$

for code tracking and codeless tracking receiver channels. PRN is the satellite's pseudo random noise number.

4.1.3.8 Carrier Cycle Slips

Carrier cycle slips are changes in the carrier phase ambiguity by an integer number of carrier wave lengths (half wave lengths for codeless tracking channels). They are induced by a temporary loss of lock of the receiver channel. To retain the full accuracy potential of carrier phase measurements, cycle slips must be detected and corrected. The detection of cycle slips can be achieved by a variety of procedures, and will not be dealt with in this study.

The occurrence of cycle slips can lead to three different situations, depending on how many channels retain lock to the GPS signals. If loss of lock occurs on all channels simultaneously and no inertial system is used, or the loss of lock lasts longer than INS can maintain the phase ambiguity, all carrier phase ambiguities have to be reestablished in the same way as at the beginning of a survey. This case does not require a separate simulation. The use of an inertial system to bridge periods of loss of lock to the GPS signals is evaluated in Section 5. Generally, if lock is retained for at least four channels and Perpendicular Dilusion of Precision (PDOP) is reasonable, instantaneous cycle slip fixing for the other channels is trivial (enough instantaneous redundancy in the measurements). Again, this case does not require simulation studies.

In the third category, lock is maintained for less than four channels, and at least for one channel. In this case, cycle slip correction is not trivial and needs simulation in the context of this study. Obviously, the problem of determining these cycle slips is identical to determining carrier phase ambiguities, with some of the carrier phase ambiguities fixed already. In this study, cycle slip recovery is simulated assuming two double difference ambiguities (lock maintained on three satellites) are fixed at their proper integer values, and all other carrier phase ambiguities are completely unknown.

4.1.3.9 Multipath

Multipath errors result from the interference of signals which have travelled along signal paths of different length. Usually, one of the signals is travelling along the line of sight, and the other components result from reflections at conducting material in the vicinity of the GPS antenna. The changing geometry between satellite, reflectors and antenna generates cyclic multipath errors. The amplitudes, phases and frequencies of these errors depend on a number of factors like:

- conductivity of the reflecting material,
- shape of the reflecting material,
- distance from the reflecting material,
- geometry between satellite, reflector and antenna,
- antenna sensitivity pattern,
- wave length (chip length) of signal.

A complete model containing these parameters is rather complicated and beyond the scope of this report. For the present study, the following simplified multipath error model is assumed:

$$\eta = D \cdot \cos(vt + \omega) \tag{4.47}$$

where: D is the multipath error amplitude, n is the multipath error frequency and ω is the multipath error initial phase. The parameters adopted for the present study are:

D - R(0, 3.0 m) for C/A-code pseudoranges.
D - R(0, 0.5 m) for P-code pseudoranges.
D - R(0, 1 cm) for carrier phases.
v - $2\pi/300$ seconds (period of five minutes).
ω - $2\pi \cdot 0.0112 \cdot$ PRN for L1 pseudoranges.
ω - $2\pi \cdot 0.0173 \cdot$ PRN for L2 pseudoranges.
ω - $2\pi \cdot 0.0133 \cdot$ PRN for L1 carrier phases.
ω - $2\pi \cdot 0.0194 \cdot$ PRN for L2 carrier phases.

Obviously, these parameters together with equation (4.47) model multipath errors as simple cosine waves with five minute periods, and with different initial phases for individual satellites. No multipath model is employed for measurements of differential ionospheric group delays as referenced in section 4.1.3.3. This somewhat optimistic assumption can be better understood as more field experience is gained with cross-correlating receivers operating in a dynamic environment.

4.1.3.10 Measurement Noise

All GPS measurements are contaminated by noise resulting from the tracking loop inaccuracies and other limitations. This measurement noise will be different in size frequency distribution for different receivers. For the purpose of this study, we will assume the measurement noise to be a normal distribution white noise with zero mean. For pseudoranges measured with code tracking and codeless tracking receiver channels, the standard deviation of the noise is chosen to be one percent of the chip length of the code [4-16]. These numbers may appear large when compared with the accuracies quoted by GPS

receiver manufacturers, since the instantaneous code measurements are often averaged over limited time periods for output.

$$\varepsilon_p = R(0,\ 0.3\ m),\ \text{for P-code pseudoranges} \tag{4.48}$$

$$\varepsilon_p = R(0,\ 3\ m),\ \text{for C/A-code pseudoranges} \tag{4.49}$$

For measurements of differential ionospheric group delays from P-code cross correlation, we assume the same noise level as for P-code pseudoranges. For carrier phase measurements, the noise level is of the order of about half a centimeter for a code tracking receiver channel, and a few centimeters for a codeless tracking receiver. For this study, the simulated carrier phase measurements will be contaminated by measurement noise according to:

$$\varepsilon_\phi = R(0,\ 0.5\ cm),\ \text{for code tracking receivers} \tag{4.50}$$

and

$$\varepsilon_\phi = R(0,\ 2\ cm),\ \text{for codeless tracking receivers.} \tag{4.51}$$

4.1.3.11 Selective Availability

S/A is the intentional degradation of the GPS capability to a level of about 100 meters horizontal position accuracy. Assuming a horizontal dilution of precision (HDOP) between 3 and 5, the range measurement errors required to achieve this level of S/A are of the order of 20 to 30 meters. These range errors can be introduced in two different procedures. The first procedure is to introduce satellite clock errors yielding the appropriate range error level. This type of S/A error is eliminated in relative positioning using double differences of pseudoranges and/or carrier phases. Therefore, this S/A error will not be simulated in this study.

The second type of S/A errors is caused by changing the satellite ephemerides. This type of S/A error does not completely cancel in relative positioning and needs to be investigated. To assess the impact on relative positioning, the ephemerides errors (c.f. section 4.1.3.1) in the simulated measurements are changed from equation (4.41) to a level of 20 meters in all three directions.

$$dr = R(0,\ 20\ m)\cdot e_{along} + R(0,\ 20\ m)\cdot e_{cross} + R(0,\ 20\ m)\cdot e_{radial} \tag{4.52}$$

4.1.4 Simulation Program Operation

The simulation program performs the following steps for each simulation run:

- Read simulation parameters from command file.
- Do Chebychev polynomial approximation for satellite orbits (computation speed!).
- Check visibility of satellites for each simulation epoch.
- Read time tag and remote receiver position from file.
- Compute satellite coordinates for all visible satellites at signal transmission times.
- Add epemerides error to computed satellite position.

- Compute geometric range between satellites and monitor station, and satellite and remote station.
- Add ionospheric delay for pseudoranges.
- Subtract ionospheric delay for carrier phases.
- Add multipath errors for both pseudoranges and carrier phases.
- Add ambiguity terms to carrier phases.
- Add noise to both carrier phases and pseudoranges.
- Form single differences (between monitor and remote station).
- Form double differences (between satellites).
- Write simulated measurements (double differences of pseudoranges and carrier phases) and satellite coordinates to output file.

4.2 Position Determination Program

This section describes the models behind a computer program for the computation of a time series of differential positions and a corresponding time series of carrier phase ambiguity estimates. In the present context, the main purpose of this program is to determine the integer values of the carrier phase ambiguities. The following steps are executed in each run of the position determination program:

- Read instructions from command file.

- Open files and initialize remote receiver position with a standard deviation of ± 1,000 km. This is replaced after the last epoch by the result of pseudorange positioning.

- For each measurement epoch:

- Read one record of simulated data (satellite coordinates, double differences of pseudoranges and carrier phases).
- Form linearized observation equations.
- Combine with information retained from previous epoch.
- Solve for remote receiver position and carrier phase double difference ambiguities.
- If real number estimate for ambiguities allows proper determination of integers, fix the ambiguity.

4.2.1 Observation Models

The measurements utilized in the position determination program are double differences of pseudoranges and carrier phases. As mentioned above, these double differences are assumed free of satellite and receiver clock errors. We obtain from the observation equations for pseudoranges and carrier phases (c.f. section 4.1.3)

$$\nabla\Delta P = \nabla\Delta\rho + \nabla\Delta(d\rho + d_{ion} + d_{trop} + A_c + \eta_c) + \nabla\Delta\varepsilon_{\|} \qquad (4.53)$$

$$\nabla\Delta\Phi = \nabla\Delta\rho + \nabla\Delta(d\rho - d_{ion} + d_{trop} + A + \eta) + \nabla\Delta\varepsilon_{\Phi} \qquad (4.54)$$

where $\nabla\Delta$ designates the double difference operator. The position information of the measurements is contained in the double difference of the geometric range, $\nabla\Delta\rho$. Because of positive spatial correlation, the double differences of range errors caused by satellite ephemerides errors, $\nabla\Delta d\rho$, and caused by

ionospheric refraction, $\nabla\Delta d_{ion}$, are greatly reduced compared with the corresponding undifferenced values. On the other hand, those errors that are uncorrelated between satellites and receivers, are increased by a factor of two (there are four measurements combined in a double difference). Usually, this will be the case for multipath induced errors, and for the measurement noise.

4.2.1.1 Pseudoranges

Pseudoranges obtained from C/A-code correlation contain an ambiguity equal to an integer multiple of the code length. As mentioned above, the determination of this ambiguity is trivial and will not be further discussed here. ($A_c = 0$). Therefore, the model for both C/A-code and P-code pseudorange double differences reads:

$$\nabla\Delta P = \nabla\Delta\rho + \nabla\Delta\varepsilon_{\|}. \tag{4.55}$$

compared to equation (4.53), the meaning of the terms in equation (4.54) has been changed in the following manner: The observation double difference on the left hand side is corrected for all correctable errors, and the error term on the right hand side contains all those errors that cannot be explicitly corrected.

4.2.1.2 Carrier Phases

Replacing the carrier phase ambiguity term by an integer multiple of the carrier wavelength according to:

$$\nabla\Delta A = \lambda\nabla\Delta N, \tag{4.56}$$

we obtain the observation model for double difference carrier phase measurements:

$$\nabla\Delta\Phi = \nabla\Delta\rho + \lambda\nabla\Delta N + \nabla\Delta\varepsilon_{\phi}. \tag{4.57}$$

4.2.2 Adjustment Model

Equations (4.55) and (4.57) are the basic non-linear description of the measurements pseudoranges and carrier phases (on the left hand side) in terms of unknown parameters (on the right). The unknown parameters are the remote receiver coordinates (hidden in the double difference of geometric ranges, $\nabla\Delta\rho$), the double difference of carrier phase ambiguities $\nabla\Delta N$, and the unmodelled residual carrier pseudorange and carrier phase errors, $\nabla\Delta\varepsilon_{\|}$ and $\nabla\Delta\varepsilon_{\phi}$ respectively. The solution of theses equations in a least squares sense consists of the following steps:

- Linearization with respect to receiver coordinates (to enable the use of matrix calculus in the solution process).
- Forming a linear system of equations based on the least squares principle, i.e. requiring the weighted sum of the estimated residuals to attain a minimum.
- Inverting the linear equation system to obtain an explicit solution for receiver coordinates and carrier phase ambiguities.

All calculations are being done in cartesian coordinates in a geocentric earth-fixed coordinate system. Input and output of the position determination program are in geodetic (ellipsoidal) coordinates.

4.2.2.1 Linearized Observation Equations

The geometric range between satellite and receiver is a non-linear function of satellite and receiver coordinates according to:

$$r = || r - R || = \{(x - X)^2 + (y - Y)^2 + (z - Z)^2\}^{1/2} \quad (4.58)$$

where we have denoted the cartesian coordinates of the satellite by lower case letters and the coordinates of the receiver by upper case letters. Linearizing this equation with respect to receiver coordinates at the approximate position $R = R_o$ we obtain:

$$r = || r - R_o || + f(d,dR) \quad || r - R || \cdot dR \quad (4.59)$$

where $dR = R - R^\circ$ is the difference between the unknown true position and the known approximate position of the receiver. Squares and higher powers of dR have been neglected in equation (4.59). Denoting the partial derivatives of the range with respect to receiver coordinates by:

$$a_R = [(\Delta x/\rho) , (\Delta y/\rho) , (\Delta z/\rho)] \quad (4.60)$$

we obtain:

$$\rho = \rho^\circ + a_R \cdot dR \quad (4.61)$$

with the unknown coordinate increment:

$$dR = [dX, dY, dZ]^T. \quad (4.62)$$

Inserting equation (4.61) into the non-linear pseudorange observation equation (4.55) we get after re-arranging the terms:

$$\nabla\Delta P - \nabla\Delta P\nabla = (\nabla a_R) \cdot dR + \nabla\Delta\varepsilon p. \quad (4.63)$$

Since the coordinates of the monitor station are known (cf. section 4.1.2.1), no coordinate increment for the monitor station is included in this equation. For the same reason, only a single difference (between satellites) of the partial derivatives, $-a_R$, needs to be included.

For n pseudorange (code phase) double differences observed simultaneously we obtain from the previous equation:

$$l_p = A_R \cdot dR + e_p \quad (4.64)$$

where l_p is the (n,1) vector of reduced pseudorange measurements containing the quantities from the left hand side of equation (4.63), A_R is the (n,3) matrix of partial derivatives of the double difference measurements with respect to remote station coordinates (design matrix), and e_p is the (n,1) vector of unmodelled pseudorange errors.

Similarly, the n simultaneously observed reduced carrier phase double difference measurements can be organized according to:

$$l_\phi = A_R \cdot dR + A_N \cdot N + e_\phi . \tag{4.65}$$

The accuracy of the pseudorange and carrier phase double difference measurements is specified by defining appropriate covariance matrices C_p and C_ϕ. These matrices contain on the diagonal the variances of e_p and e_ϕ respectively, and the corresponding covariances in the off-diagonal elements. In our simulation study, all covariances were neglected.

If we have some a priori information N° about the carrier phase ambiguity unknowns or about the accuracy of the approximate coordinates used in the linearization process described above, we can write additional pseudo-observation equations:

$$N^\circ = N + e_N . \tag{4.66}$$

The pseudo-observation equation for approximate coordinates

$R^\circ = R + e_R$ can be re-arranged to read:

$$0 = dR + e_R \tag{4.67}$$

The a priori information is specified by defining appropriate covariance matrices C_N and C_R. These matrices contain the variances and covariances of e_p and e_ϕ respectively.

4.2.2.2 Combining Code and Carrier

Combining all observation equations (4.64) through (4.67) yield the following linear equation system:

$$L = A \cdot q + e \tag{4.68}$$

with the observation vector:

$$L = [\, l_p^T, \; l_\phi^T, \; N^{\circ T}, \; 0^T]^T , \tag{4.69}$$

the unknowns:

$$q = [\, dR^T, \; N^T]^T \tag{4.70}$$

and the design matrix:

$$A = \begin{bmatrix} A_R & 0 \\ A_R & A_N \\ 0 & I \\ I & 0 \end{bmatrix} \tag{4.71}$$

The least squares solution of (4.68) is given by:

$$q = (A^T C^{-1} A)^{-1} A^T C^{-1} L \tag{4.72}$$

with C being a block-diagonal matrix:

$$C = \text{diag}\ (C_p,\ C_\Phi,\ C_N,\ C_R). \tag{4.73}$$

In numerical applications, the special structure of the design matrix (4.71) with zero and identity sub-matrices is utilized for a reduction of the computational burden in the inversion according to equation (4.72). The expected accuracy of the determined parameters is given by:

$$C_q = (A^T C^{-1} A)^{-1} \tag{4.74}$$

i.e. the square roots of the diagonal elements of Cq are the estimated standard deviations of the errors of the parameters q. More information about the least squares procedure can be found in any textbook on least squares adjustment.

4.2.2.3 Parameter Transition Model

The a priori information on carrier phase ambiguities and approximate receiver coordinates is obtained from a parameter transition model. A parameter transition model describes how a parameter changes from epoch to epoch. Since carrier phase ambiguities are invariant in time, their parameter transition model is simple.

$$N_{t+1} = N_t \tag{4.75}$$

and if an estimate for N and its associated covariance matrix C_N exists from the previous epoch, it can be easily incorporated in the solution for the next epoch according to equation (4.66). The transition model for the moving receiver position has to be derived from the assumed dynamics model of the vessel in the particular environment (sea, state, etc.). Since a very general linear prediction model assuming constant velocity proved insufficient, and a more detailed model was seen to limit the usefulness of the parameter transition model to particular applications, the idea of a transition model for the receiver position was abandoned altogether. This, on the other hand, makes the position determination procedure independent of the dynamics of the receiver motion. It can be used without modification for any type of vehicle.

4.2.2.4 Wide-Laning

Wide-laning is a procedure to obtain from two carrier signals at different wave lengths a linear combination with a longer wave length and at the same time retaining the integer nature of the carrier ambiguity. For GPS carrier signals with wavelength λ_1 and λ_2 this particular combination is given by:

$$\Phi_w = (1/\lambda_1 - 1/\lambda_2)^{-1}\ [\Phi_1/\lambda_1 - \Phi_2/\lambda_2] \tag{4.76}$$

and

$\lambda_w = (1/\lambda_1 - 1/\lambda_2)^{-1}$ 86 cm is the wide lane signal wave length.

If the second frequency is observed with a squaring type of receiver, its effective wave length is only half of λ_2. In this case, the wide-lane

combination can be formed according to:

$$\Phi_W = (2/\lambda_2 - 1/\lambda_1)^{-1} [2\Phi_2/\lambda_2 - \Phi_1/\lambda_1] \quad (4.77)$$

and

$$\lambda_W = (2/\lambda_2 - 1/\lambda_1)^{-1} \approx 34 \text{ cm}$$

is the wide-lane signal wave length. Alternatively, the wide-lane can be formed:

$$\Phi_W = (2/\lambda_1 - 2/\lambda_2)^{-1} [2\Phi_1/\lambda_1 - 2\Phi_2/\lambda_2] \quad (4.78)$$

and:

$$\lambda_W = (2/\lambda_1 - 2/\lambda_2)^{-1} \approx 43 \text{ cm}.$$

The reason for wide-laning dual frequency carrier phase measurements is to use the effective longer wave length of the signal for ambiguity resolution. The non-zero elements of the design matrix A_N for ambiguities (cf. equation (4.65)) are filled with the effective wave length of the carrier signal. The larger this wave length is, the easier can the integer values of the carrier phase ambiguities N be determined in the solution (4.72) and (4.73). Obviously, all of the above wide-lane combinations have wave lengths larger than the single frequency GPS measurements.

The major drawbacks in wide-laning are increased measurement noise, and a slightly increased sensitivity to the ionosphere. If P-code pseudoranges are observed on both GPS signal frequencies, it is possible to find a particular linear combination of these pseudoranges that is the same way affected by the ionosphere as the 86 cm wide-lane combination of the carrier phases [40]. Using this particular pseudorange combination together with the 86 cm carrier wide lane allows an ambiguity resolution that is not adversely affected by ionospheric delays.

In a similar fashion, a C/A-code pseudorange and the differential ionospheric delay measured through cross correlation of the P-code bit structure can be combined into a pseudorange that is the same way affected by the ionosphere as the wide-lane carrier phase combination.

The effect of the ionosphere on single frequency C/A-code pseudoranges is different from the ionospheric delay in the 34 cm or 43 cm carrier phase wide-lane combinations. Therefore, the wide-lane ambiguity resolution through C/A-code pseudoranges will be hampered by ionospheric delay.

4.2.2.5 Ambiguity Resolution

Ambiguity resolution means that the integer value of the carrier phase double difference ambiguity term (either single frequency or wide lane) is determined. If this is possible, the ambiguity term N is not an unknown parameter anymore and can be removed from the adjustment procedure described above. After removing the ambiguities, GPS becomes effectively a carrier signal ranging system and individual kinematic positions can be determined with the accuracy of the carrier phase measurement. If the integer values of the ambiguities are determined incorrectly, all positions will be in error.

Therefore, the integrity of the ambiguity resolution procedure has to be guaranteed through appropriate measures.

For every measurement epoch, the least squares algorithm yields a real number estimate for the ambiguity, and an associated error standard deviation (the square root of the corresponding diagonal element of the covariance matrix). The following four criteria are used to decide on the quality of the ambiguity resolution. The ambiguity is fixed if:

- the real number ambiguity estimate is within ±0.25 cycle of an integer,
- the estimated error standard deviation of the real number ambiguity estimate is less than 0.1 cycle,
- the scaled estimated error standard deviation of the real number ambiguity estimate is less than 0.1 cycle and
- the difference between the real number estimate and the nearest integer is within three times the estimated and scaled error standard deviation for the real number ambiguity estimate.

Obviously, the first criterion ensures that only real number estimates close to integers are considered for ambiguity fixing. The second criterion ensures that the nearest integer is the only possible integer for ambiguity fixing. The third criterion needs a longer explanation. The estimated standard deviation of the real number estimates is based on the covariance matrix used to describe the stochastic model for the measurements. Since the measurement covariance matrix described above does not account for temporal correlations, the estimated error standard deviation of the real number ambiguity estimate is based on uncorrelated input data. On the other hand, the error model for multipath described in section 4.1.3.9 introduces strong positive temporal correlation into the measurement errors. Neglecting these correlations yields overly optimistic ambiguity error standard deviations. A simple procedure has been derived to correct this problem. It can be shown, that for uncorrelated input the least squares ambiguity estimate accuracy is roughly inversely proportional to the square root of the number of measurement epochs processed. It also can be shown, that for errors with sinusoidal components with typical periods, T, the least squares ambiguity estimate accuracy is roughly inversely proportional to the angular frequency $2\pi/T$ times elapsed time. Based on these findings, the estimated error standard deviations were scaled by multiplying them with:

$$\text{scale} = \frac{T\sqrt{n}}{2\pi t} \tag{4.79}$$

where n is the number of measurement epochs since lock on, and t is the elapsed time since lock on. In this study the measurement rate is 1 Hz, and the multipath period is 5 minutes. With these numbers, the scale factor is greater than 1 for elapsed time less than one half hour. This simple scaling restores to a great extent the effect of the neglected temporal correlations. The fourth criterion listed above ensures that the real number estimate of the ambiguity, its error standard deviation, and the nearest integer are compatible. Once all ambiguities are determined and fixed to integers, the task of the simulation program is completed. Any loss of phase lock

afterwards is assumed to be detected by the receiver. Depending on the number of lost signals, the different procedures outlined in Section 4.1.3.8 would have to be invoked then.

4.3 Simulation Results

This section discusses the results obtained using the measurement simulation and position determination programs described above.

4.3.1 Selection of Simulation Parameters

The performance of GPS (and any other satellite positioning system) is different for different locations. This difference is caused by the number of visible satellites and the geometry between these satellites and the user position. Especially in those periods when only the minimum number of satellites required for a position fix is available, a weak satellite geometry can lead to poor or even useless positioning results. A complete simulation study would have to assess the system performance at all possible user locations during 24 hours a day. However, to keep the number of simulations as low as possible, a representative simulation location was chosen. Since satellite visibility also changes in time, representative time windows were chosen. The effect of certain measurement errors depends on the separation between monitor station and user site. Several representative separation distances are chosen. These selection processes are described below. For all simulations, an elevation cut-off angle of 15 degrees is assumed, i.e. measurements to satellites below 15 degrees of elevation are not included.

4.3.1.1 Selection of Simulation Location

To assess the variability in the number of satellites available in different parts of the U.S.A., satellite visibility was predicted at the three locations:

- Washington, D.C. (Φ 39°, λ -77°)
- Anchorage, AK (Φ 61°, λ -150°)
- New Orleans, LA (Φ 30°, λ -90°).

These locations were chosen to represent an east coast mid-latitude site, a west coast northern latitude site and a site in the Mississippi delta. For each site, the number of visible GPS and GLONASS satellites was predicted every half hour on December 30, 1990, between 0:00 hours and 24:00 hours UT, using the software package MacGEPSAL [29]. Ephemerides files for GPS satellites were generated based on the full 24 satellite constellation as described in [12]. Ephemerides files for GLONASS satellites are based on the constellation described in [6]. Figures 4.8 through 4.13 show the prediction results. It can be seen, that the number of visible GPS and GLONASS satellites drops below 5 occasionally, for an elevation cut-off angle of 15°. Each data point represents a visibility prediction at 30 minute intervals. Obviously, there are no two subsequent epochs with less than 5 satellites.

The visibility prediction results are summarized in the following statistic:

Washington, D.C.:	Minimum number of GPS/GLONASS/total satellites:	4/4/8
	Maximum number of GPS/GLONASS/total satellites:	8/8/16
	Average number of GPS/GLONASS/total satellites:	6/6/12
Anchorage, AK.:	Minimum number of GPS/GLONASS/total satellites:	4/6/10
	Maximum number of GPS/GLONASS/total satellites:	9/9/16
	Average number of GPS/GLONASS/total satellites:	6/7/13
New Orleans, LA:	Minimum number of GPS/GLONASS/total satellites:	4/5/9
	Maximum number of GPS/GLONASS/total satellites:	8/9/16
	Average number of GPS/GLONASS/total satellites:	6/6/12

Obviously, there are only minor differences in the satellite visibility at the three locations involved. In terms of minimum and average number of visible satellites, the Washington, D.C., results are slightly inferior to the other locations. **Therefore, Washington, D.C., was chosen to evaluate the kinematic GPS performance.**

A geostationary satellite is permanently in view at all three sites, if placed in an appropriate equatorial orbit. Therefore, including a geostationary satellite in the simulation increases the number of visible satellites by one.

4.3.1.2 Selection of Simulation Time Intervals

It can be seen in Figure 4.8, that in Washington, D.C., the average number of visible satellites is six. This average visibility occurs for an extended period of around midnight. **To assess the kinematic GPS ambiguity resolution under these average conditions, the time interval 0:00 - 01:00 UT is chosen for simulation.** The same time interval was kept for the simulations involving a geostationary satellite and the GLONASS-type satellites.

4.3.1.3 Distance to Monitor Station

Several errors in differential GPS positioning increase with the separation distance between monitor station and remote user. To assess the resulting decrease in position accuracy, and the corresponding increase in convergence time for the carrier phase ambiguity resolution, the simulations were performed for several representative separation distances. Distances chosen are 10 km. 20 km, 40 km and 100 km. If for a particular satellite constellation and receiver configuration an ambiguity resolution at a particular distance was not successful, no attempt was made to resolve ambiguities for greater distances.

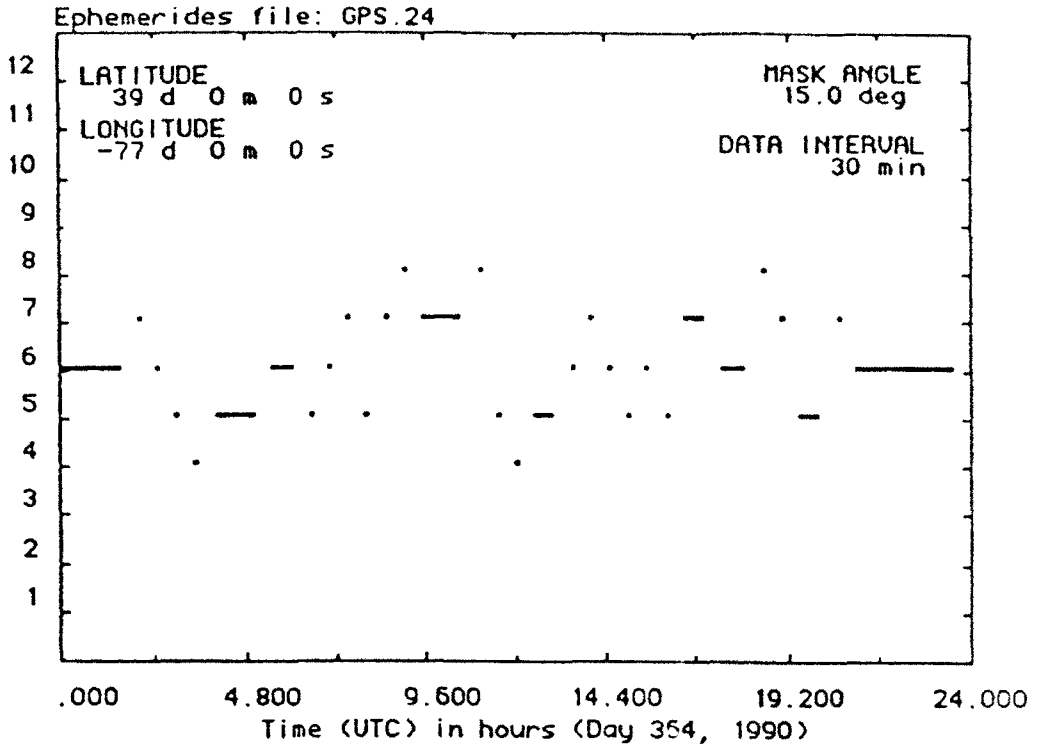

Figure 4.8: Number of GPS satellites visible in Washington, D.C.

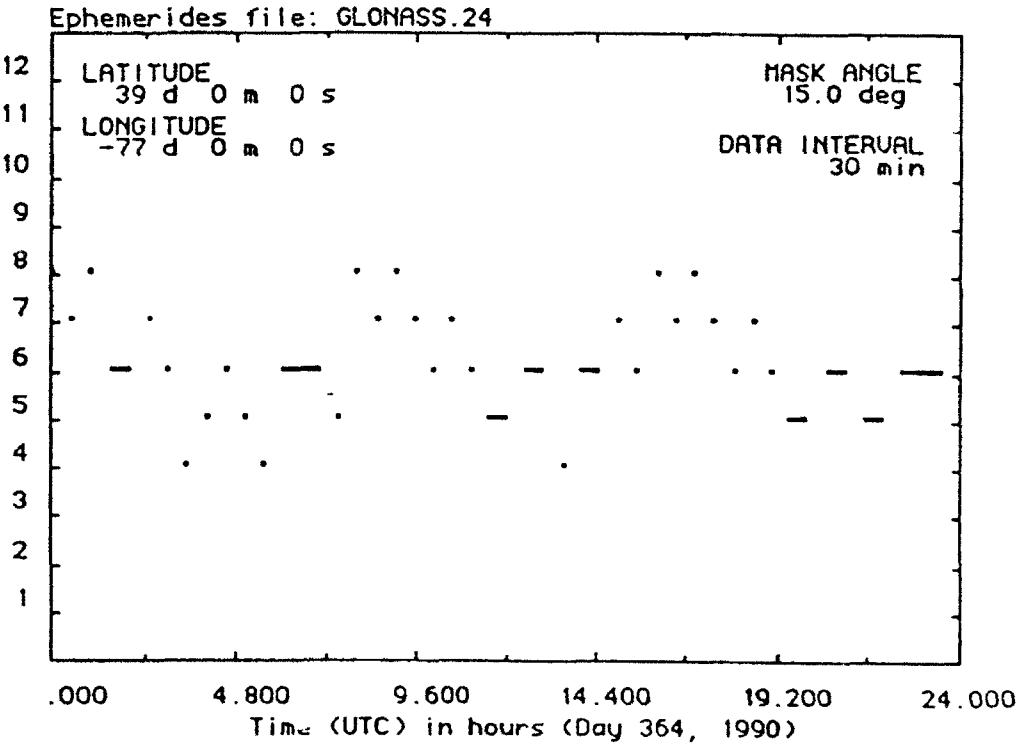

Figure 4.9: Number of Glonass satellites visible in Washington, D.C.

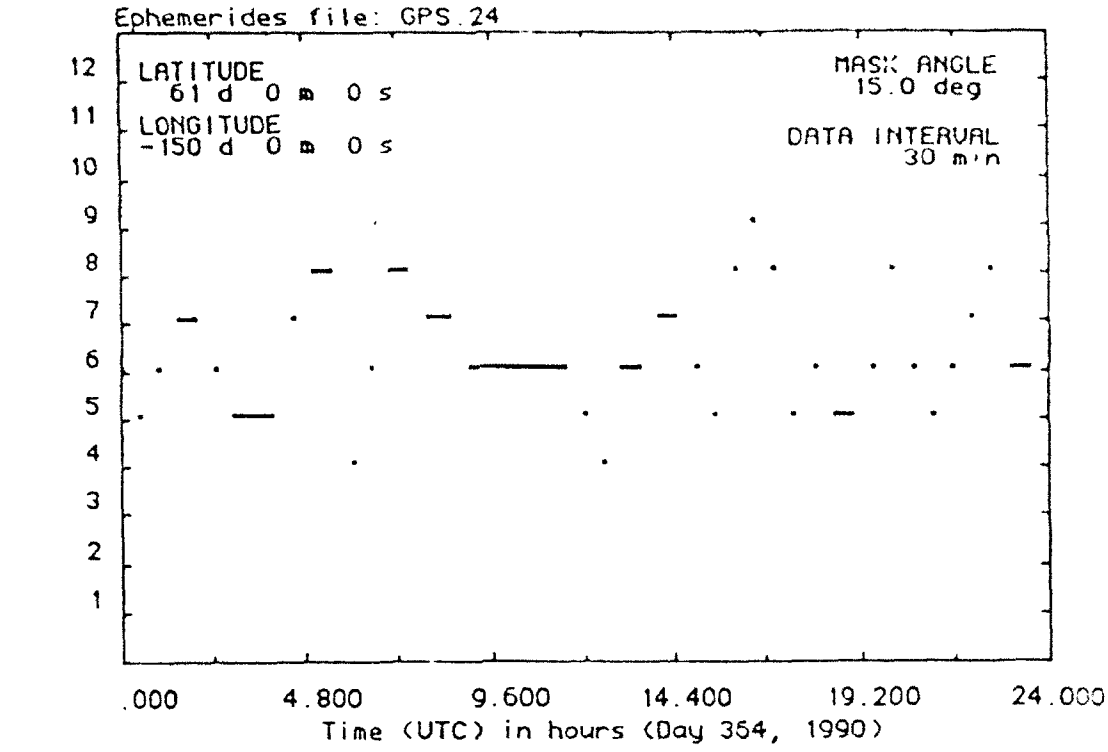

Figure 4.10: Number of GPS satellites visible in Anchorage, AK

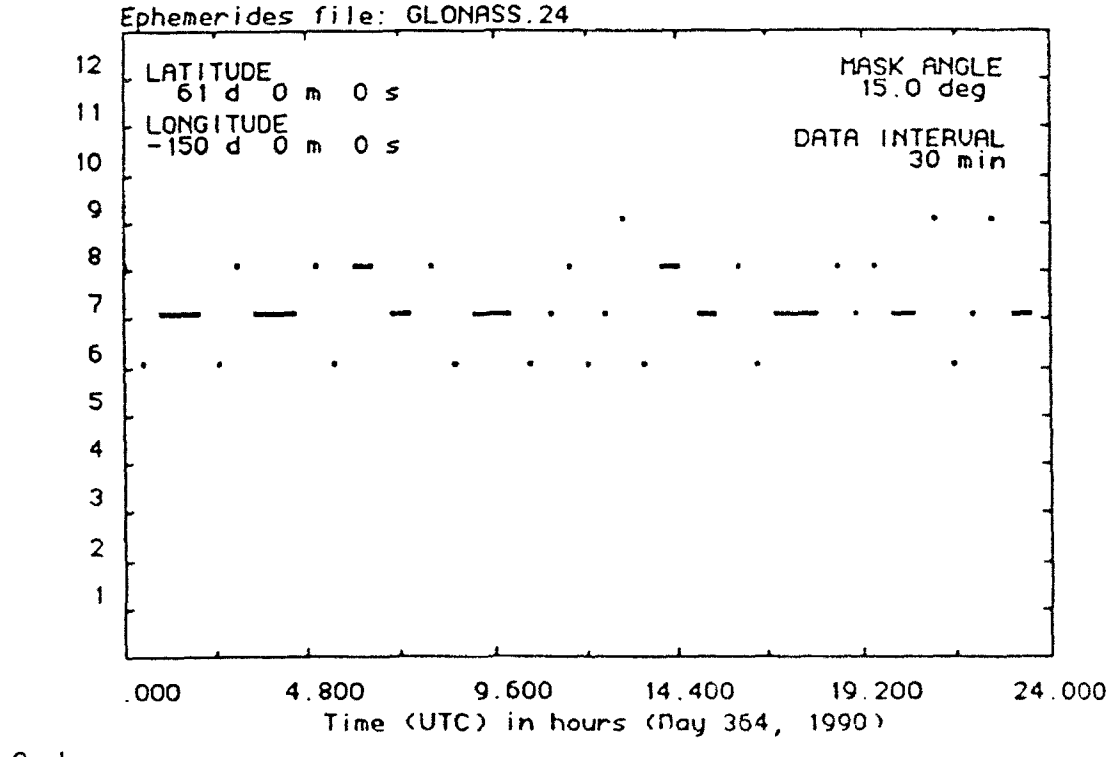

Figure 4.11: Number of Glonass satellites visible in Anchorage, AK

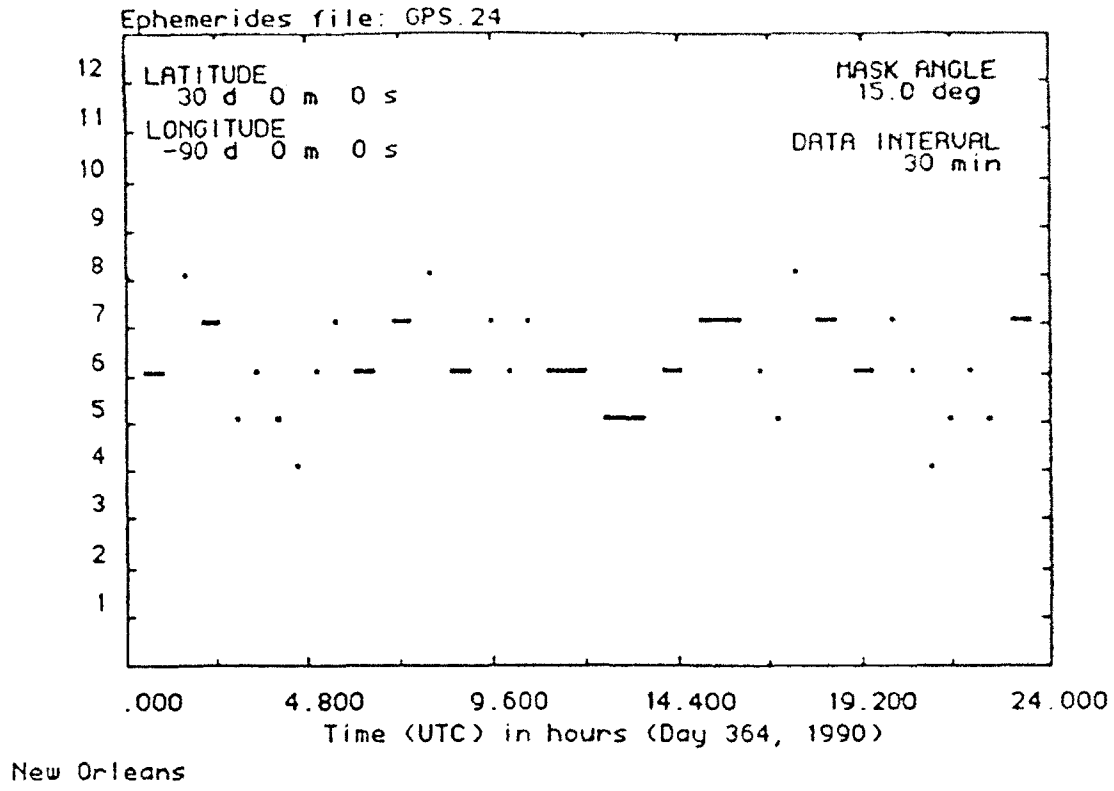

Figure 4.12: Number of GPS satellites visible in New Orleans, LA

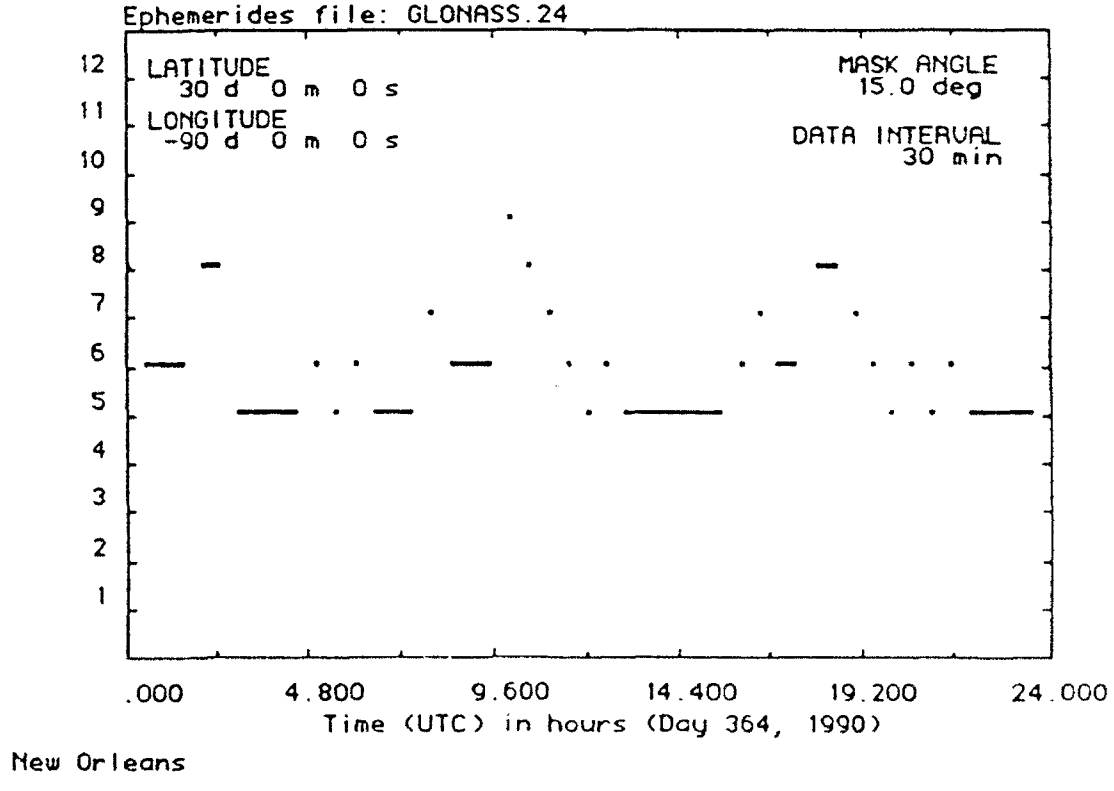

Figure 4.13: Number of Glonass satellites visible in New Orleans, LA

4.3.2 GPS Satellites Alone

· · GPS satellites are available in the simulation time interval.

4.3.2.1 Single Frequency C/A-code

Carrier phase double difference ambiguities did not converge to their integer values within 15 minutes for 10 km distance between monitor and remote station. Obviously, the same can be expected for longer distances. Continuing the measurements longer than 15 minutes will not improve the results, because the difference in ionospheric delay effects on pseudorange and carrier signal leads to a divergence for single frequency observations.

The primary reason for this failure is the size of multipath introduced in the C/A-code pseudorange measurements (3 meter error amplitude). Probably, a significant reduction of C/A-code multipath error levels (less than 1 meter) through appropriate measures would enable ambiguity resolution with a C/A-code system.

An alternative to the procedure of combining pseudoranges and carrier phases is to use carrier phase measurements to multiple satellites alone [24]. This procedure is free from any pseudorange multipath errors, but requires long convergence intervals.

If at least two carrier phase double difference ambiguities are fixed to their integer values, the remaining unknown ambiguities converge to their correct integer values within 13 minutes (± 5 minutes) for a distance between monitor and remote station of 20 km. Cycle slip recovery after partial phase lock loss is possible.

4.3.2.2 Single Frequency C/A-code Plus Codeless Second Carrier

For all simulations involving C/A-code receivers with codeless second frequency, the 34 cm wide-lane wave length was chosen (cf. Section 4.2.2.4). For a discussion of the possible improvement with the 43 cm wide lane wave length, see Section 4.4 Conclusions.

Carrier phase double difference wide-lane (squaring) ambiguities do not converge to their integer values within 15 minutes for 10 km distance between monitor and remote station. Obviously, the same can be expected for longer distances. Continuing the measurements longer than 15 minutes will not improve the results, because the difference in ionospheric delay effects on pseudorange and carrier signal leads to divergence even larger than for single frequency measurements. The primary reason for non-convergence is again multipath introduced in the C/A-code pseudorange measurements.

Cycle slip recovery after partial phase lock loss was not successful for 20 km separation distance, primarily because of the contamination by ionospheric delay effects.

4.3.2.3 Code and Codeless Dual Frequency Pseudorange and Carrier Phase

For both receiver types, full wide-laning is possible. The remaining main differences are the larger noise and multipath contamination of the pseudoranges in the codeless system.

For the full P-code receiver, the wide-lane carrier phase ambiguities converge to their correct integer values within 6 minutes (± 2 minutes) for both 10 km and 20 km separation distance, and within 7 minutes (± 2 minutes) for distances of 40 km and 100 km between monitor and remote station. Cycle slip recovery after partial phase lock loss was possible after 3 minutes (± 2 minutes).

For the P-codeless type of receiver, the wide lane carrier phase ambiguities did not converge to integers within 15 minutes for any of the above distances. The prime reason for this failure is the multipath in the L1 C/A-code derived pseudoranges. Simulations with reduced multipath amplitudes (1 meter instead of 3 meters) yielded convergence to correct integers within 10 minutes for 10 km separation distance, and within 15 minutes for 100 km separation distance.

4.3.3 GPS Plus GLONASS

A total of 12 satellites are utilized in this part of the simulation study (6 GPS satellites and 6 GLONASS satellites).

4.3.3.1 Single Frequency C/A-code

Improvement compared to GPS alone, but still no convergence to integer values for the carrier phase double difference ambiguities within 15 minutes.

If at least two carrier phase double difference ambiguities are fixed to their integer values, the remaining unknown ambiguities converge to their correct integer values within 8 minutes (± 5 minutes) for a distance between monitor and remote station of 20 km. This is a slight improvement compared to GPS alone.

4.3.3.2 Single Frequency C/A-code Plus Codeless Second Carrier

Carrier phase double difference wide-lane (squaring) ambiguities did converge to their integer values within about 15 minutes for 10 km separation distance.

Cycle slip recovery after partial phase lock loss was successful for 20 km separation distance after about 7 minutes.

4.3.3.3 Code and Codeless Dual Frequency Pseudorange and Carrier Phase

For both receiver types, the additional measurements lead to improvements in convergence time compared to GPS satellites alone. For the full P-code receiver, the wide-lane carrier phase ambiguities converge to their correct integer values within 4 minutes (± 2 minutes) for all separation distances between monitor and remote station.

For the P-codeless type of receiver, the wide-lane carrier phase ambiguities did converge to their correct integer values within 9 minutes for separation distances of 10 km and 40 km, and within 10 minutes for 100 km separation distance. Reducing the multipath amplitude to 1 meter, convergence was achieved within 6 minutes for distances of 10 km and 100 km between monitor and remote station.

4.3.4 GPS Plus Geostationary Satellite

4.3.4.1 Single Frequency C/A-code

Improvement compared to GPS alone, but still no convergence to integer values for the carrier phase double difference ambiguities within 15 minutes.

If at least two carrier phase double difference ambiguities are fixed to their integer values, the remaining unknown ambiguities converge to their correct integer values within 11 minutes (± 5 minutes) for a distance between monitor and remote station of 20 km. This is a slight improvement compared to GPS alone.

4.3.4.2 Single Frequency C/A-code Plus Codeless Second Carrier

No significant difference compared to GPS alone for ambiguity convergence. However, cycle slip recovery after partial phase lock loss was successful for 20 km separation distance after about 8 minutes.

4.3.4.3 Code and Codeless Dual Frequency Pseudorange and Carrier Phase

For both receiver types, the measurements to the additional geostationary satellite lead to slight improvements in convergence time compared with GPS satellites alone. For the full P-code receiver, the wide-lane carrier phase ambiguities converge to their correct integer values within 4 minutes (± 2 minutes) for 10 km and 20 km separation distance, and within 5 minutes for separation distances of 40 km and 100 km between monitor and remote station. As for GPS satellite alone, cycle slip recovery was possible after 3 minutes (± 2 minutes).

For the P-codeless type of receiver, the wide-lane carrier phase ambiguities did converge to their correct integer values within 11 minutes for all separation distances. Reducing the multipath amplitude to 1 meter, convergence was achieved within 7 minutes for distances of 10 km and 100 km between monitor and remote station.

4.4 Summary and Conclusions

We have simulated the capability of four different GPS receiver configurations for carrier phase ambiguity resolution with simultaneous differential positioning. The four receiver configurations were

- Single frequency C/A-code receiver.
- Single frequency C/A-code receiver with codeless (squaring) second frequency.
- Dual frequency codeless pseudorange and carrier phase receiver (Rogue type).
- Dual frequency P-code receiver (pseudorange and carrier).

It was assumed that any of these configurations can be used in a kinematic environment. The simulated satellite constellations included the complete 24 satellite GPS configuration, the GPS constellation plus one geostationary satellite and a combined GPS-GLONASS constellation with a total of 48 satellites.

The simulation results can be summarized as follows. Wide-lane ambiguities were not successfully resolved with single frequency C/A-code receivers, and with C/A-code receivers providing a second "squared" carrier phase measurement. The convergence times for full P-code receivers and P-codeless receivers (Rogue type) are summarized in Table 4.2. Results for the codeless type are provided for the two pseudorange multipath levels 3 meter (M = 3) and 1 meter (M = 1). Obviously, multipath is the dominating error in the codeless receiver type.

Obviously, there is some gain in convergence time by including a geostationary satellite or GLONASS satellites in the solution. For C/A-code single frequency receivers with codeless second frequency, ambiguity resolution was not possible for separation distances of 20 km and more, and even for 10 km separation distance the convergence was not achieved for all tested satellite constellations. Results were even worse with a C/A-code single frequency receiver without the codeless second frequency.

The prime reason for the failure of the C/A-code receiver systems in the present context is the pseudorange multipath model used in the simulations. The C/A-code multipath model consists of sinusoidal variations with amplitudes of 3 meters and periods of 5 minutes. The convergence time can be shown to depend linearly on both the amplitude and the period of the multipath. Therefore, a significant reduction in either of these two parameters would be required to reduce the convergence time significantly. Test runs with a reduced multipath amplitude of 1 meter for 20 km separation distances showed the expected improvement, but did not allow complete ambiguity resolution within 15 minutes.

The big advantage of a dual frequency system is best understood if we look at the ratio between wavelength and multipath error amplitude. For the simulation parameters chosen in this investigation, this ratio is about 1.7 for wide-laning with a full dual frequency P-code receiver and about 0.3 (M=3) or 0.9 (M=1) for the P-codeless receiver type, compared to 0.11 for the 34 cm wide-lane with the codeless second frequency carrier described above. A change to the other possible wide-lane combination yielding a 43 cm wide-lane would improve this factor to a value of 0.14.

Table 4.2: Wide-Lane Ambiguity Convergence Times (minutes) for Dual Frequency receiver configurations.

	Distance between monitor and remote station			
	10km	20km	40km	100km
GPS alone (6 satellites)				
Full P-code Rx	6	6	7	7
P-codeless Rx, M=3	no convergence any distance			
P-codeless Rx, M=1	10	10	11	15
GPS and geostationary sat. (7 satellites)				
Full P-code Rx	4	4	5	5
P-codeless Rx, M=3	11	11	11	11
P-codeless Rx, M=1	7	7	7	7
GPS and GLONASS (12 satellites)				
Full P-code Rx	4	4	4	4
P-codeless Rx, M=3	9	9	9	10
P-codeless Rx, M=1	6	6	6	6

5.0 Measurement Gap Filling Studies

5.1 Requirements Review

The measurement gap filling simulation was developed to determine the maximum gap lengths which could be tolerated before it became necessary to reinitiate an integer search. High, medium, and low quality INSs were integrated with receivers capable of wide-laning, half-wide-laning and normal laning. In addition, the use of a barometric altimeter and a rubidium clock are considered to enhance the coasting performance. No specific goals (in terms of minimum tolerable gap length) were established; however, it was generally understood that gaps due to signal obscuration by bridges could be up to a minute in length.

5.2 Simulation Description

5.2.1 Overview

An optimal covariance simulation was used to first determine the extent to which the raw inertial drift could be calibrated using GPS, and then to determine how the calibrated INS would perform with partial or complete loss of GPS. Figure 5.2-1 illustrates the major components of the simulation and their interaction. The vehicle motion model and INS, GPS and baro altimeter error models provide the necessary parameters for running the optimal covariance equations, which generate the predicted one sigma error values for each of the modelled states as a function of time. The equations are first run for a 60 second period with complete (i.e., 4 satellite) GPS coverage (this time period permits the calibration of INS position and velocity errors to reach a near steady state condition); following this, a measurement gap of specified length is simulated, during which time a specified number of GPS satellites are assumed obscured; at the completion of the simulated obscuration period, a 20 second period with full coverage is simulated, to enable the filter to reestablish the correct integer count. Obviously, inclusion of more than the minimum number of satellites will enhance INS calibration and so permit longer coasting periods. The simulations reported on are limited to 4 satellites to ensure conservative predictions.

The predicted one sigma values output from the simulation represent the performance of a fully optimal Kalman filter, with complete statistical and dynamic knowledge of all sources of error. These predictions, however, should be only slightly optimistic, since reduced state filters can in general be designed to perform nearly as well as optimal filters through appropriate choice of modelled process and measurement noise statistics [10].

5.2.2 Simulation Models

Each of the models used in the covariance simulation is described in this section; where appropriate, equation-level descriptions are provided. In addition, references for the error models and their parameters are provided wherever possible.

Figure 5.2-1 Measurement Gap Filling Simulation Overview

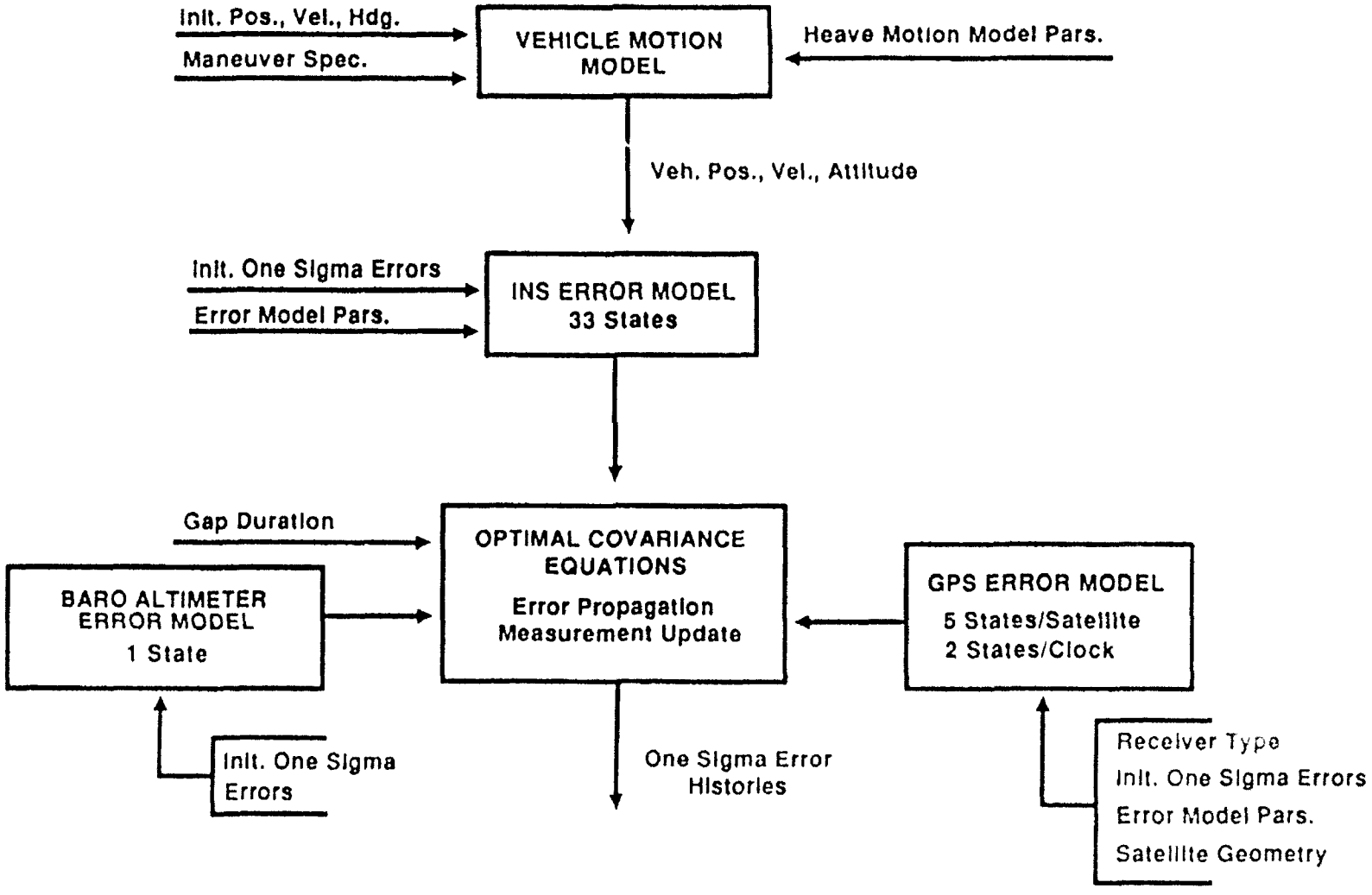

5.2.2.1 Vehicle Motion Model

The motion of the ship is represented by straight line segments (corresponding to a constant ship velocity at specified heading) separated by a single turn, which is specified by a fixed turn rate and duration. Superimposed upon this nominal trajectory is a sinusoidal heave motion of specified amplitude and frequency. For the results reported in this section, the ship is initially located at 45 degrees latitude with a 45 degree heading and a velocity of 10 knots. A turn is simulated after 80 seconds, completing a course reversal after 110 seconds. Note that the turn begins and is completed during the simulated gap in GPS coverage, to make INS error projections somewhat pessimistic. The simulated heave motion is 1 meter in amplitude, with a period of 20 seconds. The equations provided below specify the form of the vehicle motion model (note that a spherical earth model is used in updating vehicle latitude and longitude):

Vehicle Motion Model Equation Summary

Given: $Ho,\ t_{manstr},\ \Delta t_{man},\ H_{man},\ L_o,\ \lambda_o,\ v,\ A_h,\ \omega_h$

If: $t_{manstr} < t < (t_{manstr} + \Delta t_{man})\quad H = H_{man}$

Else: $H = 0$

Heading Update Equation:

$$H_{k+1} = H_k + H\ \Delta t$$

Latitude Update Equation:

$$L_{k+1} = L_k + v\ \cos H_k\ /\ R_e$$

Longitude Update Equation:

$$\lambda_{k+1} = \lambda_k + v\ \sin H_k\ /\ (Re\ \cos L_k)$$

Altitude Equation:

$$h_{k+1} = A_h\ \sin\ \omega_h(t_{k+1})$$

In the above equations, H and H denote vessel heading and heading rate, respectively, t_{manstr} and Δt_{man} denote the start and duration of the specified maneuver, respectively, v denotes vessel speed and ω_h represents the frequency of the heave oscillation.

5.2.2.2 INS Error Model

The INS error model is abstracted from [39]; it represents the position, velocity and attitude errors in a geographic frame (i.e., east, north, up) and includes both Schuler and earth rate error dynamics. Both local level and strapdown mechanizations are readily accommodated in this formulation. The dynamics matrix for the fundamental (i.e., unforced) error dynamics, abstracted from [39], is repeated here in Tables 5.2-1 through 5.2-3. Two minor changes have been made to the dynamics matrix appearing in Table 5.2-1: the longitude and latitude errors were replaced by east and north position

Table 5.2-1 Fundamental Matrix of the INS General Error Differential Equations

		$\delta\lambda$ 1	δL 2	δh 3	δv_e 4	δv_n 5	δv_z 6	ε_e 7	ε_n 8	ε_z 9
$\dot{\delta\lambda}$	1	0	$\rho_z/\cos L$	$-\rho_n/R\cos L$	$1/R\cos L$	0	0			
$\dot{\delta L}$	2	0	0	ρ_e/R	0	$1/R$	0		0	
$\dot{\delta h}$	3	0	0	0	0	0	1			
$\dot{\delta v}_e$	4	0	F_{42}	F_{43}	F_{44}	$(\omega_z+\Omega_z)$	$-(\omega_n+\Omega_n)$	0	$-f_z$	f_n
$\dot{\delta v}_n$	5	0	F_{52}	F_{53}	$-2\omega_z$	$-k_z$	ρ_e	f_z	0	$-f_e$
$\dot{\delta v}_z$	6	0	$-2\Omega_z v_e$	F_{63}	$2\omega_n$	$-2\rho_e$	0	$-f_n$	f_e	0
$\dot{\varepsilon}_e$	7	0	0	$-\rho_e/R$	0	$-1/R$	0	0	ω_z	$-\omega_n$
$\dot{\varepsilon}_n$	8	0	$-\Omega_z$	$-\rho_n/R$	$1/R$	0	0	$-\omega_z$	0	ω_e
$\dot{\varepsilon}_z$	9	0	F_{92}	$-\rho_z/R$	$\tan L/R$	0	0	ω_n	$-\omega_e$	0

Table 5.2-2 Notation Used in Fundamental Matrix

L	Latitude of vehicle
Ω	Earth rotation rate
R	Earth radius
g	Magnitude of gravity vector
v_e, v_n, v_z	Components of vehicle velocity with respect to earth
f_e, f_n, f_z	Components of specific force
$\Omega_n = \Omega \cos L$ $\Omega_z = \Omega \sin L$	Components of earth rate
$\rho_e = -v_n/R$ $\rho_n = v_e/R$ $\rho_z = v_e \tan L/R$	Components of angular velocity of E-N-Z frame with respect to earth
$\omega_e = \rho_e$ $\omega_n = \rho_n + \Omega_n$ $\omega_z = \rho_z + \Omega_z$	Components of angular velocity of E-N-Z frame with respect to inertial space

$$k_z = v_z/R$$

$$F_{42} = 2(\Omega_n v_n + \Omega_z v_z) + \rho_n v_n/\cos^2 L$$

$$F_{43} = \rho_z \rho_e + \rho_n k_z$$

$$F_{44} = -\rho_e \tan L - k_z$$

$$F_{52} = -2\Omega_n v_e - \rho_n v_e/\cos^2 L$$

$$F_{53} = \rho_n \rho_z - \rho_e k_z$$

$$F_{63} = 2g/R - (\rho_n^2 + \rho_e^2)$$

$$F_{92} = \omega_n + \rho_z \tan L$$

Table 5.2-3 Error Forcing Functions of the INS General Error Error Differential Equations

$\underline{w}_r = \underline{0}$	Position error components
$\underline{w}_v = C_p^n \, \delta\underline{f}^p + \delta\underline{g}'^n$	Velocity error components
$\underline{w}_\epsilon = C_p^n \, \delta\underline{\omega}_{ip}^p$	Attitude error components
where	
$\delta\underline{f}^p = \hat{\underline{f}}^p - \underline{f}^p$	Specific force measurement error (measured minus actual platform components)
$\delta\underline{g}'^n = \hat{\underline{g}}^n - \underline{g}^n$	Gravity model error (computed minus actual) in geographic coordinates, not including position error effect
$\delta\underline{\omega}_{ip}^p = \underline{\omega}_{ip}^p - \hat{\underline{\omega}}_{ip}^p - \underline{u}_\epsilon^p$	Platform angular velocity error (actual minus estimated platform components of the angular velocity of the platform in inertial space, less any alignment correction rate)
C_p^n	Transformation from platform to geographic coordinates

errors, respectively, which resulted in terms involving the inverse of the radius of the earth being removed in the coupling to velocity and altitude errors, and added in the attitude error rate coupling; in addition, the term in the 6,3 element of the matrix ($2g/R$) which results in the exponential growth in uncalibrated INS altitude error (caused by the positive feedback of altitude error into gravity computation error) has been dropped, since it is assumed that gravity compensation will be based upon a constant ship altitude.

In addition to these basic 9 error states, a total of 15 gyro error sources, 6 accelerometer error sources and 3 gravity computation errors are modelled, resulting in a total of 33 INS error states. The gyro errors include 3 g-insensitive drifts, 3 g-sensitive drifts, 3 gyro scale factor errors and 6 input axis misalignments. Each g-insensitive drift is modelled as a random walk, with a power spectral density selected to produce an error growth which is 10% of the initial value over a 100 second period. The initial one sigma value is a function of the INS quality considered (see Table 5.2-4, which summarizes the gyro error model parameters). Note that, in Table 5.2-4 (as well as in Table 5.2-5), the high quality INS numbers are derived from an error budget for MAPS DRU Ring Laser Gyro (RLG) based INS, while the medium and low quality numbers are representative of generic INSs of lower quality. Scale factor errors are modelled as Markov processes with 1800 second correlation times. The relatively long time constant reflects the near bias-like nature of the scale factor error, and is consistent with models presented elsewhere [27]. The process noise variance associated with each Markov process is computed from the initial state error variance and the correlation time based upon steady state conditions, as described in [10]. The g-sensitive drifts are expected to be significant only for mechanical gyros; i.e., RLGs are modelled with zero g-sensitive drifts. Thus, the three qualities of INSs represented in Table 5.2-4 are assumed to utilize RLGs. Gyro input axis misalignments are represented as random biases.

Modelled accelerometer error sources include accelerometer biases and scale factor errors (modelled as slowly varying Markov processes), and input axis misalignments, represented as random biases. Table 5.2-5 summarizes the accelerometer error source magnitudes as a function of INS quality. The horizontal components of gravity computation error (often referred to as deflections of the vertical) are modelled as Markov processes with one sigma value of 10 arc-seconds, and correlation distances of 25 nm, while the vertical component (often referred to as gravity anomaly) has a one sigma value of 50 micro-g's and a correlation distance of 60 nm. These values are generally consistent with levels which are discussed in [39]. The magnitudes selected for both the horizontal and vertical components may appear larger than values published elsewhere [32,23]; this is partially due to a desire to make the simulation performance predictions somewhat conservative, but also to include (approximately) the effect of bias components in each gravity error component (as referenced in [39]) without the inclusion of additional states.

5.2.2.3 Barometric Altimeter Error Model

Barometric altimeter updates are processed each second by the filter to assist in stabilizing the INS vertical channel during GPS outages. When full GPS coverage exists, the bias error of the barometric altimeter can be calibrated. The baro error model consists of a single Markov process, with a

Table 5.2-4 Gyro Error Model Parameters

INS Quality	Drift (deg/hr)	SF (ppm)	G-Sensitivity (deg/hr)/(m/sec^2)	Axis Misalign (arc-min)	Angle Walk
High	0.004	10	0.00	0.067	0.002 deg/hr$^{1/2}$
Medium	0.100	250	0.00	1.000	0.02 deg/hr$^{1/2}$
Low	1.000	1000	0.00	1.000	0.20 deg/hr$^{1/2}$

Table 5.2-5 Accelerometer Error Model Parameters

INS Quality	Bias (ug)	SF (ppm)	Axis Misalign (arc-min)
High	40	120	0.167
Medium	200	250	1.000
Low	500	1000	1.000

one sigma value of 10 meters, and a correlation time of 100 seconds. In addition, a measurement noise variance of 0.09 meter squared is assigned to the baro measurement when it is processed by the optimal filter.

5.2.2.4 GPS Measurement Geometry

Due to the relatively short time periods of interest, GPS satellite geometry is assumed fixed, with the four satellite azimuths and elevations indicated in Table 5.2-6, below. These satellite lines of sight are derived from real data obtained on 30 April 1983, from GPS satellites 9, 11, 13 and 19. This set of four satellites (at 0600 UTC) results in a PDOP of 2.5, and a HDOP of 1.5 (the Vertical Dilusion of Precision (VDOP) is therefore 2.0). Thus, a good nominal GPS geometry is assumed.

Table 5.2-6: Assumed GPS Satellite Geometry

Simulation No.	GPS Satellite No.	Azimuth Angle (°)	Elevation Angle(°)
SV1	9	170	40
SV2	11	40	30
SV3	13	340	66
SV4	19	310	29

5.2.2.5 GPS Error Model

The GPS error model includes receiver clock phase and frequency error, and a maximum of 5 error states for each satellite; these errors include carrier multipath error, residual (i.e., post-differentially corrected) tropospheric, ionospheric and S/A errors, and integer ambiguity error. Thus, a maximum number of 22 states can be modelled for 4 satellites. GPS carrier pseudorange measurements are processed each second with a one sigma noise value of 1 cm.

The receiver clock is assumed to be a rubidium frequency standard (a sensitivity analysis is reported on later in which a non atomic clock is considered). Its error model is derived from [28], and consists of a random walk frequency error with an initial one sigma value of $1x10^{-11}$, driven by a white noise with power spectral density computed from an Allen variance of $5x10^{-26}$ over 2000 seconds. In addition, a phase noise with a power spectral density $1.x10^{-23}$ sec^2/sec is included. Computation of the appropriate power spectral densities from the Allen variance statistic is discussed in [35]. The selection of a random walk in lieu of a Markov process is based upon the fact that frequency correlation times on the order of several days (corresponding to aging effects) are typical for rubidium standards, which is not a significant effect for the simulation durations considered. Due to the relative magnitudes of the phase and frequency power spectral densities and the simulation duration, the phase noise is expected to be the dominant error contributor.

Carrier multipath error is modeled by a Markov process with a 5 minute correlation time and a one sigma value of 1 cm; these values are consistent with roof-top tests performed using TNL 4000 (i.e., survey quality) receivers

[22]. Residual tropospheric, ionospheric, and S/A errors are computed as a function of the separation distance between the ship and the (master) reference station using the equations below:

Residual Tropospheric Error

$\sigma^2_{tropo} = \sigma^2_{tropoo}\ (1-e^{-2d/d_{tropo}})$
$\dot{\sigma}^2_{tropo} = -2\beta_{tropo}\ \sigma^2_{tropo} + q_{tropo}$
σ^2_{tropo} = calculated tropospheric error variance
σ^2_{tropoo} = non differentially corrected tropospheric error variance
d = distance from master reference station
d_{tropo} = correlation distance for tropospheric error
$\dot{\sigma}^2_{tropo}$ = time rate of change of tropospheric error variance
β_{tropo} = inverse of tropospheric error correlation time
q_{tropo} = power spectral density for tropospheric error model ($8x10_{-3}$ cm^2/sec)

Residual Ionospheric Error

$\sigma_{iono} = \sigma_{ionoo} \bullet d\ /\ d_{iono}$
$\dot{\sigma}^2_{iono} = -2\beta_{iono}\sigma^2_{iono} + q_{iono}$
σ^2_{iono} = calculated ionospheric error variance
σ^2_{ionoo} = non differentially corrected ionospheric error variance
d = distance from master reference station
d_{iono} = correlation distance for ionospheric error
$\dot{\sigma}^2_{iono}$ = time rate of change of ionospheric error variance
β_{iono} = inverse of ionospheric error correlation time
q_{iono} = power spectral density for ionospheric error model ($1.8x10^{-2}$ m^2/sec)

Residual S/A Error

$\sigma_{sa} = \sigma_{sao} \cdot d\ /\ d_{sa}$
$\dot{\sigma}^2_{sa} = -2\beta_{sa}2_{sa} + q_{sa}$
σ^2_{sa} = calculated sa error variance
σ^2_{sao} = non differentially corrected sa error variance
d = distance from master reference station
d_{sa} = correlation distance for sa
$\dot{\sigma}^2_{sa}$ = time rate of change of sa error variance
β_{sa} = inverse of sa correlation time
q_{sa} = power spectral density for sa (8×10^{-2} m^2/sec)

Table 5.2-7 summarizes the parameters of these error models. The values utilized for tropospheric and ionospheric error are consistent with parameters published in the open literature [3,13,19,18]. The parameters used for the SA error model are representative of only the so-called epsilon term, since the dither term (resulting from the perturbation of each satellite's oscillator) is common to both the ship and the reference station, and will drop out at all separation distances. The residual error due to the epsilon term, since it represents a satellite position error, is strictly a function of ship/station relative geometry, which behaves linearly with separation distance for distances which are small compared with the distance to the GPS

Table 5.2-7 GPS Error Model Parameters

Error	Nominal Induced (meters)	Corr. Dist. (km)	Corr. Time (secs)
Tropo	0.02 / sin (el)	50.0	600
Iono	3.0 / sin (el)	3000.0	1000
SA	20.0	20000.0	10000

satellite. The constant relating the two is roughly the inverse of the distance to the satellites (i.e., 20000 km). The very long correlation time associated with the S/A error reflects the slowly varying nature of the induced orbital errors.

Integer ambiguity error is modelled as a random bias, with a one sigma value dependent upon the simulation conditions. It is initialized to zero, assuming that a correct set of integers has been found; during a period of continuous satellite coverage, it remains zero, assuming that carrier lock is maintained without cycle slips occurring. Following a simulated measurement gap, it is set to a one sigma value of 100 meters, reflecting no knowledge of the integer count (other than through the pseudorange measurement, assumed to be S/A-corrupted). As the carrier pseudoranges (some with unresolved integers) are processed and the one sigma error associated with the integers decrease, a test is made to see if the integer can be resolved. As a function of the receiver utilized (i.e., wide, half wide or normal laning), the integer is considered to be resolved if 2.5 times the one sigma error is less than one half of the lane width. This test corresponds to a 0.99 probability of correct determination of the integer. It is difficult to compare this criterion directly with the criteria used in the ambiguity resolution simulation, since that was a Monte Carlo, rather than a covariance simulation. Certainly, the covariance test utilized here is more conservative than the covariance test used in the ambiguity resolution simulation. However, the additional tests performed there, which do not have a counterpart in the covariance simulation, may make the two sets of tests for lane convergence more nearly equivalent. Once an integer can be resolved, an artificial perfect measurement of the integer error is formed, which results in the one sigma error associated with that state being set to zero, and all errors correlated with that state being correspondingly reduced. Note that, alternatively, integer error could be modelled fractionally. Given that a conservative measure of correct integer determination is utilized (which is the case here), integer modelling is preferred, since filter estimation errors will generally be reduced. Once any integer has been resolved, the carrier phase measurements are reprocessed, making use of this information. The process (at each time instant) is concluded when no new integers are resolved in the current measurement epoch. Note that a separate integer ambiguity is modelled for each satellite, while double differencing algorithms consider pair-wise differences of these integers. Since a rubidium frequency standard is part of the recommended system, the use of double differencing (which removes the effect of user clock error) will not change the performance predictions significantly. If operating without an atomic clock, the use of additional satellites (beyond the minimum 4 utilized in the simulations reported in this section) will enable, through double differencing or processing by the optimal filter, removal of receiver clock errors. The Kalman filter will effectively make use of double differencing when presented with redundant satellites and a clock with excessive drift characteristics.

5.3 Simulation Results

5.3.1 Scenario Definition

Given the error models just described, measurement gaps of different durations were simulated following an assumed 60 second calibration period with full GPS coverage (i.e., carrier pseudorange measurements available from 4 satellites each second). This period was previously determined to be sufficiently long to enable the filter to achieve a near steady state error condition. Except when specifically noted, the barometric altimeter was assumed available in all cases.

5.3.2 Cases Considered

Of primary interest in running the gap filling simulation is the determination of the maximum gap length which can be tolerated without permanent loss of the integer ambiguities over the full range of operating conditions. This includes separation distances ranging from 0 to 100 km, high, medium and low quality INSs, wide-laning, half-wide-laning and normal laning receivers, and loss of from 1 to 4 GPS satellites during the simulated gap. The zero separation distance was included as a limiting case for which the residual correlated errors could be completely removed. Due to the large number of runs involved, the simulation was configured to automatically (without operator intervention) select the maximum tolerable gap length by iterating from an initial supplied length. It tests the current length, then either doubles the gap length or halves the previous change in gap length, based upon whether the integers were maintained or not, respectively. To better understand the summary curves presented in this section, consider Figures 5.3-1a. and b., which plot the one sigma errors along each satellite line of sight as a function of time, starting with the simulated measurement gap. As illustrated in Figure 5.3-1a., the initial errors are very small following the 60 second calibration period with full GPS coverage. A gap of 50 seconds with complete loss of GPS is considered, using a high quality INS and wide-laning GPS receiver. The separation distance for this case was 100 km. Note that each of the one sigma errors along the 4 lines of sight converges to less than 0.2 of a wide-lane wavelength (86 cm), indicating reacquisition of the correct set of integers for all 4 satellites. Figure 5.3-1b. is a blowup of the integer reacquisition sequence from Figure 5.3-1a., illustrating how the second carrier measurement enables initial separation of INS position errors and integer errors, and the integer "snap in" below the 1$ confidence level.

Of secondary interest in the utilization of this simulation is the resultant navigation performance of the integrated GPS/INS navigation filter (navigation performance is addressed in Section 5). To illustrate the differences between navigation performance and integer convergence, consider Fig. 5.3-2, which plots the position error components corresponding to the line of sight error components presented in the previous figure. Note the significant differences in the error level magnitudes.

Position error components prior to the gap and following integer reconvergence range from about 0.2 meter to more than 0.5 meter, while the integer ambiguity errors along each line of sight are a fraction of a centimeter. This apparent inconsistency (which is more than an order of magnitude larger than the scaling attributable to PDOP), is caused by the near unity negative correlation coefficient which develops between position errors and correlated errors in the measurements (i.e., residual tropospheric and

Figure 5.3-1a. Reacquisition of Widelane Integers with INS after 50 Second Gap

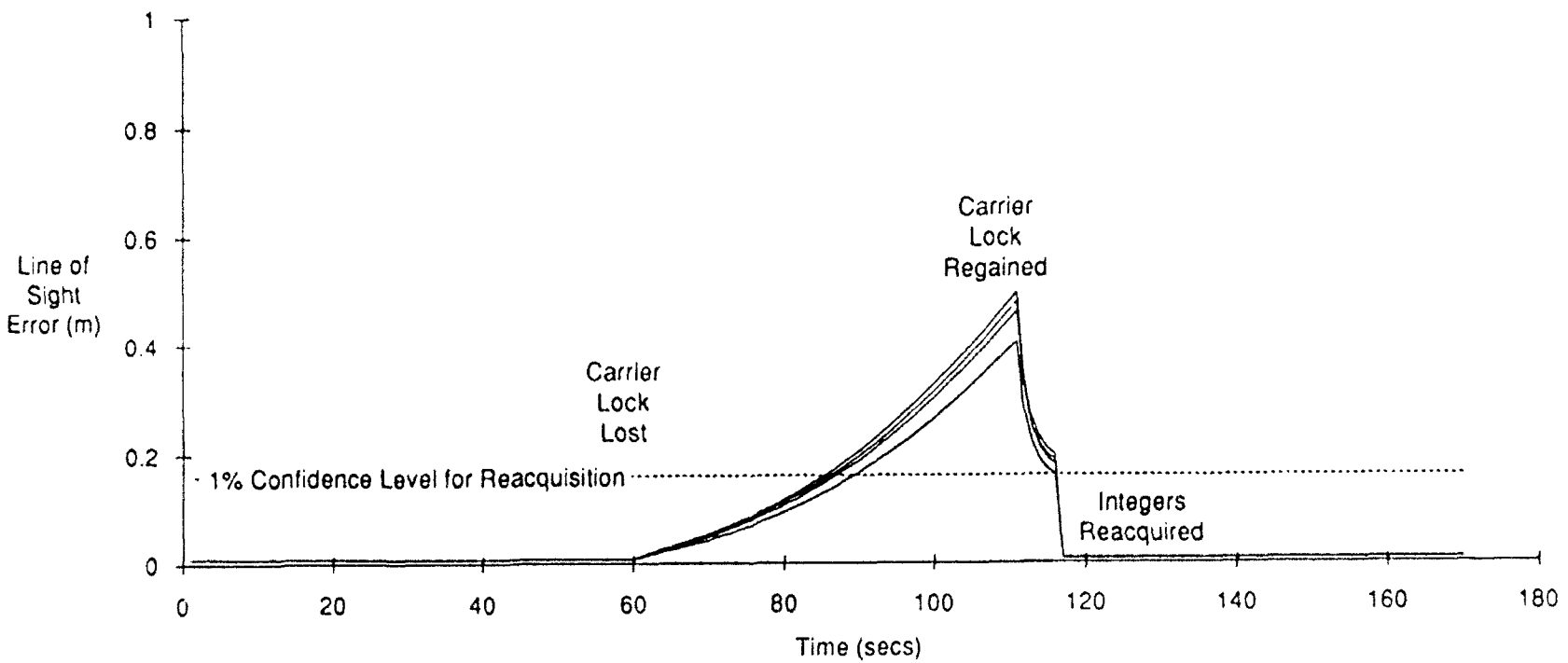

Figure 5.3-1b. Reacquisition of Widelane Integers with INS after 50 Second Gap

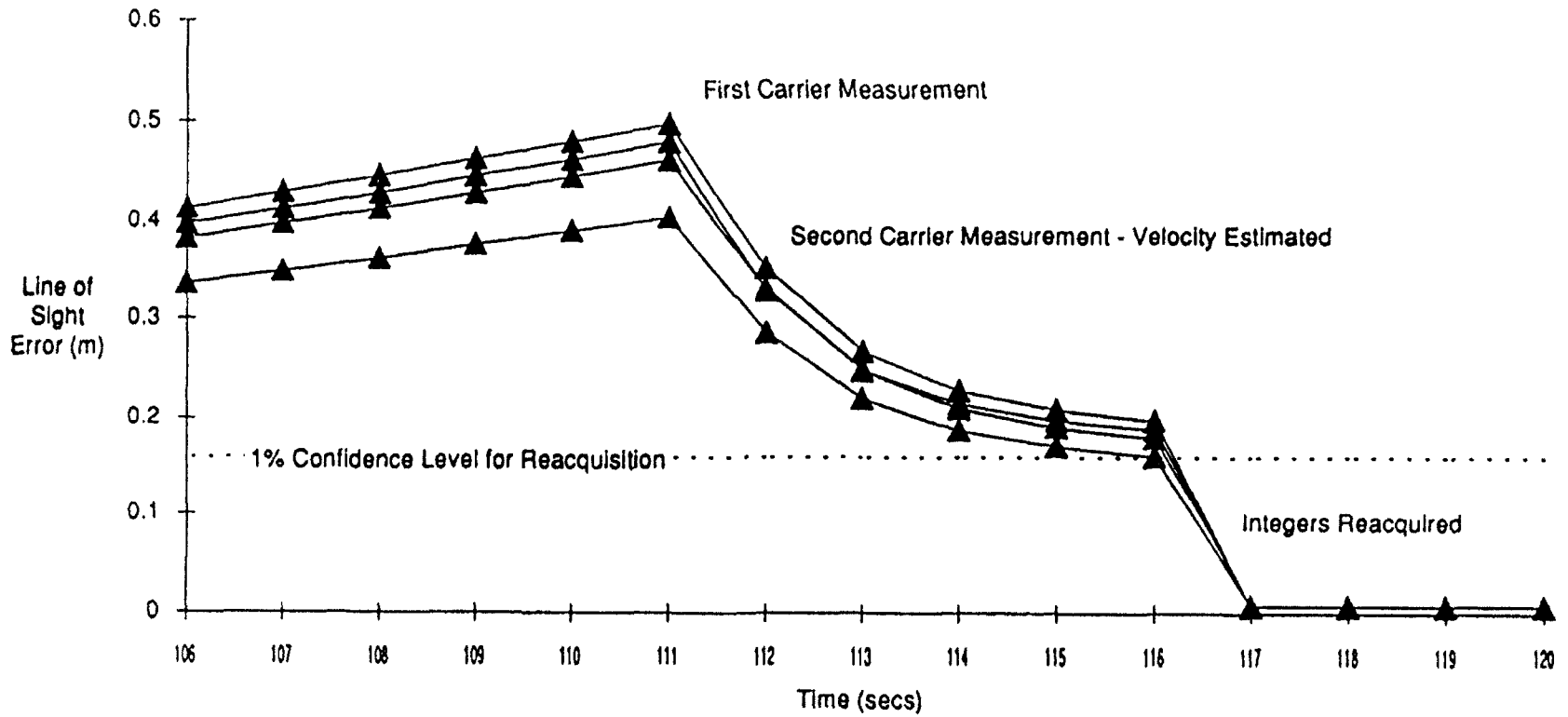

Figure 5.3-2 Position Error History 50 Second Gap in GPS Coverage

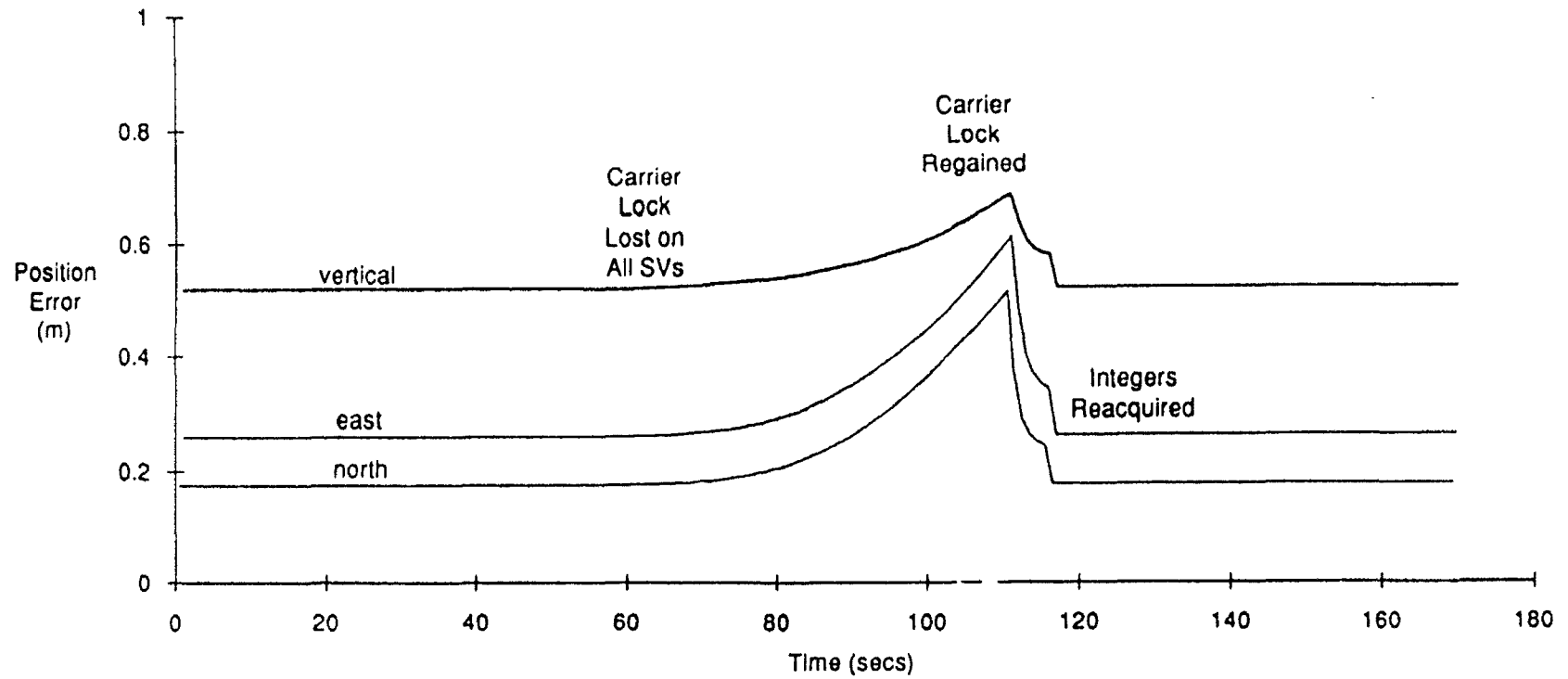

ionospheric errors and S/A). In simpler terms, the sum of these residual errors and the position errors along each line of sight can be estimated at a level below the one sigma measurement noise, but it is not possible to separate the effects of the two. This is thus representative of a classical observability problem [10]. Nevertheless, the filter is able to correctly resolve the integer ambiguities following the gap, even with relatively large uncertainties in position; a correct integer does not reflect absolute range information along a given line of sight, but includes the effects of residual correlated ranging errors, which induce the positioning error in the resulting solution.

5.3.2.1 Complete Loss of GPS

Results for complete loss of GPS are summarized by Figure 5.3-3. The maximum tolerable gap length (in seconds) is plotted on the vertical axis, while the separation distance (in kilometers) is the horizontal scale. A total of 9 individual curves appear on the plot, corresponding to all possible combinations of high, medium and low quality INSs (designated by the use of a solid line, a dashed line and a dotted line, respectively) and wide, half-wide and normal laning receivers (designated by squares, diamonds and triangles, respectively). Note the very significant variations in performance with INS quality; a high quality INS is able to tolerate gaps between 60 and 70 seconds when operating with a wide-laning receiver, while a low quality INS can at best tolerate a gap of less than 20 seconds. Also note that the variation of gap length with separation distance is relatively minor; a maximum variation over the full range of separation distances of roughly 12 seconds occurs for the high quality INS operating with the normal laning GPS receiver. This is not surprising, based on the discussion at the end of the previous section. The larger separation distances significantly degrade positioning performance, but the ability to resolve the integers is based upon the total error along each line of sight, which is dominated by the INS position error growth during the gap (this error is of course, uncorrelated with the residual correlated ranging errors).

5.3.2.2 Three GPS Satellites Tracked During Gap

Results when three satellites are still being tracked during the gap are summarized in Fig. 5.3-4. Note the significantly different behavior from the previous case: much longer measurement gaps can generally be tolerated, especially for the wide-laning receiver; significant variation of gap length with separation distance occurs; and, for a given receiver type, results are relatively insensitive to INS quality. The longer gap lengths can be attributed to the filter reliance upon the rubidium frequency standard as a "pseudo satellite" to maintain an accurate clock during the gap. The maximum tolerable gap length is therefore no longer strongly dependent upon INS quality. In fact, maximum tolerable gap lengths of more than 200 seconds should be attainable without an INS. The more significant variation with separation distance can be attributed to the temporal decorrelation of the residual correlated errors, since the gap lengths for this case (especially for the wide-laning receiver, which exhibits the more pronounced variation with separation distance) are now significant relative to the correlation times of the errors.

Figure 5.3-3 Gap Length v. Separation Distance Loss of Four GPS Satellites

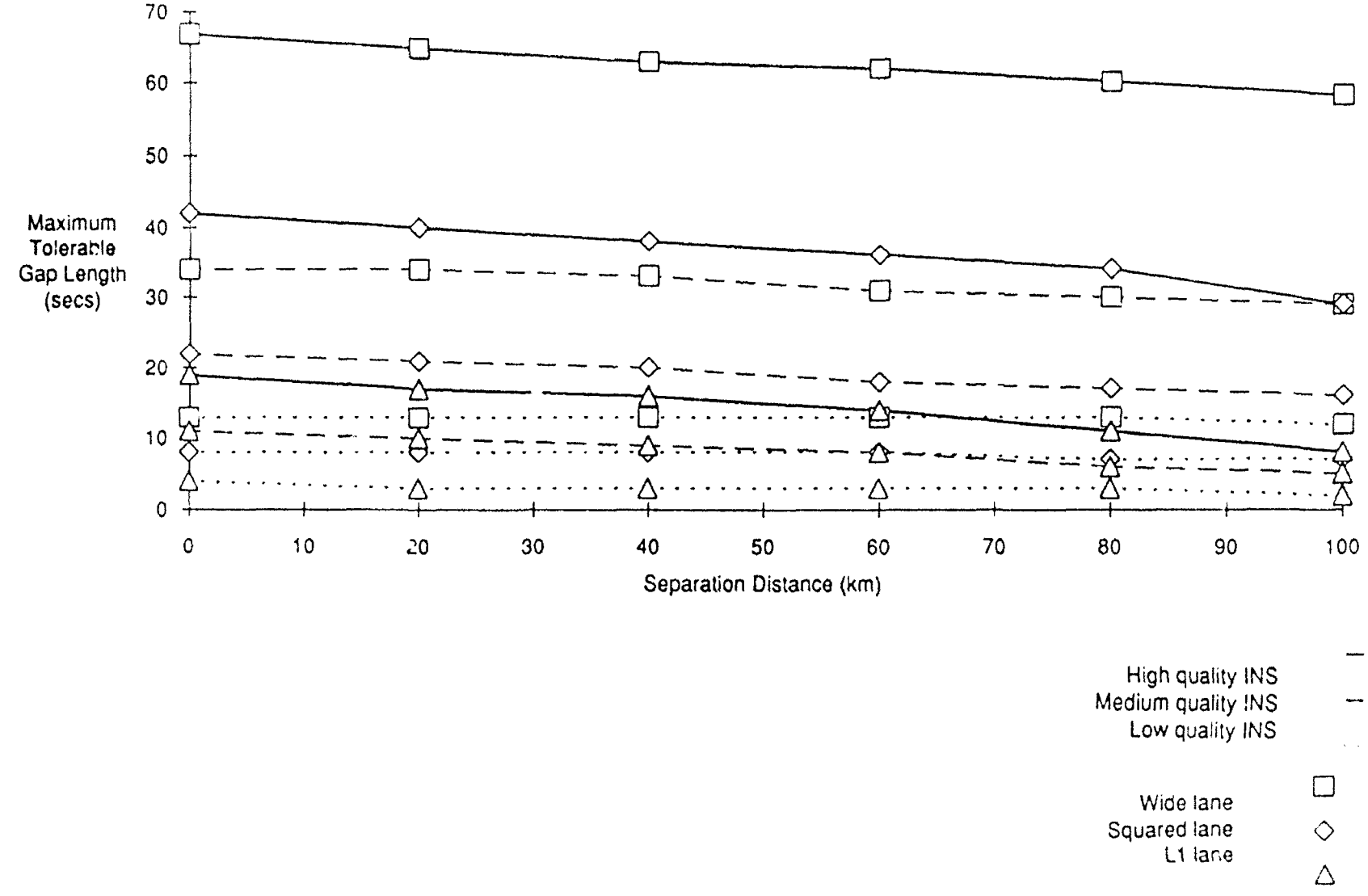

Figure 5.3-4 Gap Length v. Separation Distance Loss of One of Four GPS Satellites

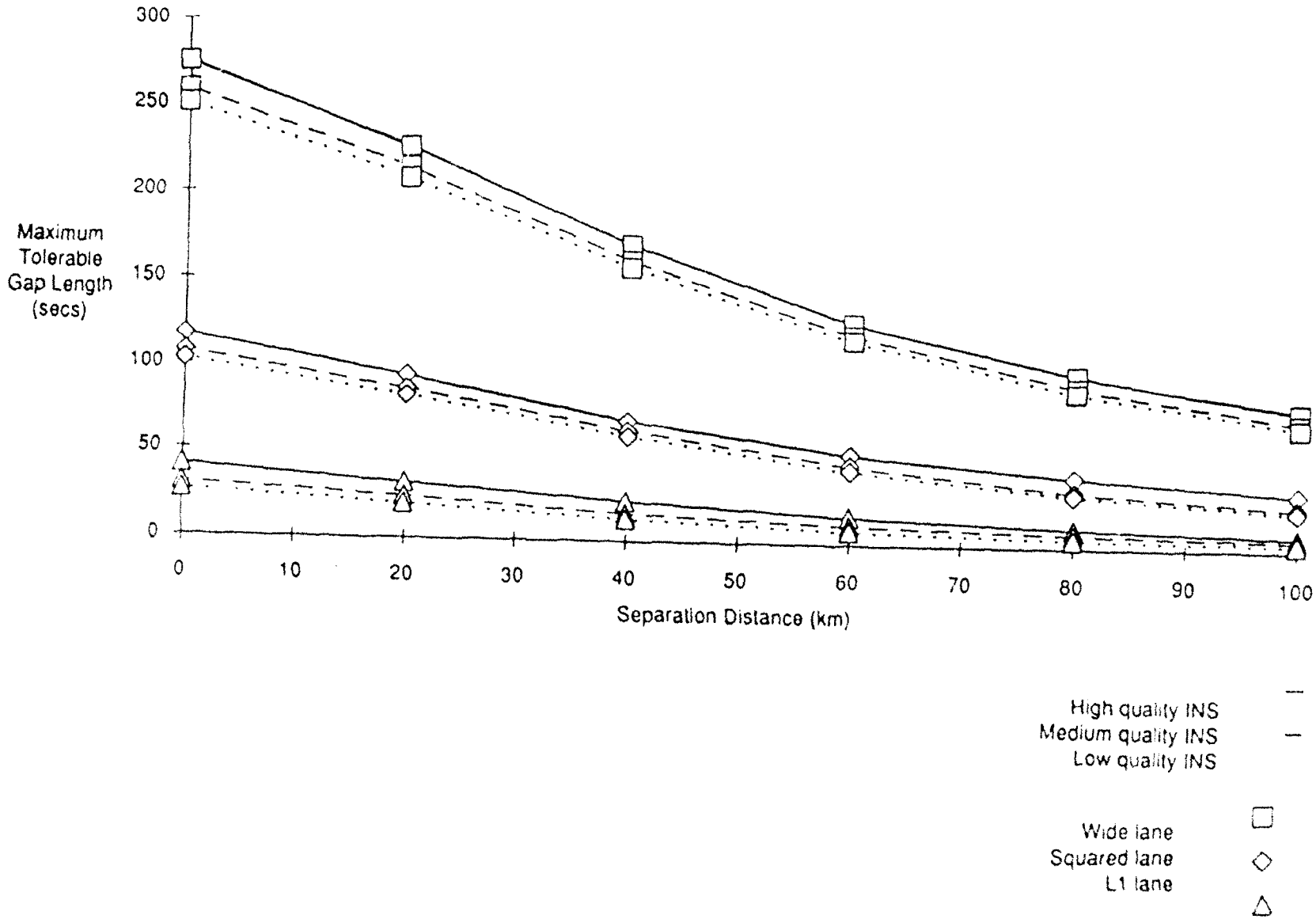

5.3.2.3 Two GPS Satellites Tracked During Gap

Results for 2 GPS satellites being tracked during the gap are presented in Figure 5.3-5. Virtually all the trends which appeared in Figure 5.3-3 for complete loss of GPS are apparent: the results are relatively insensitive to variations in separation distance, but differ significantly as a function of INS quality. The only difference from Figure 5.3-3 is the small improvement in tolerable gap length for all cases, e.g., about 10% for the high quality INS operating with wide-laning.

5.3.2.4 One GPS Satellite Tracked During Gap

Results for this case are presented in Figure 5.3-6, and are approximately midway between the results for loss of 2 satellites and 4 satellites. All the trends appearing in Figures 5.3-3 and 5.3-5 are therefore repeated in Figure 5.3-6.

5.3.2.5 Operation Without the Barometric Altimeter

Although the barometric altimeter is expected to be a relatively low cost item, it nevertheless represents an additional hardware component which must be integrated into the system, which can be costly and/or troublesome. Note, however, that even though the barometric altimeter may prove to have an insignificant role in coasting during GPS outages, it is probably required as a meteorological sensor for generation of the tropospheric model corrections. An additional set of simulations were performed to determine the tolerable gap length versus separation distance without barometric altimeter updates for a complete loss of GPS during the gap. Comparison of these results with the corresponding results from Figure 5.3-3 indicated that there was virtually no difference between the two (differences in gap length were generally less than 1 second). This implies that the INS vertical drift has been sufficiently calibrated during the assumed 60 second calibration period prior to the gap. Since the case corresponding to a complete loss of GPS was expected to produce the most significant differences when operating without the baro, there does not seem to be any motivation for including the baro altimeter in the system. Only when the INS vertical channel has not been accurately calibrated should the baro input be expected to affect performance. In this case, as discussed in the next paragraph, the use of a zero mean sea level input to an appropriately designed complementary filter should produce the same effect as the baro input.

In place of the barometric altimeter, altitude error growth can be bounded by use of a zero mean sea level input, which can be used in a manner similar to the conventional damping of an INS vertical channel using an externally supplied altitude. Figure 5.3-7 illustrates the concept; INS vertical acceleration, corrected by the last available update from the Kalman filter, is compensated by the feedback of the difference between computed and reference altitude, and then integrated to produce a vertical velocity estimate. Vertical velocity is similarly corrected by feedback of the difference between indicated and reference altitude, and then integrated to produce indicated altitude. Since the loop (as indicated) is second order, the loop gains can be expressed directly in terms of the resultant damping ratio and natural frequency, as indicated in the Figure. (A third order loop can be used). The loop represents what is generally referred to as a complementary filter: the INS is used as a source of high frequency

Figure 5.3-5 Gap Length v. Separation Distance Loss of Two of Four GPS Satellites

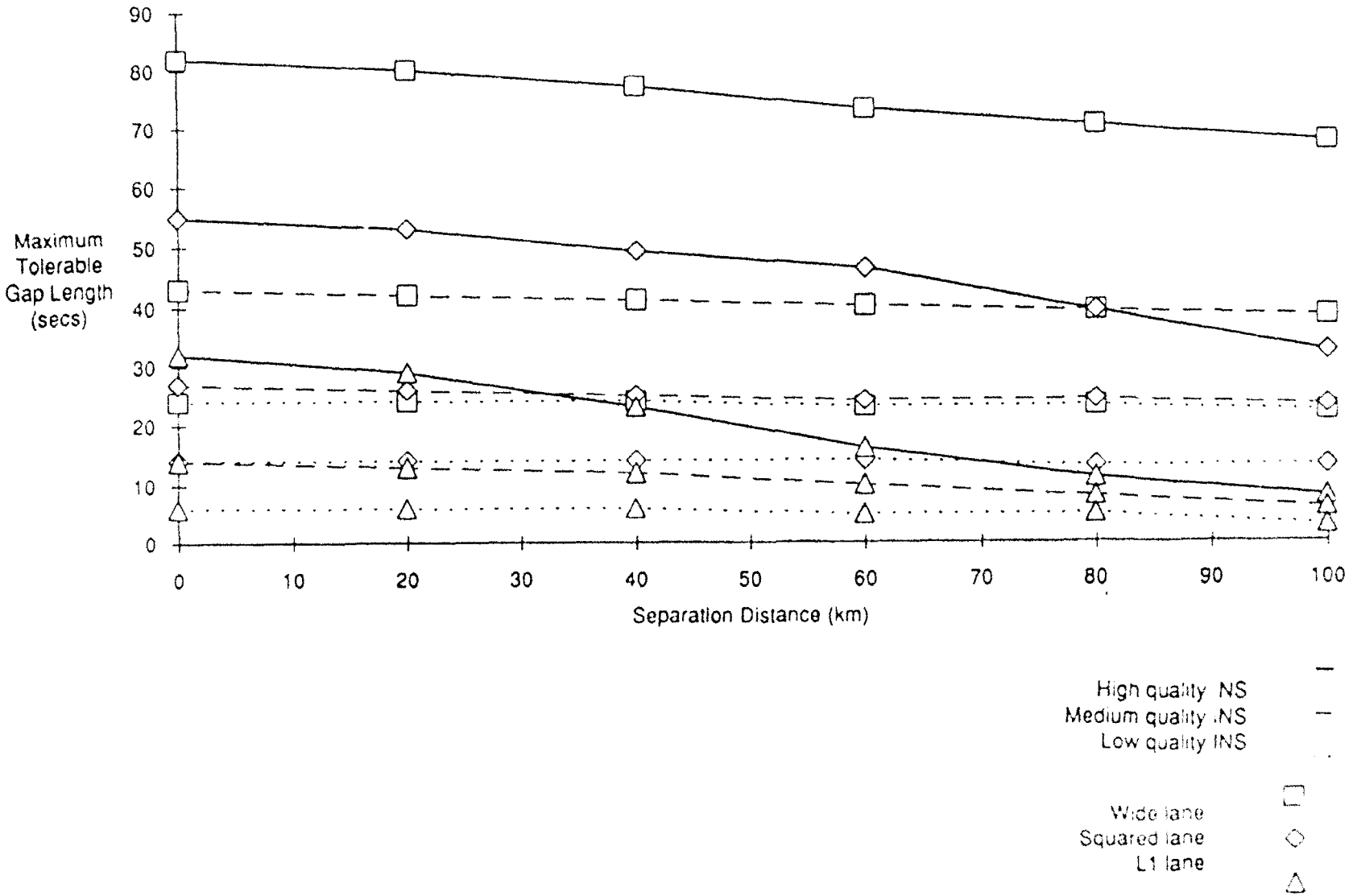

Figure 5.3-6 Gap Length v. Separation Distance Loss of Three of Four GPS Satellites

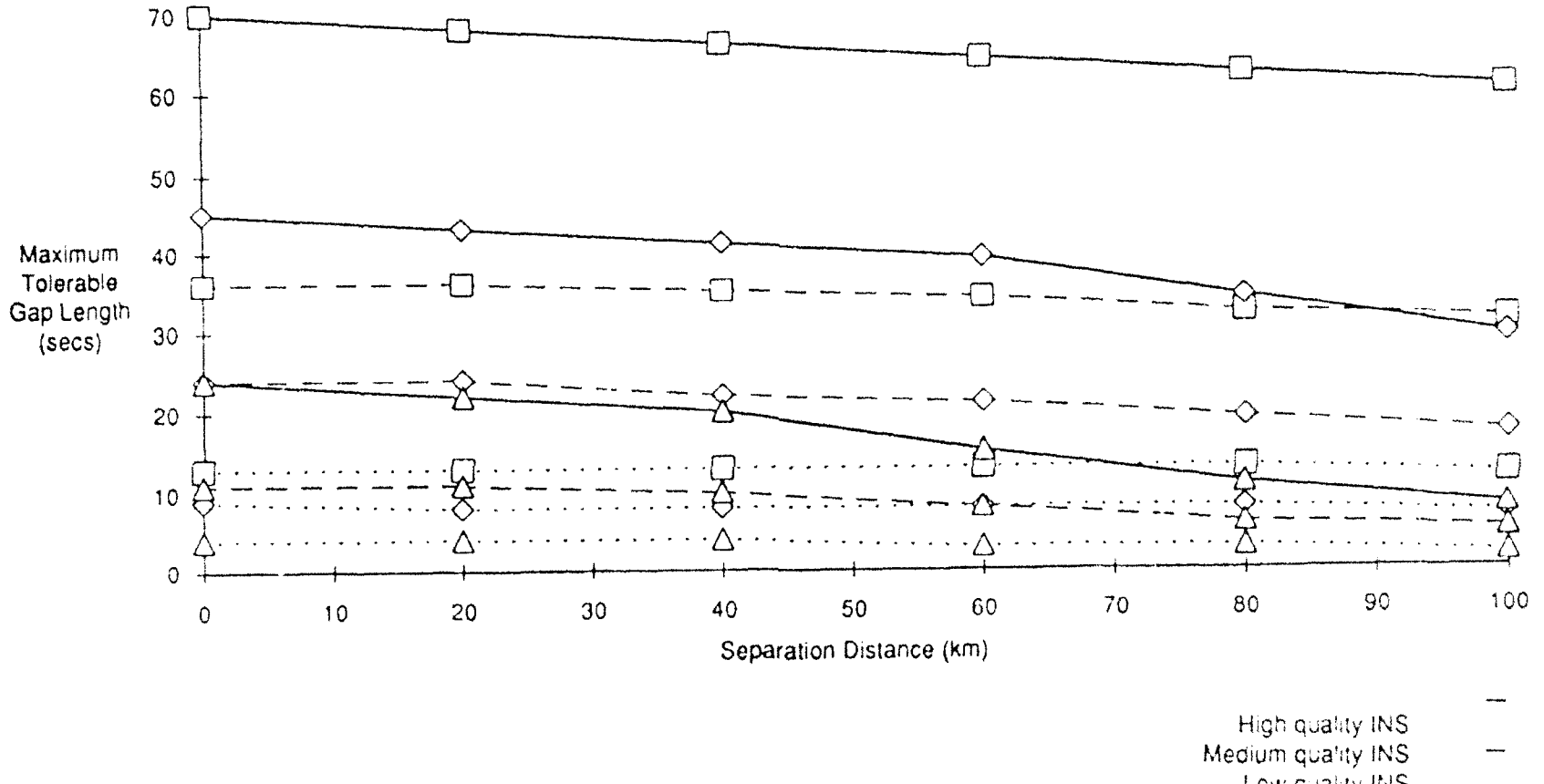

Figure 5.3-7 Zero Mean Sea Level Damping of Altitude Error Growth

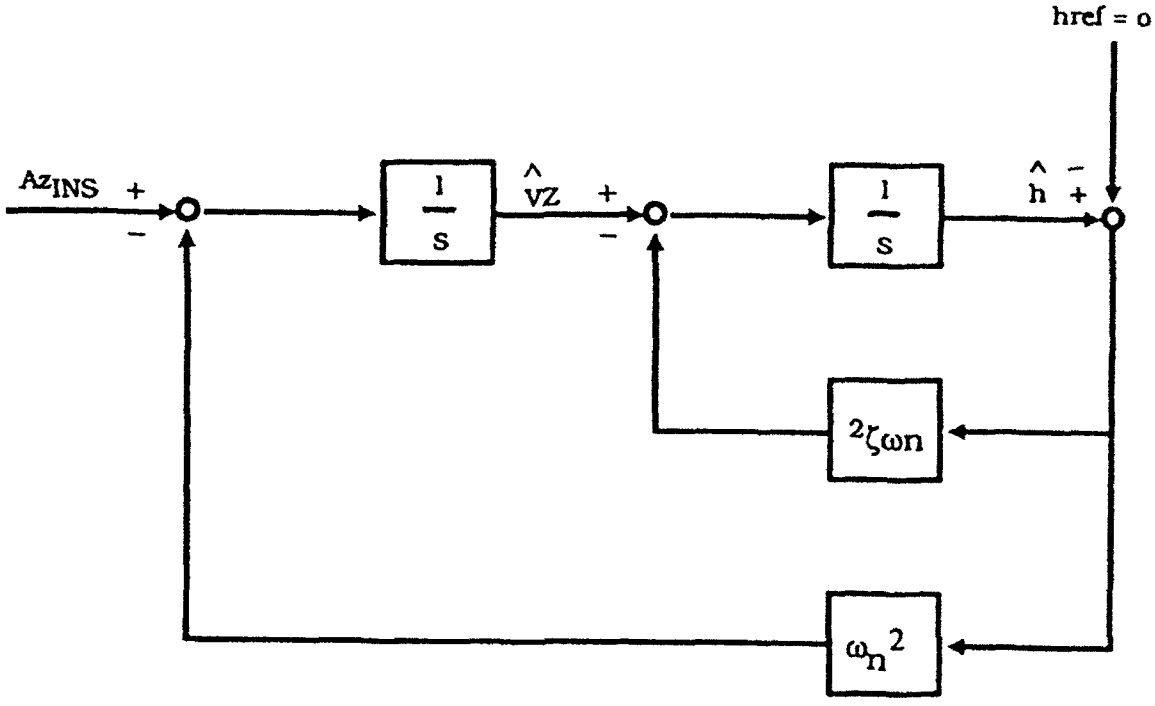

h_{ref}: Externally-supplied altitude reference

$A_{z_{INS}}$: Kalman filter compensated INS derived vertical acceleration

$\hat{V}z$: Vertical velocity estimate

ζ: Filter damping ratio

ω_n: Filter natural frequency

information, and so will be used to track the deviations from steady state caused by ocean wave motion; the steady state solution for altitude will be that supplied by the reference. The performance of the resultant scheme should therefore very closely follow the performance of a system equipped with a barometric altimeter.

5.4 Summary and Conclusions

When more than a single GPS satellite is lost, the use of a high quality INS can significantly increase the maximum tolerable gap length, permitting rapid reacquisition of the correct set of integer ambiguities. Maximum gap lengths range from 10 to 80 seconds for the high quality INS, as a function of separation distance and receiver type. Of these, receiver type plays a more important role than separation distance. Variation with separation distance for a given INS quality and receiver type is relatively minor; at most, 15 seconds over the range from 0 to 100 km is observed. On the other hand, variations with receiver type are significant for all INS qualities, e.g., a high quality INS can withstand a gap of 70 seconds when operating with a wide-laning receiver, but the length is reduced to roughly 40 seconds when using a half-wide-laning receiver.

Significantly different trends are observed when only a single satellite is lost. Here, only minor differences can be attributed to INS quality and greater variations with separation distance occur (especially for the longer gap lengths). Maximum gap lengths of more than 250 seconds can be accommodated, due to the assumed use of a rubidium frequency standard.

Use of a barometric altimeter, as an aid for gap filling, is not necessary. When the INS vertical channel has been given sufficient time with full GPS coverage (i.e., 60 seconds), no significant performance benefits are derived from the incorporation of the baro inputs. Periods following inaccurate calibration of the baro can be handled using a zero mean sea level damping input to a complementary filter (Figure 5.3-10).

6.0 Navigation Performance Prediction

6.1 Discussion of Differential GPS Operation

In this section, the navigation performance of the kinematic phase positioning system is predicted. The error budget proposed here is essentially the budget for high-precision differential GPS, with identical error sources: differential troposphere, differential ionosphere, computed satellite position, multipath and tracking loop error. Resolution of the integer or lane ambiguity, using techniques previously described, is assumed to have been successfully performed. Although knowledge of the lane integers implies a pseudorange accuracy of better than a half-wavelength, this does not necessarily translate directly into differential position accuracy of the same order. When the mobile receiver is far from the reference receiver, the differential position accuracy is affected by differential tropospheric and ionospheric refraction and miscomputation of the satellite position, as well as carrier phase noise and multipath at the individual receivers. Although most of the GPS error due to these error sources is common to all receivers in a wide area, over tens of kilometers the effect of each error changes slightly. This is often referred to as spatial decorrelation of the pseudorange error.

Since much of the change in the pseudorange error is linear over distance, spatial decorrelation effects can to a certain extent be removed by a network of reference receivers. The efficacy of networked corrections is addressed in this portion of the study as well as the accuracy of differential corrections. To illustrate the concept of networked corrections, consider a master reference station and two additional "monitor" reference stations, one directly to the north of the master and another directly to the east. Using the two master/monitor pairs of reference stations, the change in pseudorange error with respect to distance in each direction can be measured in real time and broadcast with the pseudorange corrections.

The user adjusts the received differential corrections for his own location by applying a simple linear function using the measured gradients as coefficients to the difference between the user position $\underline{x}^{user}$ and the master reference position $\underline{x}^{ref1}$:

$\partial PRC/\partial N$ = gradient of PRC in northerly direction
$\partial PRC/\partial E$ = gradient of PRC in easterly direction

$$PRC^{user} = PRC^{ref} + (\partial PRC/\partial N,\ \partial PRC/\partial E,\ 0) * (\underline{x}^{user} - \underline{x}^{ref1})$$

The gradients $\partial PRC/\partial N$ and $\partial PRC/\partial E$ (the vertical gradient is assumed to have negligible importance) are obtained by best linear fit of measurements from the monitor and master stations. In general the stations will not be placed directly north and east of the master reference stations, and the pseudorange corrections can be computed directly as a linear function of the PRCs at the reference stations in the network:

$$PRC^{user} = a_1\ PRC^{ref1} + a_2\ PRC^{ref2} + a_3\ PRC^{ref3}.$$

where the coefficients a_i are obtained by solving for the (horizontal) position of the user, $\underline{x}^{user}$, in terms of the positions of three reference stations, and minimizing the error $\underline{\varepsilon}$:

$$\underline{x}^{user} = a_1 \underline{x}^{ref1} + a_2 \underline{x}^{ref2} + a_3 \underline{x}^{ref3} + \underline{\varepsilon}.$$

The term $\underline{\varepsilon}$ is an error term that absorbs altitude errors or, in the case of two reference stations, lateral error perpendicular to the line between the stations. By picking an imaginary $\underline{x}^{user}$ directly north or east of the master station, one can obtain the north and east gradients described above.

The gradients are broadcast as a relatively short message at relatively low rates from the master station. The impact of the message is lessened because the spatial decorrelation errors are small compared to the total error carried by the high-rate differential correction message. Precision requirements for reporting the gradients is only a few digits, all that is required to maintain ranging accuracy to a level of well under one part per million. The message update rate depends primarily on how quickly the gradients change over time. Note that the gradients change much more slowly than the total error, which is dominated by the clock dither error function of S/A. The highest expected contributor to gradient dynamics is ionospheric activity, which probably produces less than 1 ppm variation in 100 seconds under operational GPS conditions. Preliminary study indicates a 100 second update rate is more than adequate. At this rate, the gradients add only a few bits per second to the master station message, and so are not included in Table 3.4-1.

The gradients are caused by three basic effects. Examining these effects in detail assists in determining the efficacy and form of a multiple reference station network. The magnitudes, decorrelation distances and the decorrelation times of the differential errors are of particular importance in designing the system.

6.2 Simulation Description

The simulation considers a number of scenarios, with separation distances from 0 to 120 km and using a single reference station or a network of two or three reference stations.

A block diagram of the simulation used in predicting navigation performance is provided in Figure 6.2-1. The simulation is a hybrid Monte Carlo/linear error covariance program. The Monte Carlo is provided by choosing random satellite geometry cases (a random time for the so-called 21+3 constellation). For each case, a linear error covariance model was used to establish accuracy performance. Results were averaged over 1000 random cases.

For each satellite geometry, models are used to compute S/A and ionospheric and tropospheric delay error statistics. These are combined into differential range error statistics, and a least squares solution algorithm is used to predict the one sigma positioning error. If monitor stations are used as well as a master station, the error statistics of the gradients are included. When operating with a 3 station network, the relative geometry depicted in Figure 6.2-2, representative of operations off the coast of

Figure 6.2-1 Navigation Error Simulation Overview

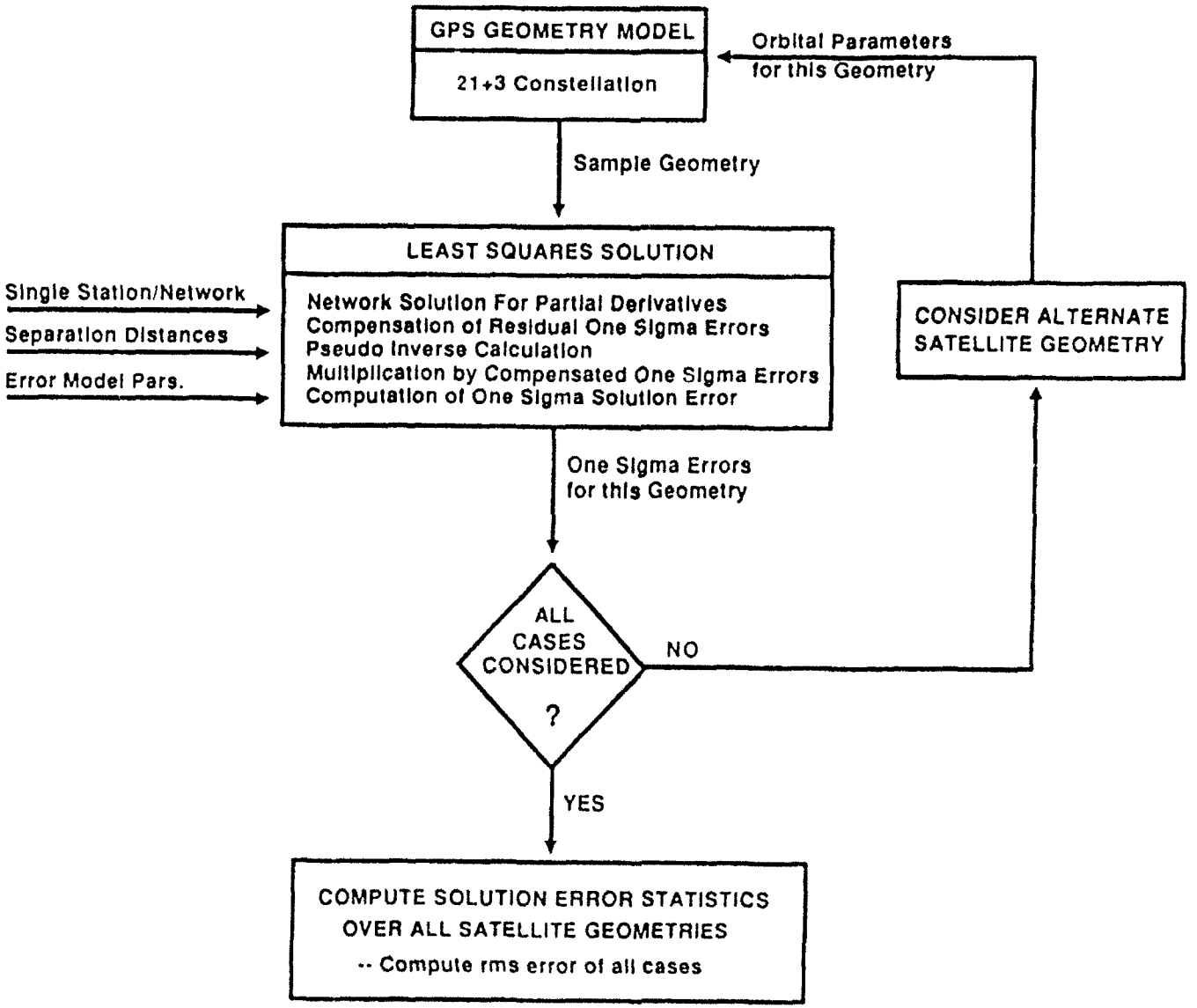

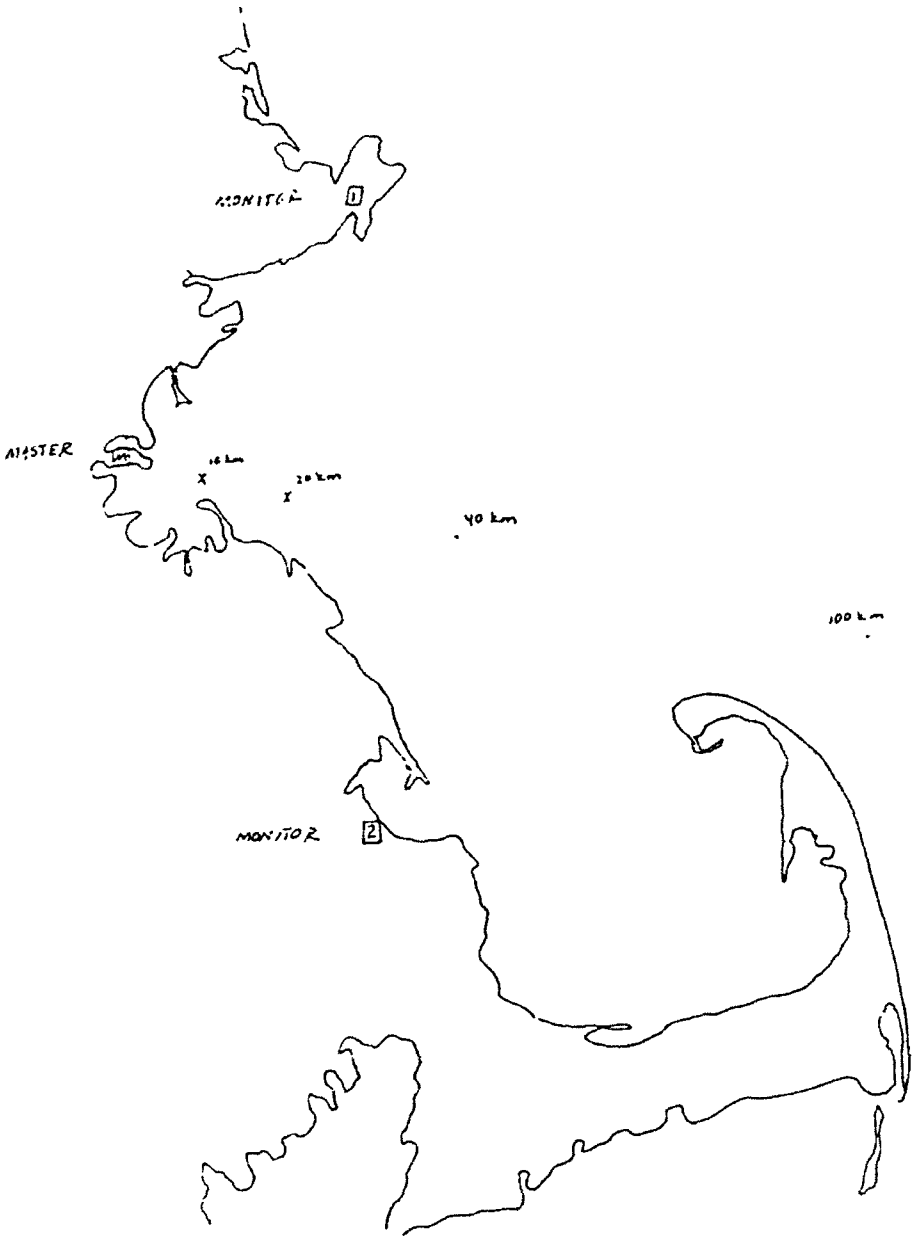

Figure 6.2-2 Simulated Network Layout in Massachusetts Bay

Massachusetts, is assumed. The master station is at Logan Airport, and two monitor stations at Gloucester to the northeast and Plymouth to the southeast. A two station mode was also studied, with two reference stations 140 km apart along the Texas coast (Figure 6.2-3). In the Massachusetts Bay case, user separation distances of 0 km to 120 km from the master reference station at Logan were considered; for the Texas coast, user separation distances of 0 km to 120 km from the midpoint of the line between the reference stations.

6.2.1 Error Modelling

6.2.1.1 Computed Orbit Error

The major component here is the intentional degradation in the broadcast orbit parameters to unauthorized users, termed Denial of Accuracy or S/A. S/A degradation is a combination of two processes, epsilon and clock dither. Only epsilon causes perceptible differential range error; clock dither is usually completely removed by differential techniques. The epsilon process comprises the broadcast of slightly incorrect orbit parameters, resulting in range error on the order of 30 meters under normal conditions. Geometry considerations produce different range error for different locations, which can be explained as follows. Given the baseline $\underline{B}$ between reference and user, the satellite position error $d\underline{S}$, and the range vector to the satellite of $\underline{R}$, the differential range error due to epsilon is roughly:

$$(\underline{k} \times (\underline{B} \times \underline{R}))^t \, d\underline{S} \, / \, \underline{R}^3.$$

The maximum differential range error is roughly (BdS)/20,000, where B is baseline distance in kilometers and dS is the radial satellite position error in meters. With typical values for the standard deviation of dS around 30 m, the range error increases with baseline length at a ratio of 0.15 cm/km, or 1.5 ppm.

The epsilon component of differential range error changes very slowly, and very predictably, over time. It is not a driver for the update rate of gradient messages.

6.2.1.2 Ionospheric Delay

If the user and the reference station both have an ionospheric error, but it is the same at the two stations, it will drop out under differencing. Under normal continental United States (CONUS) ionospheric conditions, one can expect the ionospheric effect on range error to vary at the rate of less than 1 mm/km. Infrequently this will rise as high as 5 mm/km, and on rare occasions into the 10 mm/km range. Outside CONUS, 3 mm/km is not uncommon and one instance of 50 mm/km position error has been reported in Antarctica. Ionospheric variations under the effects of the auroras in the polar and subpolar regions can be quite severe. The simulation used an ionospheric rate standard deviation of 1 mm/km. It is reasonable to assume that large scale ionospheric effects, such as moving ionospheric waves and diurnal activity, are to a large extent linear with distance on the 100 km scale. Other ionospheric activity, such as scintillations or storms, may be very local. Because the latter effects are not linear over a wide area, they will not be mitigated by networked corrections, and are modeled in the simulation as a correlated process over distance.

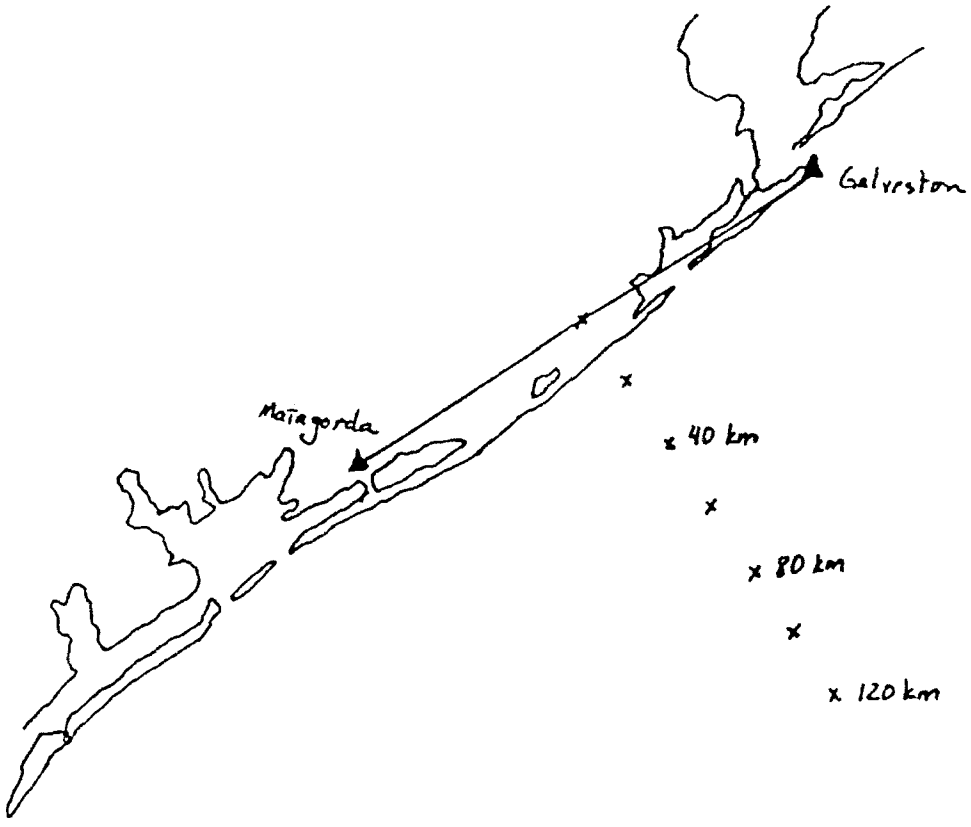

Figure 6.2-3 Simulated Network Layout in Texas Bay

Ionospheric delay affects the user only if he is relying on a differential ionospheric model rather than direct dual-frequency measurement of the ionosphere. The model becomes important if only one carrier frequency is being used or if linear combinations of both frequencies are used which preclude use for ionospheric correction (e.g. wide-lane).

6.2.1.3 Tropospheric Delay

Like ionospheric delay, most tropospheric error will drop out under differencing. Compared to ionospheric delay, tropospheric delay tends to decorrelate over shorter distances. The wet part of troposphere effect seems to decorrelate particularly quickly. As a general rule, the more accurate the tropospheric modelling, the shorter the modelling error correlation distance. For a good tropospheric model (e.g., the Hopfield model), field experience has indicated differential tropospheric error on the order of 2-3 cm decorrelating over tens of kilometers. At worst, unusual tropospheric events, such as severe electrical storms, can cause short-term errors on the order of many centimeters; these are considered rare enough to not be included in the statistics. Decorrelation distances are short enough on differential tropospheric ranging error that it acts similar to receiver noise at longer distances.

Table 6.1 shows the major differential range error sources and the range of error standard deviation values attributed to them, as well as the values used in the performance simulations.

Table 6.1: Differential Range Error Contributors

error type	std dev-range	std dev-sim value
tropsphere	0.1 - 0.5 cm/km$^{1/2}$	0.3 cm/km$^{1/2}$
inonsphere (trend)	0.0 - 1.0 cm/km	0.1 cm/km
ionosphere (random)	0.0 - 0.2 cm/km$^{1/2}$	0.07 cm/km$^{1/2}$
orbit error	0.0 - 0.2 cm/km	0.15 cm/km
multipath/noise	0.5 - 3.0 cm	1.0 cm

6.2.2 Results Summary

The simulation results are summarized in Figures 6.2-4 through 6.2-6. The results show that decimeter-level positioning is indeed achievable, although in the vertical it is somewhat dicey at longer separation distances. The accuracy figures represent an average over 1000 random satellite geometries in Massachusetts Bay for both a single reference receiver and a three station network, and both dual and single frequency receivers.

Accuracies are presented as standard deviations in horizontal (RSS of east and north) and vertical directions, in centimeters.

As expected, dual frequency receivers (used in ionosphere-corrected mode) have an "error floor" roughly three times higher than single frequency (L1) receivers at zero separation. This is because receiver noise and multipath is misinterpreted in the ionosphere correction process as ionospheric delay, resulting in a range error. In a well-designed system, the two frequencies would be averaged at short ranges to reduce noise and multipath effects, with the averaging gradually turning into ionospheric correction at longer distances. This would result in better performance than a single frequency system at zero baseline. The results shown below are strictly ionospheric-corrected dual frequency (ICDF) and do not reflect such a system design. In fact, the results indicate that ionospheric correction is a hindrance rather than a help in the network. This is expected under the assumption that ionosphere effects are roughly linear with distance over the area under consideration and thus completely observable by the network.

A note is appropriate about the general performance of the network. First, performance of the network and the differential (single station) are identical at zero separation, because the gradients are not used (equivalently, the weighting coefficients a_2 and a_3 are zero). Second, network performance degrades at distances much larger than 30 km for the network in this study. Up to this distance, the user lies inside the triangle formed by the three reference stations and the PRCs are interpolated, which tends to average the noise effects. The optimal point is at the centroid of the triangle (at roughly 20 km), where all weighting coefficients $a_1 = a_2 = a_3 = 0.33$ and the noise is diminished by a factor of $(3)^{1/2}$. At longer distances the PRCs must be extrapolated, the weighting coefficients a_i become quite large, and their effect on the noise increases proportionately with distance. This especially hurts the ICDF system, whose higher measurement noise is effectively multiplied by the RSS of the weighting coefficients. The weighting coefficients for the different distances are listed in Table 6.2.

Table 6.2: Massachusetts Bay Network Weighting Coefficients

separation	a_0	a_1	a2	RSS
0 km	1.00	0.00	0.00	1.41
10 km	0.64	0.17	0.17	1.21
20 km	0.29	0.35	0.35	1.15
40 km	-0.40	0.70	0.70	1.46
60 km	-1.10	1.05	1.05	2.10
80 km	-1.80	1.40	1.40	2.86
100 km	-2.51	1.75	1.75	3.67
120 km	-3.21	2.10	2.10	4.49

The horizontal accuracy (Figure 6.2-4a) indicates that a single frequency network is the most effective in providing high-quality positioning,

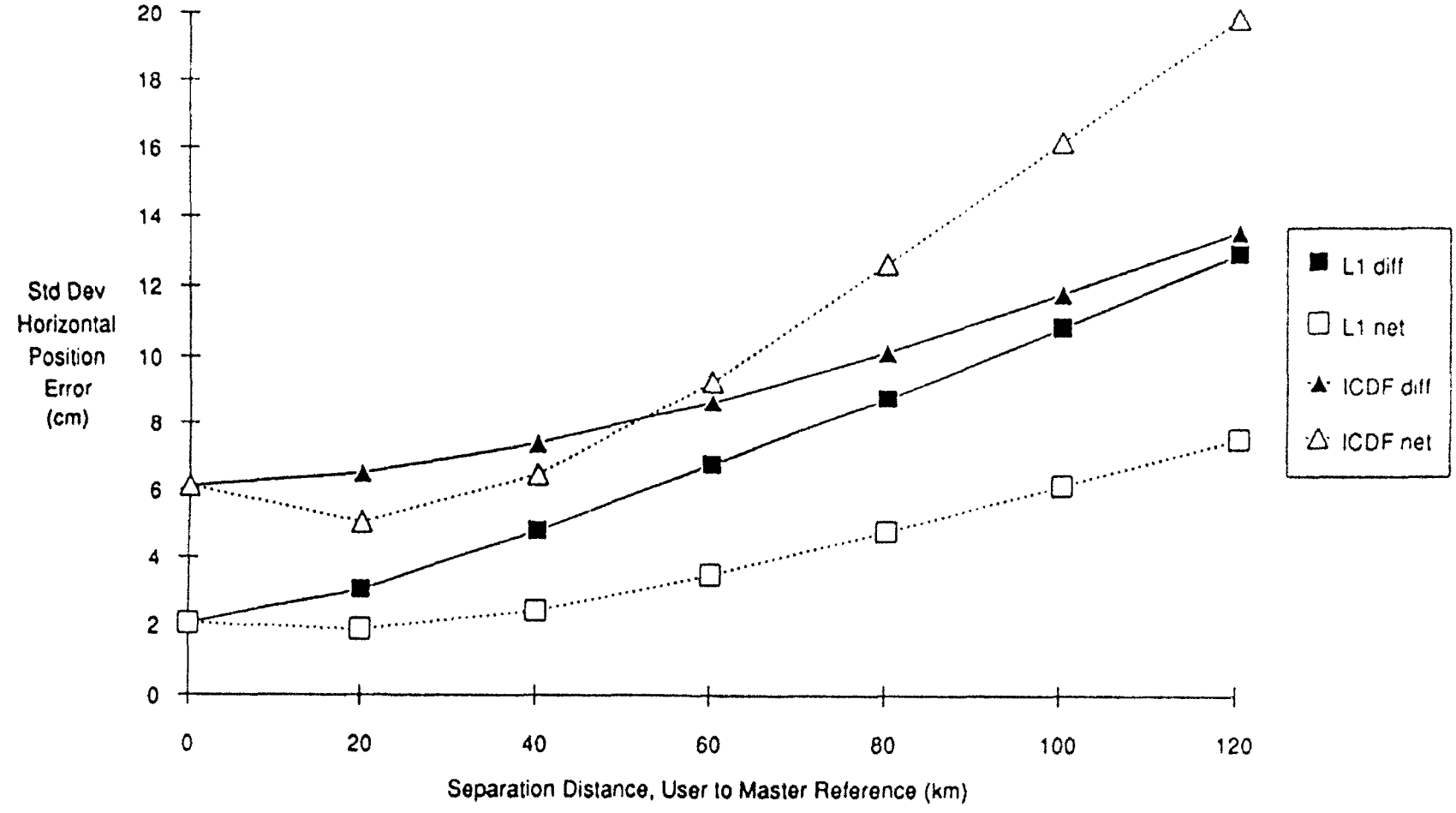

Figure 6.2-4a Differential Horizontal Accuracy: Network vs. Single Reference

performing better than a single reference differential or ICDF networks. The ICDF network degrades badly at longer distances due to the extra noise in the carrier measurements due to the ionospheric correction process and the size of the weighting coefficients a_i.

The vertical accuracy (Figure 6.2-4b) is roughly three times worse than the horizontal accuracy, with maximum error standard deviations on the order of 20-25 cm at 120 km. Note again the relatively good performance of the single frequency network and also the ICDF single-station differential. This indicates that ionospheric error is perhaps the largest contributor to vertical error at the larger separation distances.

Table 6.3 shows a breakdown of the accuracy results both for the two cases illustrated in the Figure 6.2-4 and a third case, the two-reference station scenario off the Texas coast, illustrated in Figure 6.2-5. In addition, the results corresponding to Figure 6.2-7 are summarized.

To test the performance of the network on single frequency under worsening ionospheric conditions, the same simulation was run but with the ionospheric trend values doubled to 2 ppm (1s). These values are typical of bad ionospheric conditions in CONUS, and the results are shown in Figure 6.2-6. The higher ionospheric values had no effect on the network solutions, as the network corrections effectively estimate and remove the ionospheric trends. Single differential stations suffered badly, barely able to meet the vertical decimeter-level accuracy at 10 km.

The last study examined the performance of wide-lane. With a two frequency receiver, especially in codeless mode, it is quite possible that the wide lane integer will be resolved but the L1 and L2 lanes will remain ambiguous. This is equivalent to uncertainty in the differential ionosphere. In this case, navigation will be done using the wide-lane phase, which is the difference between L1 and L2 phases. The sensitivity of this to troposphere and orbit error are identical to the previous cases, as these are independent of frequency. However, the effect of differential ionosphere is increased by a factor of 30% over single frequency, and the effect of multipath and noise is increased by nearly six-fold over single frequency and doubled over ICDF. Because of these, response is much worse than either single frequency or ICDF. A comparison of the wide-lane and single frequency performances is shown in Figure 6.2-7a and 6.2-7b for the Massachusetts Bay three station network.

Although the results for wide-lane are not by themselves impressive, the accuracy from the wide-lane positioning technique can conceivably be used to acquire the L1 and L2 lanes. The leap from wide-lane to the base frequencies is equivalent to measuring, or knowing a priori, the differential ionospheric effect on the L1 and L2 frequencies fairly accurately. This is probably possible over a few kilometers, and probably can be resolved over longer distances with a network. The dependence on good modeling of ionospheric behavior over these distances is so critical that we feel an effective study can not be done in a simulation with the current knowledge of ionospheric models.

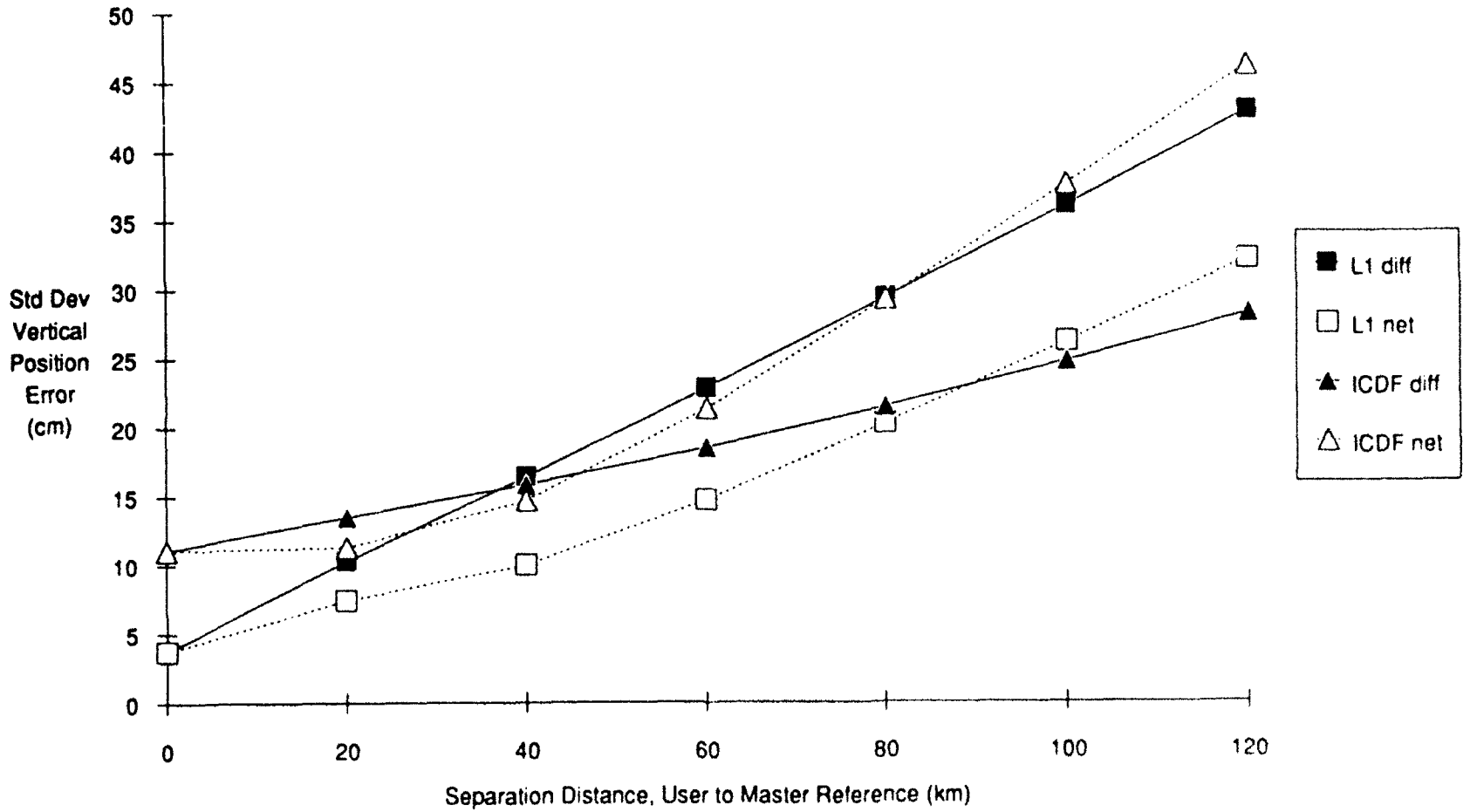

Figure 6.2-4b Differential Vertical Accuracy: Network vs. Single Reference

Table 6.3: Network Differential Accuracy Budget
(horizontal/vertical standard deviation in cm)

single reference station differential (Massachusetts Bay)

single frequency

km	noise	iono	tropo	orbit	total
0	2.05 / 3.71	0.00 / 0.00	0.00 / 0.00	0.00 / 0.00	2.05 / 3.71
20	2.05 / 3.71	0.68 / 5.65	0.80 / 6.63	2.00 / 4.07	3.05 /10.31
40	2.05 / 3.71	1.36 /11.31	0.96 / 7.98	4.00 / 8.14	4.79 /16.48
60	2.05 / 3.71	2.04 /16.96	1.02 / 8.52	5.99 /12.21	6.73 /22.88
80	2.05 / 3.71	2.72 /22.63	1.05 / 8.75	7.99 /16.28	8.75 /29.45
100	2.05 / 3.71	3.40 /28.29	1.06 / 8.85	10.00 /20.36	10.81 /36.15
120	2.05 / 3.71	4.08 /33.96	1.07 / 8.90	12.00 /24.43	12.88 /42.93

ionospherically corrected dual frequency

km	noise	iono	tropo	orbit	total
0	6.12 /11.06	0.00 / 0.00	0.00 / 0.00	0.00 / 0.00	6.12 /11.06
20	6.12 /11.06	0.00 / 0.00	0.80 / 6.63	2.00 / 4.07	6.49 /13.52
40	6.12 /11.06	0.00 / 0.00	0.96 / 7.98	4.00 / 8.14	7.37 /15.88
60	6.12 /11.06	0.00 / 0.00	1.02 / 8.52	5.99 /12.21	8.63 /18.55
80	6.12 /11.06	0.00 / 0.00	1.05 / 8.75	7.99 /16.28	10.12 /21.54
100	6.12 /11.06	0.00 / 0.00	1.06 / 8.85	10.00 /20.36	11.77 /24.80
120	6.12 /11.06	0.00 / 0.00	1.07 / 8.90	12.00 /24.43	13.51 /28.25

wide lane

km	noise	iono	tropo	sa	total
0	11.80 /21.32	0.00 / 0.00	0.00 / 0.00	0.00 / 0.00	11.80 /21.32
20	11.80 /21.32	0.87 / 7.25	1.78 /14.81	2.00 / 4.07	12.13 /27.26
40	11.80 /21.32	1.74 /14.51	2.14 /17.84	4.00 / 8.14	12.76 /32.39
60	11.80 /21.32	2.61 /21.77	2.29 /19.04	5.99 /12.21	13.68 /37.95
80	11.80 /21.32	3.49 /29.04	2.35 /19.55	7.99 /16.28	14.86 /44.10
100	11.80 /21.32	4.36 /36.31	2.38 /19.78	10.00 /20.36	16.24 /50.78
120	11.80 /21.32	5.23 /43.58	2.39 /19.88	12.00 /24.43	17.78 /57.85

two station network differential (Texas coast)

single frequency

km	noise	iono	tropo	orbit	total
0	1.68 / 3.26	0.04 / 0.07	0.80 / 8.53	0.04 / 0.07	1.87 / 9.13
20	1.68 / 3.26	0.57 / 6.08	0.81 / 8.59	1.75 / 3.67	2.62 /11.61
40	1.68 / 3.26	1.14 /12.10	0.82 / 8.72	3.48 / 7.29	4.11 /16.92
60	1.68 / 3.26	1.71 /18.13	0.83 / 8.84	5.21 /10.92	5.80 /23.16
80	1.68 / 3.26	2.28 /24.15	0.84 / 8.92	6.95 /14.54	7.55 /29.75
100	1.68 / 3.26	2.84 /30.18	0.85 / 8.97	8.68 /18.16	9.32 /36.49
120	1.68 / 3.26	3.41 /36.21	0.85 / 9.00	10.41 /21.79	11.12 /43.33

ionospherically corrected dual frequency

km	noise	iono	tropo	orbit	total
0	5.02 / 9.70	0.00 / 0.00	0.80 / 8.53	0.04 / 0.07	5.08 /12.92
20	5.02 / 9.70	0.00 / 0.00	0.81 / 8.59	1.75 / 3.67	5.37 /13.47
40	5.02 / 9.70	0.00 / 0.00	0.82 / 8.72	3.48 / 7.29	6.16 /14.94
60	5.02 / 9.70	0.00 / 0.00	0.83 / 8.84	5.21 /10.92	7.28 /17.07
80	5.02 / 9.70	0.00 / 0.00	0.84 / 8.92	6.95 /14.54	8.61 /19.63
100	5.02 / 9.70	0.00 / 0.00	0.85 / 8.97	8.68 /18.16	10.06 /22.46
120	5.02 / 9.70	0.00 / 0.00	0.85 / 9.00	10.41 /21.79	11.59 /25.49

three station network differential (Massachusetts Bay)

single frequency

	km noise	iono	tropo	orbit	total
0	2.05 / 3.71	0.00 / 0.00	0.00 / 0.00	0.00 / 0.00	2.05 / 3.71
20	1.68 / 3.03	0.01 / 0.00	0.81 / 6.77	0.01 / 0.01	1.87 / 7.42
40	2.13 / 3.85	0.02 / 0.01	1.11 / 9.25	0.01 / 0.01	2.40 /10.02
60	3.06 / 5.54	0.03 / 0.04	1.64 /13.63	0.02 / 0.02	3.47 /14.71
80	4.17 / 7.53	0.05 / 0.09	2.27 /18.89	0.03 / 0.03	4.74 /20.34
100	5.33 / 9.64	0.07 / 0.16	2.93 /24.38	0.06 / 0.11	6.08 /26.21
120	6.53 /11.80	0.11 / 0.24	3.59 /29.92	0.10 / 0.18	7.46 /32.16

ionospherically corrected dual frequency

	km noise	iono	tropo	orbit	total
0	6.12 /11.06	0.00 / 0.0	0.00 / 0.00	0.00 / 0.00	6.12 /11.06
20	5.00 / 9.03	0.00 / 0.00	0.81 / 6.77	0.01 / 0.01	5.06 /11.29
40	6.34 /11.47	0.00 / 0.00	1.11 / 9.25	0.01 / 0.02	6.44 /14.73
60	9.12 /16.49	0.00 / 0.00	1.64 /13.63	0.02 / 0.03	9.27 /21.39
80	12.41 /22.42	0.00 / 0.00	2.27 /18.89	0.03 / 0.06	12.61 /29.32
100	15.88 /28.71	0.00 / 0.00	2.93 /24.38	0.06 / 0.11	16.15 /37.66
120	19.45 /35.16	0.00 / 0.00	3.59 /29.92	0.10 / 0.18	19.78 /46.16

wide-lane

	km noise	iono	tropo	sa	total
0	11.80 /21.32	0.00 / 0.00	0.00 / 0.00	0.00 / 0.00	11.80 /21.32
20	9.64 /17.42	0.01 / 0.00	2.08 /17.34	0.01 / 0.01	9.86 /24.58
40	12.23 /22.11	0.02 / 0.02	2.84 /23.69	0.01 / 0.02	12.56 /32.41
60	17.59 /31.79	0.04 / 0.06	4.19 /34.89	0.02 / 0.03	18.08 /47.20
80	23.92 /43.23	0.06 / 0.12	5.81 /48.38	0.03 / 0.06	24.61 /64.88
100	30.62 /55.35	0.09 / 0.20	7.49 /62.42	0.06 / 0.11	31.53 /83.42
120	37.51 /67.78	0.14 / 0.31	9.20 /76.61	0.10 / 0.18	38.62/102.29

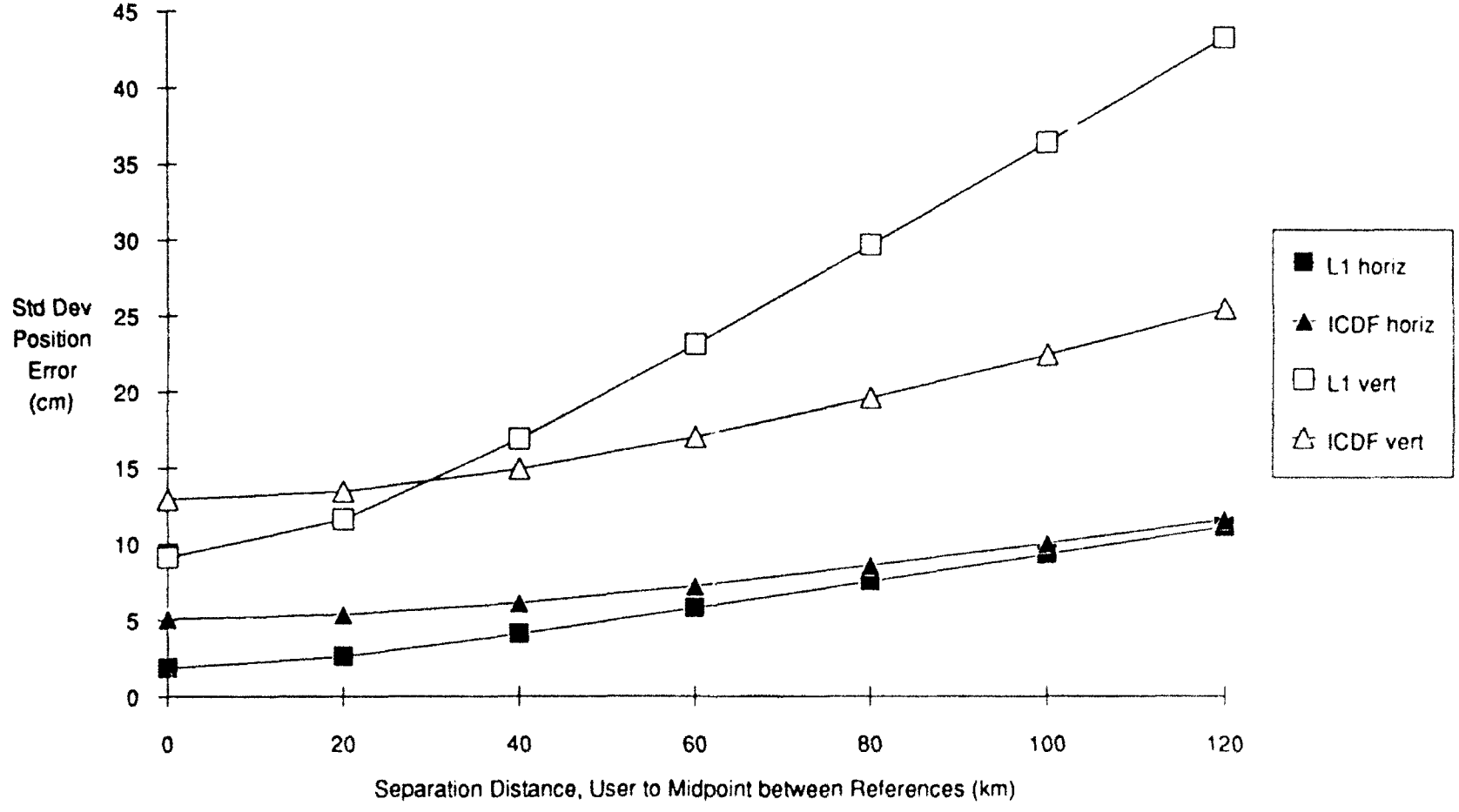

Figure 6.2-5 Differential Accuracy: Two Reference Network

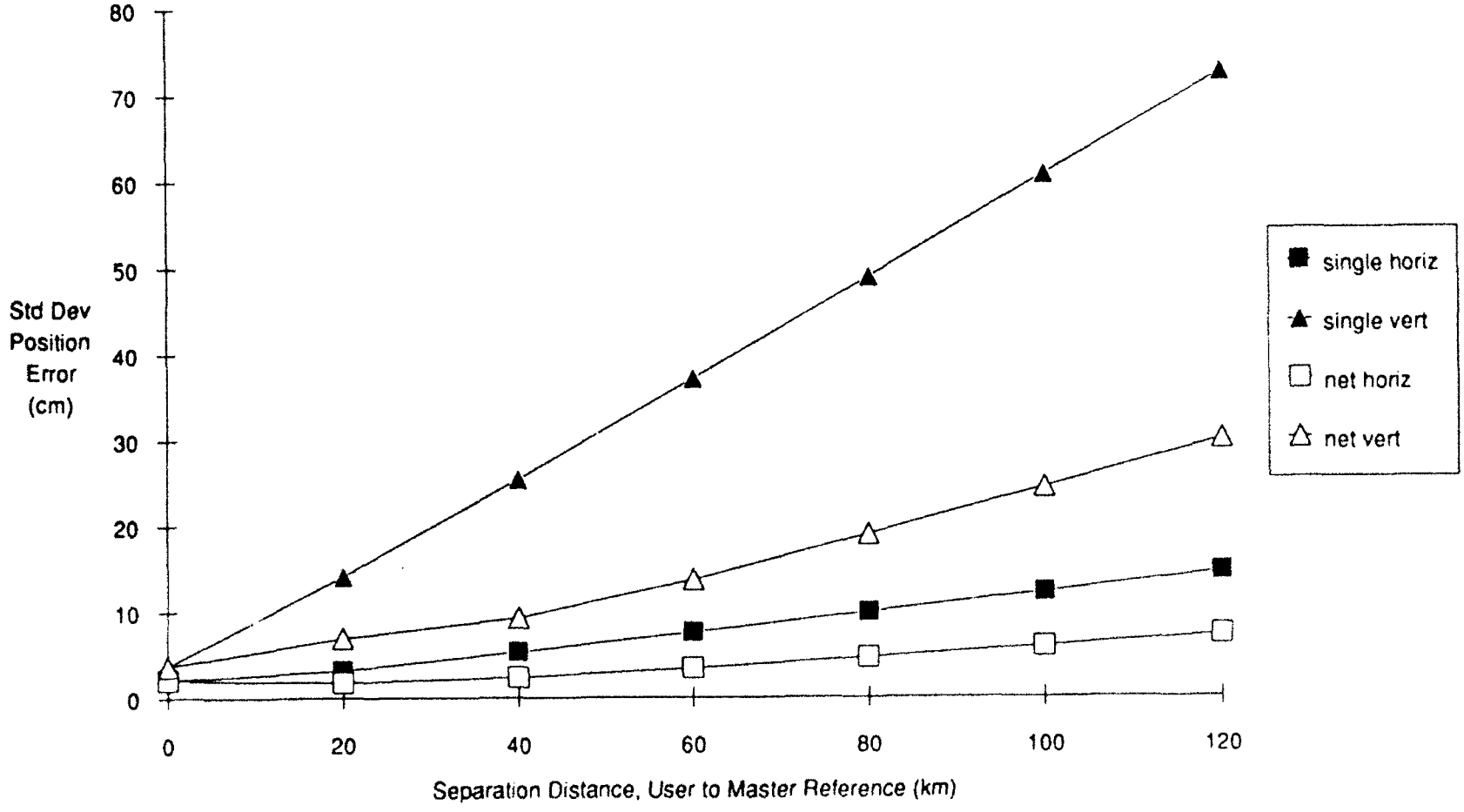

Figure 6.2-6 Single Frequency Differential Accuracy Under Severe Ionosphere Conditions

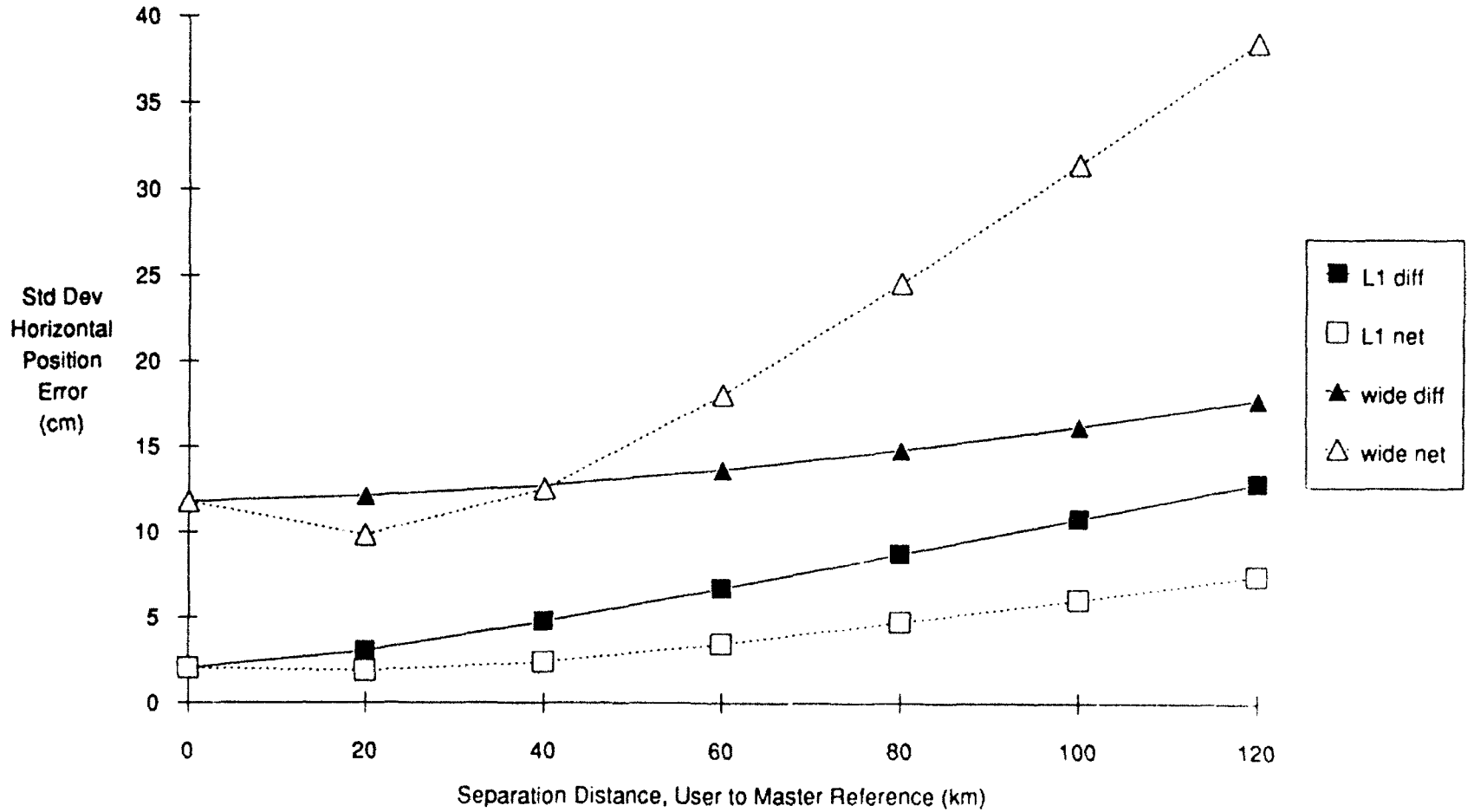

Figure 6.2-7a - Comparison of Widelane and Single Frequency Accuracies

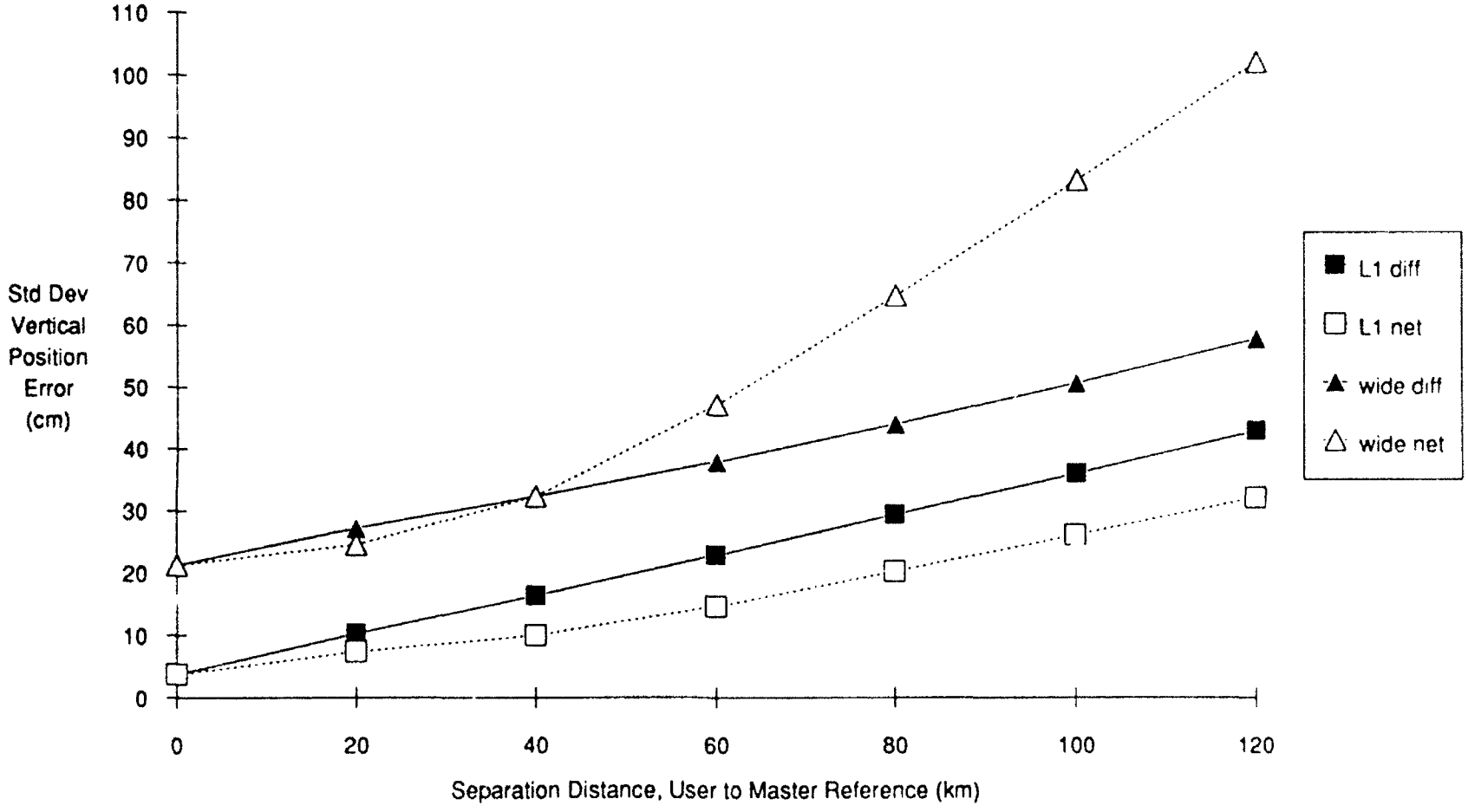

Figure 6.2-7b - Comparison of Widelane and Single Frequency Accuracies

6.3 Summary and Conclusions

The results of the simulations indicate that the performance of the differential system is sensitive to networking in the environments expected to be encountered in normal dredging operations. A decimeter-level vertical accuracy can be sustained out to 20 km with single frequency differential and 40 km or perhaps further with a network of three reference stations surrounding the user. Lastly, if dual frequency is used, the system must not perform a simple ionospheric correction on the carrier data, as this will hinder performance considerably.

The subject of wide-area networks, those with several hundred kilometers between stations, must also be viewed with suspicion in the light of the above simulation results. Wide-area networks postulate that the gradients are relatively constant over wide areas. Specifically, these gradients could be measured and broadcast from a network of perhaps ten to thirty monitor stations over CONUS, as might be established by the US Coast Guard (USCG), National Oceanographic and Atmospheric Administration (NOAA) or USACE. This would work quite well for dual frequency receivers, which can measure ionosphere; in fact, such a system has been proposed to the National Aeronautics and Space Administration (NASA) for shuttle emergency landing navigation. For single frequency and wide-laning situations, however, the wide-area concept is considerably higher risk, mainly because of the dominance of ionospheric effect. The wide-area concept depends on the linearity of the differential range error over large areas, and such linearity for ionospheric behavior has not been tested or documented. If, as expected, wide-laning is a critical technique in performing the dredging surveys, the wide-area network might be the only method to guarantee decimeter level vertical accuracy. Field testing on large scale fiducial networks focusing on this specific problem is required.

7.0 Cost and Risk Analysis

7.1 GPS Receiver Costs

Table 7.1-1, abstracted from [26], lists current off-the-shelf, survey quality GPS receivers. Summary cost data, also abstracted from [26], appears as Figure 7.1-1. As can be seen from the figure, costs range from $35K to $50K for high quality receivers. Excluded from the cost data is the Rogue receiver, designed by Jet Propulsion Laboratories (JPL) and built by Allen Osborne, which sells for $80K. A lower size, weight and power version of the Rogue, named Turbo-Rogue, which should also have improved tracking performance, is being developed and is expected to cost in the neighborhood of $40K, which should be competitive with other survey quality receiver designs. In addition, the Mini-Rogue, also expected to sell for $40K, is being developed by Allen Osborne; its projected availability date is December 1990. Note that, of the off-the-shelf GPS receiver designs listed in Table 7.1-1, only the Rogue is able to utilize a full wide-lane capability without use of the P-code. Of course, all designs which have a P-code tracking capability support wide-laning, e.g., the TI4100 and the WM102. Half-wide-laning is possible with MM2816, MM2816AT, and Macrometer II, in addition to the LD-X11, and the 4000ST and 4000SLD.

Limited design efforts are underway for the development of an integrated GPS/GLONASS receiver: Magnavox has financed an International Research and Development (IRAD) project for about 2 years [7], Ashtech is beginning a joint development with the former USSR, and the Federal Aviation Administration (FAA) has sponsored a development at Lincoln Laboratory. Due to the relatively immature state of these developments, no reliable cost data are available.

7.2 Reference Station Costs

As indicated in Figure 3.1-1, the major components of the reference stations are the GPS Receiver, a processor and display and a communications subsystem. The receiver costs have already been addressed; the processor and display costs are expected to be in the $3K-$5K range, assuming a 10 mHZ AT clone, with hard disk, and a monachrome graphics capability. The communications subsystem costs vary significantly between the master and monitor reference stations. For the master station:

- $4K for VHF/UHF radio.
- $300 for each of 2 modems (reception of monitor station data).

For each monitor station, a modem costing $300 is required.

7.3 INS Costs

Reliable cost data has only been obtained for the high quality INS. Costs are generally expected to be in the $80K to $100K range; specifically, the MAPS DRU unit, available to the Army for approximately $86K, meets or exceeds the navigation accuracy requirements for the high quality INS as assumed in this study. Since the MAPS DRU unit was not designed for this particular application, however, some adaptation (specifically of the interface to the outside world) will be needed.

Table 7.1-1 "Off-The-Shelf" Code GPS Survey Receivers [7-1]

GPS Survey Receivers

Reference for detailed data: *GPS Receivers - Characteristics and Performance Survey,* K.D. McDonald and B.P. Parkinson

Model Abbrev.	Manufacturer	Class	Chan's	Notes
MM1816	Aero Services Div. of Western Atlas Int'l	S1	8	MiniMac 1816®
MM1616		S1	6	MiniMac 1616®
MM2816		S3	8	MiniMac 2816®
MM2816AT		S3	8	MiniMac 2816AT®
Macrom. II		S3	6	Macrometer II®
SNR-8	Allen Osborne	S4	8	Rogue®
SNR-8A		S4	8	Rogue®
S-XII	Ashtech, Inc.	S1	12	Ashtech XII(discont'd.)
M-XII		S1	12	Ashtech XII
L-XII		S1	12	Ashtech XII
LT-XII		S1	12	Ashtech XII
LD-XII		S3	12	Ashtech XII
1005	Del Norte Technology	S1	5 or 7	
Geotrak	EDO Canada, Ltd.	S1	8	JMR Geotrak®
WM101	Wild Magnavox	S1	4	
WM102		S4	8	S2 transition to S4
Eagle	Motorola	S1	4	
Eagle VIII		S1	8	
MRGS		S1	4	Mini Ranger Geodetic System®
XR3-P	Polytechnic Electronics	S1	5 or 9	
TR5S	Sercel	S1	5	
NR52		S1	5	
TI4100	Texas Instruments	S2	1	No longer mfg'd, multiplexed set
4000AX	Trimble Navigation	S1	10	No longer mfg'd
4000SX		S1	10	
4000ST		S1, 3	8 or 12	All L1 or half L1 and L2
4000SL		S1	10	
4000SLD		S1, 3	10	L1 (+ S1) and S3

S1 - C/A Code L_1 Only
S2 - P Code
S3 - C/A Code Dual Freq
S4 - P Code / C/A Code Dual Freq

Figure 7.1-1 GPS Receiver Price vs. Year of Receiver Introduction [7-1] with Indicated Trend

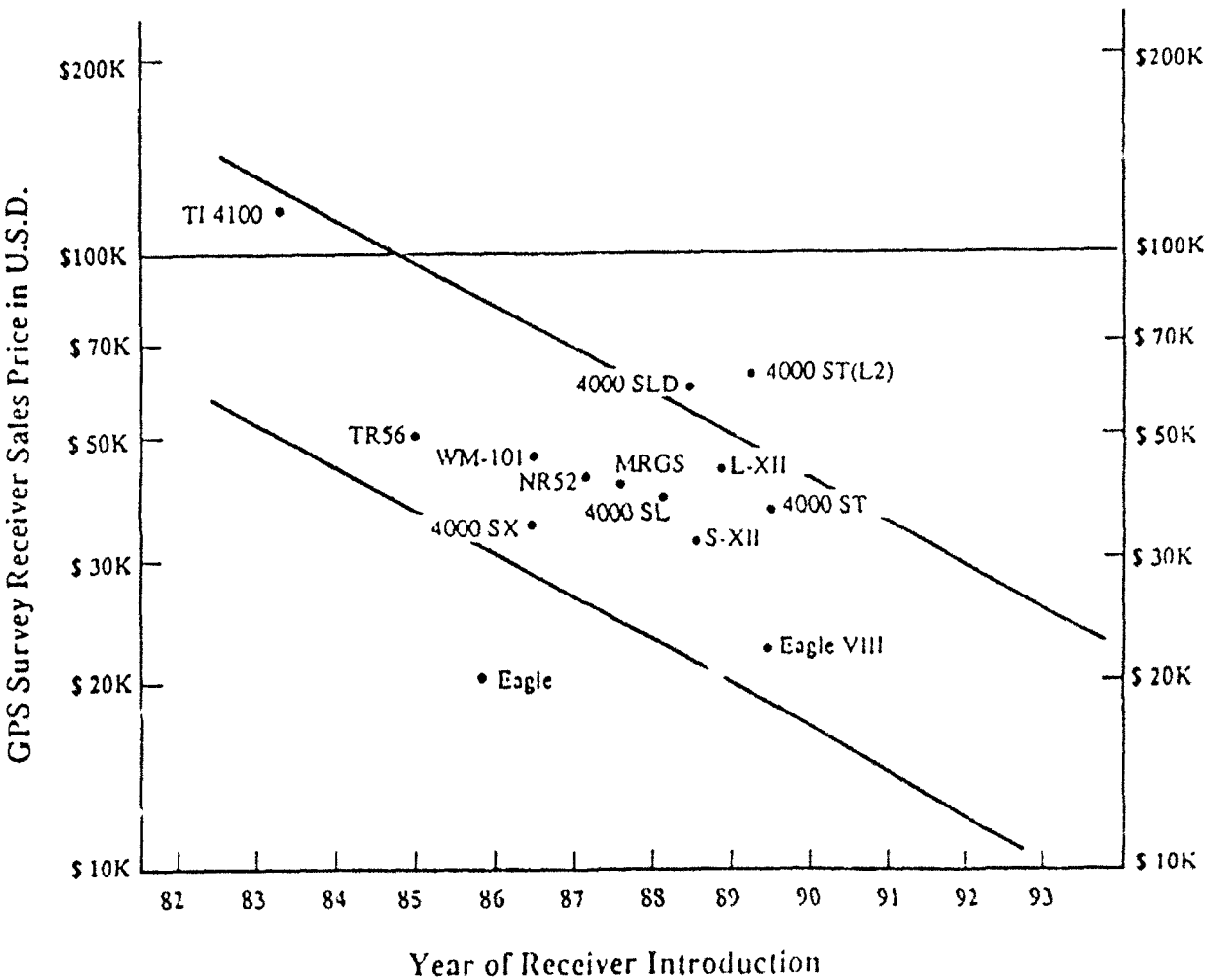

7.4 Barometric Altimeter Costs

Two barometric altimeter units adequate for use on this system are the following:

- A digital barometer, built by Atmospheric Instrumentation Research, Inc., which sells for $800.
- The Rosetta Microsystems Falcon Altitude Encoder, which sells for $100-$200.

7.5 Rubidium Frequency Standard

As shown in Section 5, the use of a rubidium frequency standard can extend maximum tolerable gap lengths significantly when operating with 3 satellites, so its use in the proposed system is highly recommended. It is expected to cost in the neighborhood of $10K.

7.6 Computer Costs

As previously referenced in Section 3, the major software functions which execute in the ship-based computer include interface software, differential correction calculation software, GPS/INS integration software, and ambiguity resolution software. The major loading on computer resources (i.e., throughput) is expected to be the GPS/INS Kalman filter and the ambiguity resolution algorithm, which run at 1 Hz and process the available (carrier) pseudorange measurements. Of course, the ambiguity resolution software will only execute when integers need to be resolved, so it will execute whenever lock is lost on a satellite in view, or whenever a satellite is added to the active tracking set. On a COMPAQ 386/25 computer at Trimble, the 56 state covariance simulation runs approximately 20 times faster than real time, so the 17 state Kalman filter can be expected to run roughly 100 times faster than real time. The ambiguity resolution software can be made to run roughly 5 timess faster than real time on a MacIntosh II computer. On a 386/25 computer this can be expected to run twice as fast as on the MacIntosh. Thus, a 386/25 seems adequate to execute the real time software. Its cost, including a monochrome display and hard disk, is conservatively estimated to be $7.5K.

7.7 Software Development Costs

It is difficult to estimate software development costs, due to the uncertainty associated with hardware integration, the level of documentation required and the extent to which existing code can be utilized. The software development costs reported herein will assume that there are no significant hardware integration problems (e.g., the need to build a custom interface between the INS and the computer), a minimum level of documentation and no portability of code. The assumed documentation level corresponds to an equation-level description of the algorithms, with heavily commented source code. Given these assumptions, the following estimates are supplied for each of the major software modules:

- Ambiguity resolution software- 18 mm.
- Kalman filter integration software- 15 mm.
- Reference station software- 9 mm (Master Station), 6 mm (Monitor Station).
- Interface software- 6 mm.
- Software installation and test- 6 mm.

Thus, a total of 60 mm are required. Assuming that a man month costs $12K, the total software development costs are roughly $720K.

7.8 Estimated Total System Costs

The total hardware costs, excluding the Rubidium frequency standard and the barometric altimeter, and operating with a single (master) station and for all hardware elements included are summarized below.

ESTIMATED TOTAL HARDWARE COSTS

(single reference station)
$207K

(all hardware elements included)
$294K

ESTIMATED TOTAL SOFTWARE DEVELOPMENT COSTS

$720K

7.9 Identified Risk Areas

Three areas of potential risk have been identified for this system:

- The use of non "off-the shelf" equipment.
- Reliance upon GLONASS in the recommended receiver design.
- Use of multiple reference stations.

Recommended use of the turbo-Rogue receiver for the kinematic phase positioning system represents a risk factor, since it is not yet commercially available. This risk can be reduced significantly if the mini-Rogue is utilized, which should be available soon and include all the necessary features of the turbo-Rogue. Use of GLONASS is considered a risk area since available information is not complete; e.g., can the signals be encrypted or turned off? Multiple reference stations are required, especially for longer distance separations (e.g., approaching 100 km). This is an undesirable feature of the system, since there is a maintenance cost associated with each reference station, and there can be a potential for vandalism. The vandalism can perhaps be reduced or eliminated by placing the reference stations at (secure) USACE facility locations. In addition, the networking concept, as analyzed in the previous section, has not been proven or demonstrated using real hardware. Since it is needed to maintain the required accuracy, it would have to be demonstrated and tested as part of the kinematic positioning system

8.0 Evaluation of Growth Potential

8.1 Alternative System Uses

Several other possible uses of a kinematic phase positioning system are referenced in the open literature, in addition to the possible use on board a helicopter of immediate interest to USACE. Its use as part of a precision range tracking system is reported in [25]. This reference documents flight test results performed at NASA/Wallops Flight Facility using TI4100 GPS receivers and a laser altimeter for a vertical reference. Agreement at the decimeter level is reported. In [21], an integrated GPS/INS system is proposed for use in highway surveying applications. A Litton LTN 90-100 strapdown INS is integrated with 2 Trimble 4000SX GPS receivers; an accuracy of 10-15 cm is expected from the tests. In [20], flight tests are performed using a kinematic phase positioning system on board an Orion P-3C aircraft: accuracies of 12 cm are reported for relatively poor GPS geometries; analytical projections for good GPS geometries are 1-2 cm..

8.2 Problems in Helicopter Integration

Two possible problems exist in the use of the system on board a helicopter: the possible increased frequency of cycle slips, increased INS error excitation caused by the more severe dynamic environment and satellite obscuration induced by the helicopter blades. The increased frequency of cycle slipping can, of course, be reduced by increasing the bandwidth of the carrier tracking loop; this unfortunately brings an inevitable increase in the noisiness of the derived carrier phase measurements. This tradeoff generally results in an optimum bandwidth selection for the expected dynamics and acceptable noise level in the measurements. This optimization requires a precise specification of the worst case dynamics and noise environment which may be experienced. Given this data for the helicopter environment, then, the probability of cycle slips can be reduced to an acceptably low level. The possible obscuration by the helicopter blades has 2 potential solutions: the GPS antenna can simply be installed above the blades or the signal processing software within the receiver can be designed to "look" for the signal in between the blade crossings. This latter approach has been demonstrated using Trimble receivers.

9.0 Conclusions and Recommendations

The major conclusions of this study are summarized in the decision matrix appearing as Table 9.0-1. Note that certain design options have been deleted from the list of possible system configurations. Only a high quality INS is considered, due to its improved gap filling performance in the absence of GPS, as demonstrated in the simulations of Section 5. The possible use of a single frequency C/A-code receiver and a C/A-code receiver which derives L2 information by signal squaring is not given serious consideration, since their ability to resolve integers is significantly degraded relative to the other receiver types (as demonstrated in the simulations of Section 4). Finally, only rubidium standard clocks are considered, based upon their enhancement of measurement gap filling capabilities, as reported in Section 5 (i.e., no consideration is given to a very low cost quartz clock).

The acronyms used to describe the GPS receiver types are: P, for P code receiver, and C/A XC, for a dual frequency C/A-code receiver which derives L2 information through cross-correlation. In the description of the possible aiding sensors, BARO denotes barometric altimeter. Finally, S denotes a single differential reference station, while N refers to a differential network comprised of 3 stations. The navigation performance measures are expressed as: one sigma horizontal position error and one sigma vertical position error, with both numbers expressed in centimeters. Note that the navigation performance appearing in the table corresponds to results for which the L1 integers have been resolved; they are therefore somewhat optimistic projections, since L1 convergence conditions were not established as part of this study. More pessimistic projections can be derived from the wide-lane performance numbers appearing in Table 6.3. Separate sets of numbers appear for 0 and 100 km separation distances. The performance of the ambiguity resolution algorithm is expressed in terms of the maximum time to converge to a correct set of wide-lane integers on all satellites in view (expressed in minutes) at the maximum indicated separation distance (in km). Constraints on the magnitude of the modelled multipath error (i.e., M=1) necessary to achieve the indicated convergence time are noted. The maximum gap length numbers (in seconds) are for 0 and 100 km separation distances, respectively, with complete loss of GPS during the gap.

Based upon this decision matrix, several possible systems emerge as strong candidates for USACE applications. The clear choice for a GPS receiver is either the Turbo Rogue, under development at JPL or the Mini-Rogue, soon to be made available by Allen Osborne; they represent the ideal combination of a P-code receiver with a backup C/A-code tracking capability which can support wide-laning. It should be competitively priced at $40K. If the risk associated with its availability is determined to be too great, use of the original Rogue (built by Allen Osborne) should yield equivalent performance, but with a cost penalty of an additional $40K (and a weight and size penalty). The (optional) use of a receiver which tracks GLONASS, in addition to GPS, increases the speed at which integers can be resolved (by roughly 40%). Its use by USACE is not strongly recommended, however, since no such receiver has been built, and information about the GLONASS system is not complete.

Table 9.0-1 Summary Decision Matrix

Possible System Configurations			System Qualities				
Rcvr	Aiding Sensors	Diff'l Sys	Nav Perf* (cm)	Amb Res Perf** (mins)	Max Gap Length***	Cost	Risk Areas
P	INS	S	2.6/6.2, 11.4/39.9	7 (100 km) 4 (100 km, GLONASS)	68 secs (0 km) 65 secs (100 km)	$213K	Low Cost Rcvr not avail
C/A XC	INS	S	2.6/6.2 11.4/39.9	15 (100 km, M=1) 6 (100 km, GLONASS,M=1)	68 secs (0 km) 65 secs (100 km)	$213K	Low Cost Rcvr not avail
P	INS	N	2.4/4.6 3.3/18.9	7 (100 km) 4 (100 km, GLONASS)	68 secs (0 km) 67 secs (100 km)	$294K	Network not proven, vandalism potential
C/A XC	INS	N	2.4/4.6 3.3/18.9	15 (100 km, M=1) 6 (100 km, GLONASS, M=1)	68 secs (0 km) 67 secs (100 km)	$294K	Network not proven, vandalism potential
P	INS/ BARO	S	2.6/6.2 11.4/39.9	7 (100 km) 4 (100 km, GLONASS)	68 secs (0 km) 65 secs (100 km)	$205K	
C/A XC	INS/ BARO	S	2.6/6.2 11.4/39.9	15 (100 km, M=1) 6 (100 km, GLONASS, M=1)	68 secs (0 km) 65 secs (100 km)	$205K	
P	INS/ BARO	N	2.4/4.6 3.3/18.9	7 (100 km) 4 (100 km, GLONASS)	68 secs (0 km) 67 secs (100 km)	$286K	Network not proven, vandalism potential
C/A XC	INS/ BARO	N	2.4/4.6 3.3/18.9	15 (100 km, M=1) 6 (100 km, GLONASS, M=1)	68 secs (0 km) 67 secs (100 km)	$286K	Network not proven, vandalism potential

* one sigma horizontal/vertical positioning error at 0, 100 km separation

** maximum convergence times for maximum separation (in km)

*** complete GPS obscuration during gap

**** excludes system development cost

A high quality INS is essential for maintenance of navigation accuracy during (complete) GPS outages. Use of a rubidium clock is warranted for fairly long periods of loss of a single satellite. Use of the barometric altimeter, even though it is relatively inexpensive, is not warranted, since it will not enhance performance significantly, and a zero mean sea level damping approach should yield equivalent performance. However, it may be required as a metrological sensor for performing local tropospheric corrections, and may prove to be useful if this system is used in helicopter operations, as described in the previous section.

The use of multiple reference stations, which is required for separation distances in excess of 20 km (when working with L1 resolved integers), represents significant risk (note that system performance even with the network does not meet the 10 cm requirement at 100 km). No differential network has ever been built, so would have to be undertaken as part of this system development. In addition, there could be significant costs associated with maintaining each reference station and securing them from vandalism.

APPENDIX 1: GPS EPHEMERIDES
[4-3]

Summary of nominal constellation:

a) Semi major axis at orbit: 26,609.000 km (same for all satellites).
b) Eccentricity: 0 (same for all satellites).
c) Inclination: 55° (same for all satellites).
d) Argument of perigee: 0 (same for all satellites).

The following variables are for the reference time 26 November 1989, 00:00:00

e) Right ascension at the ascending mode:

325.730284° (SV1 - SV4)
25.730284° (SV5 - SV8)
85.730284° (SV9 - SV12)
145.730284° (SV13 - SV16)
205.730284° (SV17 - SV20)
265.730284° (SV21 - SV24)

f) Mean anomaly

190.96	SV1
220.48	SV2
330.17	SV3
83.58	SV4
249.90	SV5
352.12	SV6
25.25	SV7
124.10	SV8
286.20	SV9
48.94	SV10
155.08	SV11
183.71	SV12
312.30	SV13
340.93	SV14
87.06	SV15
209.81	SV16
11.90	SV17
110.76	SV18
143.88	SV19
246.11	SV20
52.42	SV21
165.83	SV22
275.52	SV23
305.04	SV24

g) Rate of right ascension: $-7.914 \cdot 10^{-9}$ $\frac{\text{rad}}{\text{sec}}$

(same for all satellites)

```
 1 573  0  0  0     0.00 000000.00 0.000000000000000D-00
0.000000000000000D-00 0.000000000000000D-00 3.332881000000000D-00
0.000000000000000D-00 0.000000000000000D-00 5.158391222000000D+03
0.000000000000000D-00 9.599310890000000D-01 0.000000000000000D-00
3.699471000000000D-00-7.914051000000000D-09 0.000000000000000D-00
0.000000000000000D-00 0.000000000000000D-00 0.000000000000000D-00
0.000000000000000D-00 0.000000000000000D-00 0.000000000000000D-00

 2 573  0  0  0     0.00 000000.00 0.000000000000000D-00
0.000000000000000D-00 0.000000000000000D-00 3.848102000000000D-00
0.000000000000000D-00 0.000000000000000D-00 5.158391222000000D+03
0.000000000000000D-00 9.599310890000000D-01 0.000000000000000D-00
3.699471000000000D-00-7.914051000000000D-09 0.000000000000000D-00
0.000000000000000D-00 0.000000000000000D-00 0.000000000000000D-00
0.000000000000000D-00 0.000000000000000D-00 0.000000000000000D-00

 3 573  0  0  0     0.00 000000.00 0.000000000000000D-00
0.000000000000000D-00 0.000000000000000D-00 5.762554000000000D-00
0.000000000000000D-00 0.000000000000000D-00 5.158391222000000D+03
0.000000000000000D-00 9.599310890000000D-01 0.000000000000000D-00
3.699471000000000D-00-7.914051000000000D-09 0.000000000000000D-00
0.000000000000000D-00 0.000000000000000D-00 0.000000000000000D-00
0.000000000000000D-00 0.000000000000000D-00 0.000000000000000D-00

 4 573  0  0  0     0.00 000000.00 0.000000000000000D-00
0.000000000000000D-00 0.000000000000000D-00 1.458746000000000D-00
0.000000000000000D-00 0.000000000000000D-00 5.158391222000000D+03
0.000000000000000D-00 9.599310890000000D-01 0.000000000000000D-00
3.699471000000000D-00-7.914051000000000D-09 0.000000000000000D-00
0.000000000000000D-00 0.000000000000000D-00 0.000000000000000D-00
0.000000000000000D-00 0.000000000000000D-00 0.000000000000000D-00

 5 573  0  0  0     0.00 000000.00 0.000000000000000D-00
0.000000000000000D-00 0.000000000000000D-00 4.361578000000000D-00
0.000000000000000D-00 0.000000000000000D-00 5.158391222000000D+03
0.000000000000000D-00 9.599310890000000D-01 0.000000000000000D-00
4.746669000000000D-00-7.914051000000000D-09 0.000000000000000D-00
0.000000000000000D-00 0.000000000000000D-00 0.000000000000000D-00
0.000000000000000D-00 0.000000000000000D-00 0.000000000000000D-00

 6 573  0  0  0     0.00 000000.00 0.000000000000000D-00
0.000000000000000D-00 0.000000000000000D-00 6.145653000000000D-00
0.000000000000000D-00 0.000000000000000D-00 5.158391222000000D+03
0.000000000000000D-00 9.599310890000000D-01 0.000000000000000D-00
4.746669000000000D-00-7.914051000000000D-09 0.000000000000000D-00
0.000000000000000D-00 0.000000000000000D-00 0.000000000000000D-00
0.000000000000000D-00 0.000000000000000D-00 0.000000000000000D-00
```

```
 7 573  0  0  0     0.00 000000.00 0.000000000000000D-00
0.000000000000000D-00 0.000000000000000D-00 0.440696000000000D-00
0.000000000000000D-00 0.000000000000000D-00 5.158391222000000D+03
0.000000000000000D-00 9.599310890000000D-01 0.000000000000000D-00
4.746669000000000D-00-7.914051000000000D-09 0.000000000000000D-00
0.000000000000000D-00 0.000000000000000D-00 0.000000000000000D-00
0.000000000000000D-00 0.000000000000000D-00 0.000000000000000D-00

 8 573  0  0  0     0.00 000000.00 0.000000000000000D-00
0.000000000000000D-00 0.000000000000000D-00 2.165954000000000D-00
0.000000000000000D-00 0.000000000000000D-00 5.158391222000000D+03
0.000000000000000D-00 9.599310890000000D-01 0.000000000000000D-00
4.746669000000000D-00-7.914051000000000D-09 0.000000000000000D-00
0.000000000000000D-00 0.000000000000000D-00 0.000000000000000D-00
0.000000000000000D-00 0.000000000000000D-00 0.000000000000000D-00

 9 573  0  0  0     0.00 000000.00 0.000000000000000D-00
0.000000000000000D-00 0.000000000000000D-00 4.995132000000000D-00
0.000000000000000D-00 0.000000000000000D-00 5.158391222000000D+03
0.000000000000000D-00 9.599310890000000D-01 0.000000000000000D-00
5.793867000000000D-00-7.914051000000000D-09 0.000000000000000D-00
0.000000000000000D-00 0.000000000000000D-00 0.000000000000000D-00
0.000000000000000D-00 0.000000000000000D-00 0.000000000000000D-00

 10 573  0  0  0     0.00 000000.00 0.000000000000000D-00
0.000000000000000D-00 0.000000000000000D-00 0.854164000000000D-00
0.000000000000000D-00 0.000000000000000D-00 5.158391222000000D+03
0.000000000000000D-00 9.599310890000000D-01 0.000000000000000D-00
5.793867000000000D-00-7.914051000000000D-09 0.000000000000000D-00
0.000000000000000D-00 0.000000000000000D-00 0.000000000000000D-00
0.000000000000000D-00 0.000000000000000D-00 0.000000000000000D-00

 11 573  0  0  0     0.00 000000.00 0.000000000000000D-00
0.000000000000000D-00 0.000000000000000D-00 2.706657000000000D-00
0.000000000000000D-00 0.000000000000000D-00 5.158391222000000D+03
0.000000000000000D-00 9.599310890000000D-01 0.000000000000000D-00
5.793867000000000D-00-7.914051000000000D-09 0.000000000000000D-00
0.000000000000000D-00 0.000000000000000D-00 0.000000000000000D-00
0.000000000000000D-00 0.000000000000000D-00 0.000000000000000D-00

 12 573  0  0  0     0.00 000000.00 0.000000000000000D-00
0.000000000000000D-00 0.000000000000000D-00 3.206344000000000D-00
0.000000000000000D-00 0.000000000000000D-00 5.158391222000000D+03
0.000000000000000D-00 9.599310890000000D-01 0.000000000000000D-00
5.793867000000000D-00-7.914051000000000D-09 0.000000000000000D-00
0.000000000000000D-00 0.000000000000000D-00 0.000000000000000D-00
0.000000000000000D-00 0.000000000000000D-00 0.000000000000000D-00

 13 573  0  0  0     0.00 000000.00 0.000000000000000D-00
0.000000000000000D-00 0.000000000000000D-00 5.450663000000000D-00
```

0.000000000000000D-00 0.000000000000000D-00 5.158391222000000D+03
0.000000000000000D-00 9.599310890000000D-01 0.000000000000000D-00
0.557879000000000D-00-7.914051000000000D-09 0.000000000000000D-00
0.000000000000000D-00 0.000000000000000D-00 0.000000000000000D-00
0.000000000000000D-00 0.000000000000000D-00 0.000000000000000D-00

14 573 0 0 0 0.00 000000.00 0.000000000000000D-00
0.000000000000000D-00 0.000000000000000D-00 5.950351000000000D-00
0.000000000000000D-00 0.000000000000000D-00 5.158391222000000D+03
0.000000000000000D-00 9.599310890000000D-01 0.000000000000000D-00
0.557879000000000D-00-7.914051000000000D-09 0.000000000000000D-00
0.000000000000000D-00 0.000000000000000D-00 0.000000000000000D-00
0.000000000000000D-00 0.000000000000000D-00 0.000000000000000D-00

15 573 0 0 0 0.00 000000.00 0.000000000000000D-00
0.000000000000000D-00 0.000000000000000D-00 1.519484000000000D-00
0.000000000000000D-00 0.000000000000000D-00 5.158391222000000D+03
0.000000000000000D-00 9.599310890000000D-01 0.000000000000000D-00
0.557879000000000D-00-7.914051000000000D-09 0.000000000000000D-00
0.000000000000000D-00 0.000000000000000D-00 0.000000000000000D-00
0.000000000000000D-00 0.000000000000000D-00 0.000000000000000D-00

16 573 0 0 0 0.00 000000.00 0.000000000000000D-00
0.000000000000000D-00 0.000000000000000D-00 3.661875000000000D-00
0.000000000000000D-00 0.000000000000000D-00 5.158391222000000D+03
0.000000000000000D-00 9.599310890000000D-01 0.000000000000000D-00
0.557879000000000D-00-7.914051000000000D-09 0.000000000000000D-00
0.000000000000000D-00 0.000000000000000D-00 0.000000000000000D-00
0.000000000000000D-00 0.000000000000000D-00 0.000000000000000D-00

17 573 0 0 0 0.00 000000.00 0.000000000000000D-00
0.000000000000000D-00 0.000000000000000D-00 0.207694000000000D-00
0.000000000000000D-00 0.000000000000000D-00 5.158391222000000D+03
0.000000000000000D-00 9.599310890000000D-01 0.000000000000000D-00
1.605076000000000D-00-7.914051000000000D-09 0.000000000000000D-00
0.000000000000000D-00 0.000000000000000D-00 0.000000000000000D-00
0.000000000000000D-00 0.000000000000000D-00 0.000000000000000D-00

18 573 0 0 0 0.00 000000.00 0.000000000000000D-00
0.000000000000000D-00 0.000000000000000D-00 1.933127000000000D-00
0.000000000000000D-00 0.000000000000000D-00 5.158391222000000D+03
0.000000000000000D-00 9.599310890000000D-01 0.000000000000000D-00
1.605076000000000D-00-7.914051000000000D-09 0.000000000000000D-00
0.000000000000000D-00 0.000000000000000D-00 0.000000000000000D-00
0.000000000000000D-00 0.000000000000000D-00 0.000000000000000D-00

19 573 0 0 0 0.00 000000.00 0.000000000000000D-00
0.000000000000000D-00 0.000000000000000D-00 2.511180000000000D-00
0.000000000000000D-00 0.000000000000000D-00 5.158391222000000D+03
0.000000000000000D-00 9.599310890000000D-01 0.000000000000000D-00
1.605076000000000D-00-7.914051000000000D-09 0.000000000000000D-00

0.000000000000000D-00 0.000000000000000D-00 0.000000000000000D-00
0.000000000000000D-00 0.000000000000000D-00 0.000000000000000D-00

20 573 0 0 0 0.00 000000.00 0.000000000000000D-00
0.000000000000000D-00 0.000000000000000D-00 4.295430000000000D-00
0.000000000000000D-00 0.000000000000000D-00 5.158391222000000D+03
0.000000000000000D-00 9.599310890000000D-01 0.000000000000000D-00
1.605076000000000D-00-7.914051000000000D-09 0.000000000000000D-00
0.000000000000000D-00 0.000000000000000D-00 0.000000000000000D-00
0.000000000000000D-00 0.000000000000000D-00 0.000000000000000D-00

21 573 0 0 0 0.00 000000.00 0.000000000000000D-00
0.000000000000000D-00 0.000000000000000D-00 0.914902000000000D-00
0.000000000000000D-00 0.000000000000000D-00 5.158391222000000D+03
0.000000000000000D-00 9.599310890000000D-01 0.000000000000000D-00
2.652274000000000D-00-7.914051000000000D-09 0.000000000000000D-00
0.000000000000000D-00 0.000000000000000D-00 0.000000000000000D-00
0.000000000000000D-00 0.000000000000000D-00 0.000000000000000D-00

22 573 0 0 0 0.00 000000.00 0.000000000000000D-00
0.000000000000000D-00 0.000000000000000D-00 2.894280000000000D-00
0.000000000000000D-00 0.000000000000000D-00 5.158391222000000D+03
0.000000000000000D-00 9.599310890000000D-01 0.000000000000000D-00
2.652274000000000D-00-7.914051000000000D-09 0.000000000000000D-00
0.000000000000000D-00 0.000000000000000D-00 0.000000000000000D-00
0.000000000000000D-00 0.000000000000000D-00 0.000000000000000D-00

23 573 0 0 0 0.00 000000.00 0.000000000000000D-00
0.000000000000000D-00 0.000000000000000D-00 4.808731000000000D-00
0.000000000000000D-00 0.000000000000000D-00 5.158391222000000D+03
0.000000000000000D-00 9.599310890000000D-01 0.000000000000000D-00
2.652274000000000D-00-7.914051000000000D-09 0.000000000000000D-00
0.000000000000000D-00 0.000000000000000D-00 0.000000000000000D-00
0.000000000000000D-00 0.000000000000000D-00 0.000000000000000D-00

24 573 0 0 0 0.00 000000.00 0.000000000000000D-00
0.000000000000000D-00 0.000000000000000D-00 5.323952000000000D-00
0.000000000000000D-00 0.000000000000000D-00 5.158391222000000D+03
0.000000000000000D-00 9.599310890000000D-01 0.000000000000000D-00
2.652274000000000D-00-7.914051000000000D-09 0.000000000000000D-00
0.000000000000000D-00 0.000000000000000D-00 0.000000000000000D-00
0.000000000000000D-00 0.000000000000000D-00 0.000000000000000D-00

APPENDIX 2: GLONASS EPHEMERIDES
[4-1]

Summary of nominal constellation:

a) Semi major axis of orbit: 25,506.783 km (same for all satellites).
b) Eccentritity: 0 (same for all satellites).
c) Inclination: 64.8° (same for all satellites).
d) Argument of perigee: 0 (same for all satellites).

The following variables are for the reference time 7 September 1987, 00:00:00

e) Right ascension at the ascending mode:

73.000°	(SV1 - SV8)
193.000°	(SV9 - SV16)
313.000°	(SV17 - SV24)

f) Mean anomaly

0.00°	SV1
45.00°	SV2
90.00°	SV3
135.00°	SV4
180.00°	SV5
225.00°	SV6
270.00°	SV7
315.00°	SV8
15.00°	SV9
60.00°	SV10
105.00°	SV11
150.00°	SV12
195.00°	SV13
240.00°	SV14
285.00°	SV15
330.00°	SV16
30.00°	SV17
75.00°	SV18
120.00°	SV19
165.00°	SV20
210.00°	SV21
255.00°	SV22
300.00°	SV23
345.00°	SV24

g) Rate of right ascension: $-5.875 \cdot 10^{-9}$ $\frac{\text{rad}}{\text{sec}}$

(same for all satellites)

25 573 0 0 0 0.00 000000.00 0.000000000000000D-00
0.000000000000000D-00 0.000000000000000D-00 3.421892000000000D-00
0.000000000000000D-00 0.000000000000000D-00 5.050424054000000D+03
0.000000000000000D-00 1.130973400000000D-00 0.000000000000000D-00
5.229631000000000D-00-5.874955000000000D-09 0.000000000000000D-00
0.000000000000000D-00 0.000000000000000D-00 0.000000000000000D-00
0.000000000000000D-00 0.000000000000000D-00 0.000000000000000D-00

26 573 0 0 0 0.00 000000.00 0.000000000000000D-00
0.000000000000000D-00 0.000000000000000D-00 4.207291000000000D-00
0.000000000000000D-00 0.000000000000000D-00 5.050424054000000D+03
0.000000000000000D-00 1.130973400000000D-00 0.000000000000000D-00
5.229631000000000D-00-5.874955000000000D-09 0.000000000000000D-00
0.000000000000000D-00 0.000000000000000D-00 0.000000000000000D-00
0.000000000000000D-00 0.000000000000000D-00 0.000000000000000D-00

27 573 0 0 0 0.00 000000.00 0.000000000000000D-00
0.000000000000000D-00 0.000000000000000D-00 4.992689000000000D-00
0.000000000000000D-00 0.000000000000000D-00 5.050424054000000D+03
0.000000000000000D-00 1.130973400000000D-00 0.000000000000000D-00
5.229631000000000D-00-5.874955000000000D-09 0.000000000000000D-00
0.000000000000000D-00 0.000000000000000D-00 0.000000000000000D-00
0.000000000000000D-00 0.000000000000000D-00 0.000000000000000D-00

28 573 0 0 0 0.00 000000.00 0.000000000000000D-00
0.000000000000000D-00 0.000000000000000D-00 5.778087000000000D-00
0.000000000000000D-00 0.000000000000000D-00 5.050424054000000D+03
0.000000000000000D-00 1.130973400000000D-00 0.000000000000000D-00
5.229631000000000D-00-5.874955000000000D-09 0.000000000000000D-00
0.000000000000000D-00 0.000000000000000D-00 0.000000000000000D-00
0.000000000000000D-00 0.000000000000000D-00 0.000000000000000D-00

29 573 0 0 0 0.00 060000.00 0.000000000000000D-00
0.000000000000000D-00 0.000000000000000D-00 6.563485000000000D-00
0.000000000000000D-00 0.000000000000000D-00 5.050424054000000D+03
0.000000000000000D-00 1.130973400000000D-00 0.000000000000000D-00
5.229631000000000D-00-5.874955000000000D-09 0.000000000000000D-00
0.000000000000000D-00 0.000000000000000D-00 0.000000000000000D-00
0.000000000000000D-00 0.000000000000000D-00 0.000000000000000D-00

30 573 0 0 0 0.00 000000.00 0.000000000000000D-00
0.000000000000000D-00 0.000000000000000D-00 1.065698000000000D-00
0.000000000000000D-00 0.000000000000000D-00 5.050424054000000D+03
0.000000000000000D-00 1.130973400000000D-00 0.000000000000000D-00
5.229631000000000D-00-5.874955000000000D-09 0.000000000000000D-00
0.000000000000000D-00 0.000000000000000D-00 0.000000000000000D-00
0.000000000000000D-00 0.000000000000000D-00 0.000000000000000D-00

```
 31 573  0  0  0     0.00 000000.00 0.000000000000000D-00
0.000000000000000D-00 0.000000000000000D-00 1.851096000000000D-00
0.000000000000000D-00 0.000000000000000D-00 5.050424054000000D+03
0.000000000000000D-00 1.130973400000000D-00 0.000000000000000D-00
5.229631000000000D-00-5.874955000000000D-09 0.000000000000000D-00
0.000000000000000D-00 0.000000000000000D-00 0.000000000000000D-00
0.000000000000000D-00 0.000000000000000D-00 0.000000000000000D-00

 32 573  0  0  0     0.00 000000.00 0.000000000000000D-00
0.000000000000000D-00 0.000000000000000D-00 2.636494000000000D-00
0.000000000000000D-00 0.000000000000000D-00 5.050424054000000D+03
0.000000000000000D-00 1.130973400000000D-00 0.000000000000000D-00
5.229631000000000D-00-5.874955000000000D-09 0.000000000000000D-00
0.000000000000000D-00 0.000000000000000D-00 0.000000000000000D-00
0.000000000000000D-00 0.000000000000000D-00 0.000000000000000D-00

 33 573  0  0  0     0.00 000000.00 0.000000000000000D-00
0.000000000000000D-00 0.000000000000000D-00 3.683692000000000D-00
0.000000000000000D-00 0.000000000000000D-00 5.050424054000000D+03
0.000000000000000D-00 1.130973400000000D-00 0.000000000000000D-00
1.040841000000000D-00-5.874955000000000D-09 0.000000000000000D-00
0.000000000000000D-00 0.000000000000000D-00 0.000000000000000D-00
0.000000000000000D-00 0.000000000000000D-00 0.000000000000000D-00

 34 573  0  0  0     0.00 000000.00 0.000000000000000D-00
0.000000000000000D-00 0.000000000000000D-00 4.469090000000000D-00
0.000000000000000D-00 0.000000000000000D-00 5.050424054000000D+03
0.000000000000000D-00 1.130973400000000D-00 0.000000000000000D-00
1.040841000000000D-00-5.874955000000000D-09 0.000000000000000D-00
0.000000000000000D-00 0.000000000000000D-00 0.000000000000000D-00
0.000000000000000D-00 0.000000000000000D-00 0.000000000000000D-00

 35 573  0  0  0     0.00 000000.00 0.000000000000000D-00
0.000000000000000D-00 0.000000000000000D-00 5.254488000000000D-00
0.000000000000000D-00 0.000000000000000D-00 5.050424054000000D+03
0.000000000000000D-00 1.130973400000000D-00 0.000000000000000D-00
1.040841000000000D-00-5.874955000000000D-09 0.000000000000000D-00
0.000000000000000D-00 0.000000000000000D-00 0.000000000000000D-00
0.000000000000000D-00 0.000000000000000D-00 0.000000000000000D-00

 36 573  0  0  0     0.00 000000.00 0.000000000000000D-00
0.000000000000000D-00 0.000000000000000D-00 6.039886000000000D-00
0.000000000000000D-00 0.000000000000000D-00 5.050424054000000D+03
0.000000000000000D-00 1.130973400000000D-00 0.000000000000000D-00
1.040841000000000D-00-5.874955000000000D-09 0.000000000000000D-00
0.000000000000000D-00 0.000000000000000D-00 0.000000000000000D-00
0.000000000000000D-00 0.000000000000000D-00 0.000000000000000D-00

 37 573  0  0  0     0.00 000000.00 0.000000000000000D-00
0.000000000000000D-00 0.000000000000000D-00 0.542099000000000D-00
0.000000000000000D-00 0.000000000000000D-00 5.050424054000000D+03
```

```
0.000000000000000D-00 1.130973400000000D-00 0.000000000000000D-00
1.040841000000000D-00-5.874955000000000D-09 0.000000000000000D-00
0.000000000000000D-00 0.000000000000000D-00 0.000000000000000D-00
0.000000000000000D-00 0.000000000000000D-00 0.000000000000000D-00

 38 573  0  0  0     0.00 000000.00 0.000000000000000D-00
0.000000000000000D-00 0.000000000000000D-00 1.327497000000000D-00
0.000000000000000D-00 0.000000000000000D-00 5.050424054000000D+03
0.000000000000000D-00 1.130973400000000D-00 0.000000000000000D-00
1.040841000000000D-00-5.874955000000000D-09 0.000000000000000D-00
0.000000000000000D-00 0.000000000000000D-00 0.000000000000000D-00
0.000000000000000D-00 0.000000000000000D-00 0.000000000000000D-00

 39 573  0  0  0     0.00 000000.00 0.000000000000000D-00
0.000000000000000D-00 0.000000000000000D-00 2.112896000000000D-00
0.000000000000000D-00 0.000000000000000D-00 5.050424054000000D+03
0.000000000000000D-00 1.130973400000000D-00 0.000000000000000D-00
1.040841000000000D-5.874955000000000D-09 0.000000000000000D-00
0.000000000000000D-00 0.000000000000000D-00 0.000000000000000D-00
0.000000000000000D-00 0.000000000000000D-00 0.000000000000000D-00

 40 573  0  0  0     0.00 000000.00 0.000000000000000D-00
0.000000000000000D-00 0.000000000000000D-00 2.898294000000000D-00
0.000000000000000D-00 0.000000000000000D-00 5.050424054000000D+03
0.000000000000000D-00 1.130973400000000D-00 0.000000000000000D-00
1.040841000000000D-00-5.874955000000000D-09 0.000000000000000D-00
0.000000000000000D-00 0.000000000000000D-00 0.000000000000000D-00
0.000000000000000D-00 0.000000000000000D-00 0.000000000000000D-00

 41 573  0  0  0     0.00 000000.00 0.000000000000000D-00
0.000000000000000D-00 0.000000000000000D-00 3.945491000000000D-00
0.000000000000000D-00 0.000000000000000D-00 5.050424054000000D+03
0.000000000000000D-00 1.130973400000000D-00 0.000000000000000D-00
3.135236000000000D-00-5.874955000000000D-09 0.000000000000000D-00
0.000000000000000D-00 0.000000000000000D-00 0.000000000000000D-00
0.000000000000000D-00 0.000000000000000D-00 0.000000000000000D-00

 42 573  0  0  0     0.00 000000.00 0.000000000000000D-00
0.000000000000000D-00 0.000000000000000D-00 4.730890000000000D-00
0.000000000000000D-00 0.000000000000000D-00 5.050424054000000D+03
0.000000000000000D-00 1.130973400000000D-00 0.000000000000000D-00
3.135236000000000D-00-5.874955000000000D-09 0.000000000000000D-00
0.000000000000000D-00 0.000000000000000D-00 0.000000000000000D-00
0.000000000000000D-00 0.000000000000000D-00 0.000000000000000D-00

 43 573  0  0  0     0.00 000000.00 0.000000000000000D-00
0.000000000000000D-00 0.000000000000000D-00 5.516288000000000D-00
0.000000000000000D-00 0.000000000000000D-00 5.050424054000000D+03
0.000000000000000D-00 1.130973400000000D-00 0.000000000000000D-00
3.135236000000000D-00-5.874955000000000D-09 0.000000000000000D-00
0.000000000000000D-00 0.000000000000000D-00 0.000000000000000D-00
```

0.0000000000000000D-00 0.0000000000000000D-00 0.0000000000000000D-00

44 573 0 0 0 0.00 000000.00 0.0000000000000000D-00
0.0000000000000000D-00 0.0000000000000000D-00 0.0185000000000000D-00
0.0000000000000000D-00 0.0000000000000000D-00 5.0504240540000000D+03
0.0000000000000000D-00 1.1309734000000000D-00 0.0000000000000000D-00
3.1352360000000000D-00-5.8749550000000000D-09 0.0000000000000000D-00
0.0000000000000000D-00 0.0000000000000000D-00 0.0000000000000000D-00
0.0000000000000000D-00 0.0000000000000000D-00 0.0000000000000000D-00

45 573 0 0 0 0.00 000000.00 0.0000000000000000D-00
0.0000000000000000D-00 0.0000000000000000D-00 0.8038990000000000D-00
0.0000000000000000D-00 0.0000000000000000D-00 5.0504240540000000D+03
0.0000000000000000D-00 1.1309734000000000D-00 0.0000000000000000D-00
3.1352360000000000D-00-5.8749550000000000D-09 0.0000000000000000D-00
0.0000000000000000D-00 0.0000000000000000D-00 0.0000000000000000D-00
0.0000000000000000D-00 0.0000000000000000D-00 0.0000000000000000D-00

46 573 0 0 0 0.00 000000.00 0.0000000000000000D-00
0.0000000000000000D-00 0.0000000000000000D-00 1.5892970000000000D-00
0.0000000000000000D-00 0.0000000000000000D-00 5.0504240540000000D+03
0.0000000000000000D-00 1.1309734000000000D-00 0.0000000000000000D-00
3.1352360000000000D-00-5.8749550000000000D-09 0.0000000000000000D-00
0.0000000000000000D-00 0.0000000000000000D-00 0.0000000000000000D-00
0.0000000000000000D-00 0.0000000000000000D-00 0.0000000000000000D-00

47 573 0 0 0 0.00 000000.00 0.0000000000000000D-00
0.0000000000000000D-00 0.0000000000000000D-00 2.3746950000000000D-00
0.0000000000000000D-00 0.0000000000000000D-00 5.0504240540000000D+03
0.0000000000000000D-00 1.1309734000000000D-00 0.0000000000000000D-00
3.1352360000000000D-00-5.8749550000000000D-09 0.0000000000000000D-00
0.0000000000000000D-00 0.0000000000000000D-00 0.0000000000000000D-00
0.0000000000000000D-00 0.0000000000000000D-00 0.0000000000000000D-00

48 573 0 0 0 0.00 000000.00 0.0000000000000000D-00
0.0000000000000000D-00 0.0000000000000000D-00 3.1600930000000000D-00
0.0000000000000000D-00 0.0000000000000000D-00 5.0504240540000000D+03
0.0000000000000000D-00 1.1309734000000000D-00 0.0000000000000000D-00
3.1352360000000000D-00-5.8749550000000000D-09 0.0000000000000000D-00
0.0000000000000000D-00 0.0000000000000000D-00 0.0000000000000000D-00
0.0000000000000000D-00 0.0000000000000000D-00 0.0000000000000000D-00

APPENDIX 3: GEOSTATIONARY SATELLITE EPHEMERIS

```
 50 573  0  0  0     0.00 000000.00 0.0000000000000000D-00
0.0000000000000000D-00 0.0000000000000000D-00 0.0000000000000000D-00
0.0000000000000000D-00 0.0000000000000000D-00 6.4993159320000000D+03
0.0000000000000000D-00 0.0000000000000000D-00 0.0000000000000000D-00
4.0142570000000000D-00 0.0000000000000000D-00 0.0000000000000000D-00
0.0000000000000000D-00 0.0000000000000000D-00 0.0000000000000000D-00
0.0000000000000000D-00 0.0000000000000000D-00 0.0000000000000000D-00
```

REFERENCES

1. Allison, T. and Eschenbach, R. Real-time Cycle-slip Fixing During Kinematic Surveys. Proceedings of the Fifth International Geodetic Symposium on Satellite Positioning, Las Cruces, NM, DMA, U.S.DoD, NGS, NOAA, 13-17 March 1989, New Mexico State University, Las Cruces, NM, pp.330-7.

2. Allison, T., Eschenbach, R., Hyatt, R., Westfall, B. C/A code Dual Frequency Surveying Receiver, Architecture and Performance. PLANS '88 Proceedings of IEEE Position Location and Navigation Symposium, Orlando, FL, 29 November - 2 December 1988, pp.434-441.

3. Altshuler, Edward E. and Kalagham, Paul M. Tropospheric Range Error Corrections for the NAVSTAR System. Air Force Cambridge Research Laboratories, AFCRL-TR-74-0198, April 1974.

4. Ashjaee, J.M., Bourne, D.R., Helkey, R.J., Lorenz, R.G., Minazio, J.B., Remondi, B.W. and Sutherland, R.R. Ashtech XII GPS Receiver, the all-in-one All-in-view. In: ION GPS-88, Preliminary Proceedings of the First International Technical Meeting, Colorado Springs, CO, 21-23 September 1988, Institute of Navigation, Institute of Navigation's Satellite Division, 7pp. Also in PLANS '88 Proceedings of IEEE Position Location and Navigation Symposium, Orlando, FL, 29 November - 2 December 1988, pp.1123-42.

5. Counselman, C.C., III. Method of Resolving Radio Phase Ambiguity in Satellite Orbit Determination. Journal of Geophysical Research, Vol.94, No.B6, 10 June 1989, pp.7058-64.

6. Daly, P. Aspects of the Soviet Union's GLONASS Satellite Navigation System. The (UK) Journal of Navigation 41(2), 1988, pp.186-98.

7. Eastwood, R.A. An Integrated GPS/GLONASS Receier. ION National Technical Meeting, San Diego, CA, January 1990.

8. Ferguson, K., Veatch, E., Sauve, R., Evers, M., Corcoran, W. Kinematic and Pseudo-kinematic Surveying With the Ashtech XII. In: ION GPS-89, Preliminary Proceedings of the Second International Technical Meeting, Colorado Springs, CO, 25-29 September 1989. The Institute of Navigation's Satellite Division, 3 pp.

9. Frei, E. and Beutler, G. Some Considerations Concerning an Adaptive, Optimized Technique to Resolve the Initial Phase Ambiguities. Proceedings of the Fifth International Geodetic Symposium on Satellite Positioning, DMA, DoD, NGS, NOAA, Las Cruces, NM, 13-17 March 1989, New Mexico University, Vol.2, pp.671-86.

10. Gelb, A. Applied Optimal Estimation, MIT Press, 1978.

11. Georgiadou, Y. and Kleusberg, A. On the Effect of Ionospheric Delay on Geodetic Relative GPS Positioning. Manuscripta Geodetica 13, 1988, pp.1-8.

12. Green, G.B., Massat, P.D. and Rhodus, N.W. The GPS 21 Primary Satellite Constellation. Navigation 36(1), 1989, pp.9-24.

13. Greenspan, R.L. and Donna, J.I. Measurement Errors in GPS Observables. Proceedings of the Forty-Second Annual Meeting of the Institute of Navigation, Seattle, WA, June 1986.

14. Hartmann, G.K. and Leitinger, R. Range Errors Due to Ionospheric and Tropospheric Effects for Signal Frequencies Above 100 MHz. Bulletin Geodesique 58, 1984, pp.109-36.

15. Hatch, R. Instantaneous Ambiguity Resolution. KIS Symposium, Banff, Canada, 11 September 1990.

16. Heroux, P. and Kleusberg, A. GPS Precise Relative Positioning and Ionosphere in Auroral Regions. Proceedings of the 5th International Symposium on Satellite Positioning, Las Cruces, NM, 1989, pp.475-86.

17. Hwang, P.Y.C. Kinematic GPS: Resolving Integer Ambiguities On-the-Fly. IEEE Position Location and Navigation Symposium, No.90CH2811-8, Las Vegas, NV, 20-23 March 1990, pp.579-86.

18. Jorgensen, P.S. An Assessment of Ionospheric Effects on the GPS User. NAVIGATION, Journal of the Institute of Navigation, Vol.36, No.2, Summer 1989.

19. Klobuchar, John A. A First-Order, Worldwide, Ionospheric, Time-Delay Algorithm. Air Force Cambridge Research Laboratories, AFCRL-TR-75-0502, September 1975.

20. Krabill, W.B. and Martin, C.F. Aircraft Positioning Using Global Positioning System Carrier Phase Data. Journal of the Institute of Navigation, Vol.34, No.1, Spring 1987.

21. Lapuche, D., et. al. The Use of GPS/INS in a Highway Survey System. 1990 PLANS Proceedings.

22. Letter from Frederick Gloeckler to Bruce Peetz, Trimble Navigation, 2 December 1988.

23. Levine, S.A. and Gelb, A. Effect of Deflections of the Vertical on the Performance of a Terrestrial Inertial Navigation System. Journal of Spacecraft and Rockets, Vol.6, No.9, September 1969, pp.978-84.

24. Loomis, P. A Kinematic GPS Double Differencing Algorithm. Proceedings of the Fifth International Symposium on Satellite Positioning, Las Cruces, NM, 1989, pp.611-20.

25. Mader, G.L. Decimeter Level Aircraft Positioning Using GPS Carrier Phase Measurements. Source unknown.

26. McDonald, K. An Analysis of GPS Receiver Performance Capabilities and Trends. ION National Technical Meeting, San Diego, CA, January 1990.

27. Nash, R.A.,Jr, Kasper, J.A.,Jr, Crawford, B.S. and Levine, S.A. Application of Optimal Smoothing to the Testing and Evaluation of Inertial Navigation Systems and Components. IEEE Transactions on Automatic Control, Vol.AC-16, No.6, December 1971, pp.806-16.

28. Precision Time and Frequency Handbook, Ball Efratom Division, 1985.

29. Quek, S.H. and Wells, D.E. Mac GEPSAL (Macintosh General Purpose Satellite Alert Program User's Guide. Geodetic Research Laboratory, University of New Brunswick, Fredericton, N.B., Canada E3B 5A3.

30. Remondi, B.W. Pseudo-kinematic GPS Results Using the Ambiguity Function Method. NOAA Technical Memorandum NOS NGS-52, Rockville, MD, May 1990.

31. Remondi, B.W. and Hofmann-Wellenhof, B. GPS Broadcast Orbits Versus Precise Orbits: A Comparision Study. CSTG GPS Bulletin 2, No.6, pp.8-20.

32. Rice, D.A. A Geoidal Section of the United States. XIIIth General Assembly of the International Union of the Geodesy and Geophysics, Helsinki, July - August 1960.

33. Santerre, R. GPS Satellite Sky Distribution: Impact on the Propagation of Some Important Errors in Precise Relative Positioning. Department of Surveying Engineering, University of New Brunswick, Technical Report No.145

34. Seeber, G. and Wübbena, G. Kinematic Positioning with Carrier Phases and "On the Way" Ambiguity Solution. Fifth International Geodetic Symposium on Satellite Positioning Proceedings, Vol.II, Las Cruces, NM, 13-17 March 1989.

35. Van Dierendonck, A.J. and McGraw, J.B. Relationship Between Allan Variances and Kalman Filter Parameters. STI-TM-42016, Stanford Telecommunication, Inc., 14 December 1984.

36. Ward, P. An Advanced NAVSTAR GPS Geodetic Receiver. Proceedings of the Third International Geodetic Symposium on Satellite Positioning, Las Cruces, NM, 8-12 February 1982, Vol.II, pp.1123-42.

37. Wells, D.E., Beck, N., Delikaraoglou, D., Kleusberg, A., Krakiwsky, E., Lachapelle, G., Langley, R., Nakiboglou, M., Schwarz, K.P., Tranquilla, J. and Vanicek, P. Guide to GPS Positioning. Canadian GPS Associates, Fredericton, N.B., Canada, 1987, E3B 5A3.

38. Westrop, J., Napier, M.E. and Ashkenazi, V. Cycle Slips on the Move: Detection and Elimination. In: ION GPS-89, Preliminary Proceedings of the Second International Technical Meeting, Colorado Springs, CO, 25-29 September 1989, The Institute of Navigation's Satellite Division, 5 pp.

39. Widnall, W.S. and Grundy, P.A. Inertial Navigation System Error Models. Intermetrics TR-03-73, 11 May 1973.

40. Wübbena, G. The GPS Adjustment Software Package GEONAP - Concepts and Models. Proceedings of the Fifth International Symposium on Satellite Positioning, Las Cruces, NM, pp.452-61.

Waterways Experiment Station Cataloging-in-Publication Data

Geier, G. J.
System analysis for a kinematic positioning system based on the Global Positioning System / by G. Jeffrey Geier, Peter V.W. Loomis, Alfred Kleusberg ; prepared for Department of the Army, U.S. Army Corps of Engineers ; monitored by U.S. Army Topographic Engineering Center.
133 p. : ill. ; 28 cm. — (Contract report ; DRP-92-8)
Includes bibliographical references.
1. Global Positioning System. 2. Hydrographic surveying. 3. Inertial navigation systems. 4. Dredging. I. Loomis, P. V. M. II. Kleusberg, Alfred. III. United States. Army. Corps of Engineers. IV. U.S. Army Topographic Engineering Center. V. U.S. Army Engineer Waterways Experiment Station. VI. Dredging Research Program. VII. Title. VIII. Series: Contract report (U.S. Army Engineer Waterways Experiment Station) ; DRP-92-8.
TA7 W34c no.DRP-92-8